Universidad de Valladolid

FACULTAD DE CIENCIAS

DEPARTAMENTO DE FÍSICA DE LA MATERIA CONDENSADA, CRISTALOGRAFÍA Y MINERALOGÍA.

TESIS DOCTORAL:

DEVELOPMENT OF NANOSTRUCTURES AND HIGHLY FUNCTIONAL SYSTEMS WITH COMPLEX MOLECULAR ARCHITECTURE BASED ON ELASTIN-LIKE RECOMBINAMERS

Presentada por Guillermo Pinedo Martín para optar al grado de Doctor por la Universidad de Valladolid

Dirigida por:
Dr. José Carlos Rodríguez Cabello
Dr. Matilde Alonso Rodrigo.

A mi familia

AGRADECIMIENTOS

Parecía imposible, pero aquí está, el final de mi tesis doctoral. Claro y cuando acabas de escribir aún faltan los agradecimientos, parte importante, tienen que quedar bien, seguramente sea la parte más leída. Esta tesis han sido 3 emocionante años, llenos de alegrías, también decepciones enfados y demás, pero sin duda una experiencia impresionante.

En primer lugar quería agradecer a mis directores Carlos y Matilde por darme la oportunidad de pertenecer a Bioforge y hacer la tesis. Sin vuestra ayuda, apoyo y consejos esto hubiera sido imposible, muchísimas gracias.

No me puedo olvidar de los "seniors", matrimonio Arias-Girotti., Merche, Ana y Luis mil gracias. Javi, muchas gracias por toda tu ayuda, paciencia y por enseñar a un pobrecillo físico un poquito de biología molecular. Ale, a pesar de que tenemos puntos de vista diferentes y no era raro que acabáramos "discutiendo" cuando te preguntaba algo, siempre has estado dispuesta a echarme una mano en lo que hiciera falta, muchísimas gracias por todo. Merche, muchas gracias por los buenos ratos, las charlas y por toda tu ayuda cuando me dio por pasar por químicos.

En la portada de esta tesis pone mi nombre, pero es un poco de todos mis compañeros de Bioforge, todos ellos me han ayudado de una manera o de otra a hacer este trabajo. Gracias a los que estaban cuando empecé (Menchu, María y Laura). Laura, bien sabes tú que sin tu ayuda, consejo y amistad esto hubiera sido mucho más duro, gracias de todo corazón.

Una de las cosas que ha hecho geniales estos años ha sido el gran ambiente en el laboratorio. He tenido la suerte de compartir mi

tesis con compañeros excepcionales. Israel, Alicia, Chus, Mohammed, Arturo, e Ito, mil gracias por todo, por todos los buenos momentos que hemos pasado juntos, por escucharme y aguantarme cuando este trabajo se ponía complicado, me llevo no solo compis sino buenos amigos. Rocío, una sola frase, sin ti imposible, muchas gracias. Vanesa e Irene, creo que habéis sido imprescindibles para no acabar majara, muchas gracias por todas nuestras charlas, gossip y buenos ratos en vuestra isla dentro del labo. BioJorge, Sergio, Doriana, Tatjana, Soraya, Javi y Reinal he compartido la parte final de esta tesis con vosotros, sois la caña, muchas gracias por vuestra ayuda, por las risas y buen rollo. No me puedo olvidar de nuestro amigo portu, Rui o Felipe como se hacía llamar en ciencias, muchas gracias.

Esta tesis me ha llevado también hasta Potenza (Italia). Muchas gracias a Ida, Antonietta y Maria Antonietta por su ayuda y gran acogida en Potenza. En especial muchas gracias a Marina Lorusso que desde el día uno me ayudo y me hizo sentir como en casa en mi estancia en Italia. En Potenza conocí a una de las personas más geniales que conozco, Lucia Maio. Empezamos esto juntos y lo acabamos juntos en Valladolid. Muchísimas gracias por todo.

A mis amigos, por estar ahí y hacer de vía de escape del mundo tesis. Alberto muchas gracias por aguantarme, escucharme y apoyarme en este último año de locos

Por último, mil gracias a mis padres y hermano, por creer en mí, por su incondicional apoyo en todo lo que hago, incluso en esto de la tesis, creo que aún no he sido capaz de explicarles de que va esto que he estado haciendo los últimos tres años.

A todos, y seguro que me olvido alguien, muchísimas gracias.

INDEX

ABSTRACT

1.0. ABSTRACT/ RESUMEN.

Material scientists are mimicking Nature to obtain protein polymers with the properties of the natural macromolecules. Protein-based polymers offer a set of interesting physical, chemical and biological properties. Elastin-like recombinamers (ELRs) are a family of biomimetic materials inspired in natural elastin, which have recently focused the attention of many researchers due to their outstanding biocompatibility, low cytotoxicity and its ability to form a variety of structures, such as, nanofibres, films or hydrogels. The aim of this thesis is the development of new nanostructures and highly functional systems with complex molecular architecture based on Elastin-like Recombinamers.

Regarding the nanostructure formation, this work explores the effect of the presences of salts and surfactants on the self-assembling behavior of Elastin-like block co-recombinamers (ELbcRs). The study was carried out using scattering and microscopy techniques, coming to the conclusion that both types of molecules are a simple and effective way of controlling the size of the ELbcRs nanoparticles.

In regard to the development of new highly functional materials, this work explore two different ways, a covalent bond with graphene oxide and the inclusion in the ELR sequence of leucine zipper domains. Graphene has interesting properties for the biomedical field, but it is hardly soluble and cytotoxic. In this work, it is explore the feasibility of covalently attached ELRs to graphene oxide (GO), which gave rise to non-cytotoxic aqueous soluble ELR-GO composites which were used to assemble micro-patterned hydrogels, nanofibers, nanoparticles and physical hydrogels.

Finally, this thesis explore the possibility of obtaining brunched recombinamers through the inclusion of leucine zippers domains within the ELRs sequence. This work comprises all the steps involved in the bioproduction of ELRs, from gene construction to recombinamer expression and purification. The formation of complex recombinamer architectures thorough coiled-coil aggregation, such as di-blocks and brush structure, were experimentally demonstrated. These results proves the feasibility of obtaining non-linear ELR superstructures.

RESUMEN

La naturaleza es una fuente de inspiración importante para muchos científicos dedicados al diseño de materiales y más concretamente al de polímeros basados en proteínas. Simular las propiedades de macromoléculas naturales es un objetivo perseguido por muchos. En este sentido, los polímeros basados en proteínas presentan una interesante serie de propiedades tanto físicas como químicas y biológicas. Más concretamente los recombinameros tipo Elastina (ELR) son una familia de materiales biomiméticos basados en la eslatina natural, que están centrando el interés de muchos investigadores debido a su excelente biocompatibilidad, baja citotoxicidad y su capacidad para formar una variedad de estructuras, tales como, nanofibras, películas o hidrogeles. El objetivo de esta tesis es el desarrollo de nuevas nano-estructuras y sistemas altamente funcionales con arquitectura molecular compleja a base de recombinameros tipo elastina.

En lo que respecta a la formación de nano-estructuras, este trabajo explora el efecto de la presencia de sales y surfactantes sobre el comportamiento de auto-ensamblado de los ELbcRs. El estudio se llevó

a cabo utilizando técnicas de dispersión y de microscopía, llegándose a la conclusión de que ambos tipos de moléculas son una forma simple y eficaz de controlar el tamaño de las nanopartículas formadas por los ELbcRs.

En lo que se refiere al desarrollo de nuevos materiales altamente funcionales, este trabajo explora dos maneras diferentes, un enlace covalente con óxido de grafeno y la inclusión en la secuencia de los ELR dominios de cremalleras de leucina. El grafeno tiene propiedades interesantes para el campo de la biomedicina, pero es difícilmente solubilizable en medio acuoso y presenta cierta citotoxicidad. En este trabajo se estudia la viabilidad de unir ELRs covalentemente al óxido de grafeno (GO), dando lugar a compuestos ELR-GO no citotóxicos y solubles en medios acuosos. Estos compuestos ELR- GO se utilizaron para fabricar hidrogeles micro-estampados, nanofibras, nanopartículas e hidrogeles físicos.

Por último, esta tesis explora la posibilidad de obtener recombinameros ramificados a través de la inclusión en la secuencia de los ELRs dominios de cremalleras de leucina. Este trabajo comprende todos los pasos involucrados en el bioproducción de ELRs, desde la construcción de los genes hasta la expresión y purificación de los recombinameros. La formación de recombinameros con arquitecturas moleculares complejas a través de la formación de coiled-coil, como di- bloques y estructura en peine, fueron experimentalmente demostrados. Estos resultados muestran la viabilidad de la obtención de superestructuras ELR no lineales.

INTRODUCTION

2.0. INTRODUCTION.

2.1. PROTEIN BASED MATERIALS: ELASTIN-LIKE RECOMBINAMERS (ELRs).

Protein based-materials have drawn attention of numerous researchers in recent years as promising advanced biomaterials for use in the field of biomedicine, especially as a result of recent improvements in recombinant DNA technology, which allow us to design and manufacture materials by exploiting the abilities of natural proteins[1]. Some of the most widely studied protein-derived materials are the so-called elastin like recombinamers (ELRs)[2-4] , taking into account its recombinant nature this new nomenclature was proposed[5] in replacement of the more conventional terminology elastin- like polymers (ELPs), which include those first chemically synthesized materials.

2.1.1. Natural Elastin.

Elastin is an elastic, insoluble protein that is present in many tissues such as lung, skin, major vascular vessels, elastin ligaments or tendon[6], where elasticity and resilience are a key requirement[7].

Elastin possesses several extraordinary characteristics, such as an ability to undergo high deformation without breaking and subsequent recovery of the original conformation once the stress disappears[8, 9].The origin of this ability resides in the structure of the recurrent sequences (VPGVG, VPGG, VGVAPG) found in the soluble elastin precursor tropoelastin[10] . It is also worth noting that this elastic behavior is an energy-conserving process, thus allowing the resulting elastic fibers to undergo billions of relaxation-stretching cycles[11].

However, the most striking behavior of this protein, which is responsible for the particular elastic properties of elastin, has been found in a particular fragment of the natural occurring protein, the so-called α-elastin. According to D. Urry., when the α-elastin is in aqueous solution and as a result of a temperature increment, it suffers a transition from a disordered state to an order state where the molecules are capable of aggregating resulting in a sticky and dense separated phase[12].

The transition to an higher ordered state as a result of an increment of the temperature is out of trend of normal physic systems, where an increment of order is expected when temperature is decreased, owing to thermal agitation is not strong enough (at low temperatures), for breaking the molecular forces which leads a material to adopt a regular conformation.

2.1.2. Elastin-like recombinamers (ELRs)

ELRs are smart, genetically engineered biomaterials inspired by natural elastin and based on the very same recurring amino acid sequences as found in tropoelastin. Some of the most relevant characteristics of ELRs, which are derived from those of the natural protein, serve as an example of how elastin's mechanical properties are retained by way of cross-linked ELR matrices[13]. These mechanical properties become more interesting in conjunction with other properties such as biocompatibility, stimuli-responsive behavior and the ability to self-assemble[14, 15]. The most widely studied ELRs are based on the recurring pentapeptide sequence Val-Pro-Gly-Xaa-Gly, where Xaa is any natural amino acid except proline.

2.1.3. Inverse temperature transition (ITT)

All functional ELRs present a reversible phase transition in response to changes in temperature.[5] In aqueous solution below a certain temperature, i.e., the transition temperature (T_t) or lower critical solubility temperature (LCST), the polymer chains remain disordered, relatively extended with a random coil conformation, and fully hydrated.[6] This hydrophobic hydration is characterized by an ordered clathrate-like water structure surrounding the apolar moieties of the polymer (**Figure 1**). This structure is somewhat similar to that described for crystalline gas hydrates, although more heterogeneous and of varying perfection and stability.[7,8] When temperature surpasses the Tt and according to Urry's model, the polymer chains hydrophobically fold and undergo a conformational transition that leads to phase separation. That "coacervate" is composed of about of 63% water and 37% polymer.[9] In the folded state, the polymer chain adopts a dynamic, regular, non-random structure called β spiral, which involves one type II β turn per pentamer stabilized by intra-spiral inter-turn and inter-spiral hydrophobic contacts.[5] (**Figure 1**)

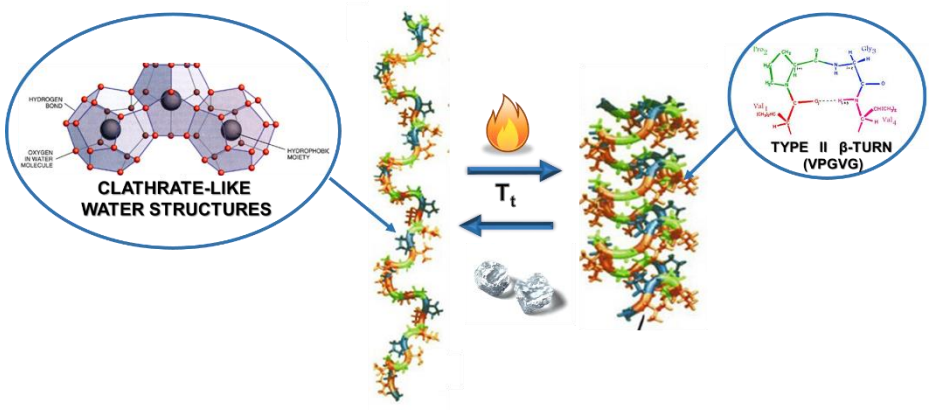

Figure 1: *Schematic representation of the thermal transition of ELRs from an extended state (low temperatures, hydrophobic moieties surrounded by clathrate water structures) to a folded state (type II β-turn in VPGVG pentapeptides)*

The process begins with the formation of filaments composed of three-stranded dynamic polypeptide β-spirals, which grow up to various hundred nanometers before settling into a visible separated state.[5,10] (**Figure 2**)

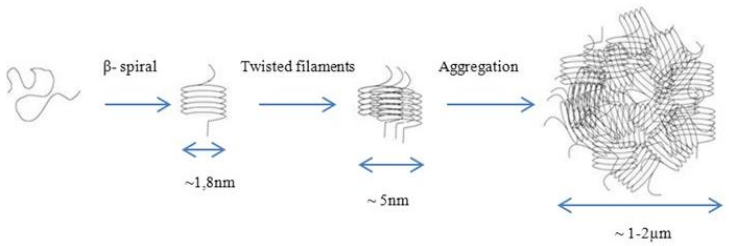

Figure 2: *Mechanism of the ELRs' ITT. From left to right: β-spiral formation, formation of twisted filaments or β-spiral supercoil and their aggregation into microaggregates. Reproduced from reference*[16]

This process is completely reversible (lowering the temperature below Tt, the initial state is recovered) and has an associated latent heat, ΔHt.[5] This ΔHt is the result of the combination of the disruption

of the water structure and the folding and stabilization owing to the Van der Waals interactions.[11] One VPGVG is enough to permit the transition from random coil to an order β turn, but higher molecular weight polymers are required to obtain materials presenting useful properties.[12]

Common proteins undergo unfolding and denaturalization when temperature raises. The shift described above from a disordered state to an ordered state upon heating is the base of the inverse temperature transition (ITT). At this point, it might seems that this behavior is not possible, because it seems to violate the second law of thermodynamics. However, this apparent mystery can be solved if the system as a whole is considered, i.e., not only the protein but also the water surrounding it. When the system moves to the ordered state, the increase in order of the protein component is less than the decrease in order of the water component. Thus, the second law of thermodynamics is indeed satisfied.

2.1.4. Factors influencing the T_t.

Several parameters are able to modify the T_t, which opens up its possible usage as a way to tune the T_t in accordance with the desire application. Parameters that might have an influence in the T_t can be classified as extrinsic or intrinsic factors.

2.1.4.1. Intrinsic factors influencing the T_t.

2.1.4.1.1. Concentration.

The effect of concentration on the T_t present two different behaviors. At low ELR concentration, the higher the concentration the lower the T_t. This decrease of temperature is a logarithm function of the concentration according to Chilkoti et al[17]. (**Figure 3**)

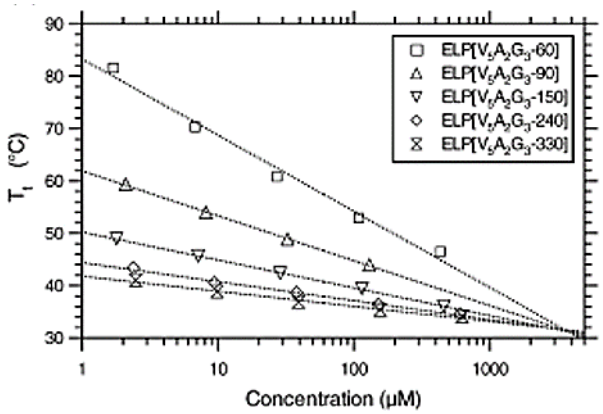

Figure 3: *Tt as a function of concentration for different ELR constuctions. Reproduced from*[17]

In a previous experiment, Urry et al[18, 19] also found a decrease in T_t as the ELP (chemical poly(VPGVG)) concentration increased. The decrease of the T_t reaches a plateau at a sufficiently high concentration (40 mg/ml for Urry's poly (VPGVG)[18]

On the other hand, Rodriguez Cabello et al[20] showed that above a certain concentration of poly(VPGVG) (125 mg/ml), the T_t trend is inverted and an increase of the T_t is observed (**Figure 4**).

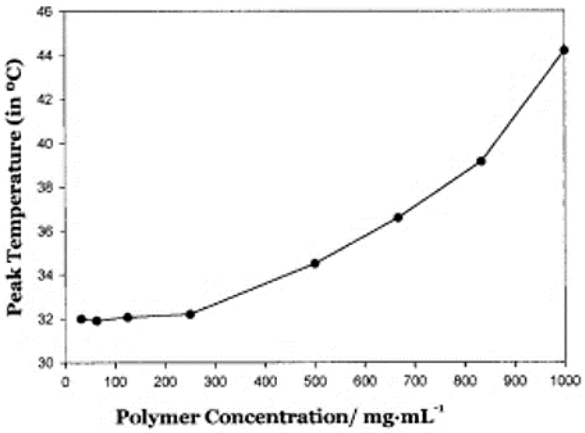

Figure 4: *T_t as a function of concentration for Poly (VPGVG). Reproduced from*[20]

This phenomena is explained due to competition for the hydration water and the heterogeneity of the hydrophobic hydration water structures taking place at such concentrated samples.

2.1.4.1.2. ELR sequence and chain length.

As mentioned above, most of the ELRs are based in the general formula (VPGXG); where X represents any natural or modified amino acid except proline. All polymers with this general formula are functional, i.e., all show smart behavior with sharp responsiveness. However, the achievement of functional ELRs by means of the substitution of any of the other amino acids in the pentamer is not so straightforward. For example, the proline cannot be substituted, the first position in the pentapeptide only accept, so far, valine, phenylalanine or isoleucine[21] and the first glycine cannot be replaced with any natural amino acid other than l-alanine. This is because the type II β-turn per pentamer involves this glycine together with the proline in the folded state of the polymer. The presence of bulky moieties in amino acids with L chirality impedes the formation of the β-turn, and the resulting polymer is not functional. Thus, the substitution by alanine is the only possibility reported that still leads to a functional polymer, though even in this case, the resulting polymer shows significantly different and out of trend mechanical and thermal properties[22].

It has been proven that the amino-acid sequence has a great influence on the T_t of ELRs[23]. Substitutions of the amino acid at the fourth position (X) of the pentamer modify the values of T_t, to an extent that depends on the polarity of the amino acid side chain. As a rule of thumb an increase in the polarity decreases the hydrophobic hydration, which causes an increase in T_t and a decrease in ΔH_t.

Taking into account the hydrophobicity scale of amino acids:

Trp > Tyr > Phe > Leu~ Ile~ Met > Val > Ala > Gly

and according to Urry's description of a pentapeptide poly[f_v(VPGVG), f_x (VPGXG)], where f_v and f_x accounts for the molar fraction of each monomer, and on the basis of a linear variation of T_t with f_x is possible to design an ELR with a particular T_t, as well as, the T_t of a pure X pentapetide by extrapolation, f_x =1, **Figure 5**.

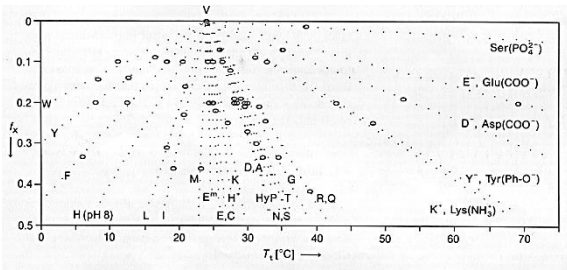

Amino acid X	T_t [°C]	Correlation coefficient
Lys(NMeN, red.) [a]	−130	1.000
Trp (W)	−90	0.993
Tyr (Y)	−55	0.999
Phe (F)	−30	0.999
His (pH 8) (H)	−10	1.000
Pro (P)	(−8)	[b]
Leu (L)	5	0.999
Ile (I)	10	0.999
Met (M)	20	0.996
Val (V)	24	[c]
Glu($COOCH_3$) (E^m)	25	1.000
Glu(COOH) (E)	30	1.000
Cys (C)	30	1.000
His (pH 4) (H^+)	30	1.000
Lys(NH_2) (K)	35	0.936
Asp(COOH) (D)	45	0.994
Ala (A)	45	0.997
HyP	50	0.998
Asn (N)	50	0.997
Ser (S)	50	0.997
Thr (T)	50	0.999
Gly (G)	55	0.999
Arg (R)	60	1.000
Gln (Q)	60	0.999
Lys(NH_3^+) (K^+)	120	0.999
Tyr(Ph-O^-) (Y^-)	120	0.996
Lys(NMeN, ox.) [a]	120	1.000
Asp(COO^-) (D^-)	170	0.999
Glu(COO^-) (E^-)	250	1.000
Ser(PO_4^{3-})	1000	1.000

[a] NMeN represents *N*-methylnicotinamide pendant on a lysyl side chain, i.e., *N*-methylnicotinate attached by amide linkage to the ε-NH_2 of lysine. The reduced state is *N*-methyl-1,6-dihydronicotinamide residue. [b] Calculated. [c] Serves as reference substance.

***Figure 5**: Plots of T_t fo poly-[f_v(VPGVG), f_x (VPGXG)], in PBS as a function of fx, at small fx. At such low X content the plots are essentially linear. The table represent the T_t for poly-[f_v(VPGVG), f_x (VPGXG)]. Reproduced from[18]*

It is worth noting, that those ELRs which contains in their X position an acid or a basic amino-acid (acid: Glu, Asp; basic: Lys, Arg, Asn or Gln) are also pH sensitive, and the ionization degree of those amino-acids will have an important effect on the T_t. In this sense, when an acid amino-acid is above its characteristic pKa, its carboxylic group is deprotonated, thus negatively charged, resulting in an increasing of the mean polarity, which leads to an increase in the T_t.

On the contrary, when a basic amino-acid is below its pKa its amino groups is protonated, thus positively charged, leading to a raise of the T_t.

Regarding the chain length, it also has an effect on the Tt. According to Meyer et. al[17]. the Tt is relatively invariant at sufficiently high chain lengths, but it is highly incremented as the chain length is reduced.

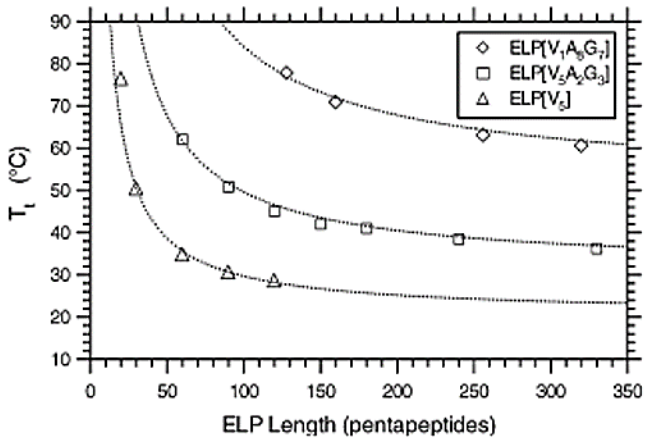

Figure 6: *T_t as a function of ELR chain length for three different ELR at 25 μM in PBS. Reproduced from[17].*

None of the three intrinsic factors, namely, concentration, sequence and chain length is to be considered independently in order to determine the T_t, because a conjunction of the three will determine the final T_t.

2.1.4.2. Extrinsic factors influencing the T_t.

2.1.4.2.1. Effect of salt.

According to the Hofmeister series[24, 25], anions to the left of Cl- (kosmotropes) have a strong tendency to salt out polymers/ proteins in the same way as cations to the right of Na+, in other words causing a decrease in polymer/protein solubility in aqueous solution. “Salting in” ions (chaotropes) provoke opposite effects.

$$CO_3^{2-} > SO_4^{2-} > S_3O_3^{2-} > H_2PO_4^- > F^- > Cl^- > Br^- > NO_3^- > I^- > SCN^-$$

$$NH_4^+ > Cs^+ > Rb^+ > K^+ > Na^+ > Li^+ > Ca^{2+} > Mg^{2+}$$

The effect of different anions into the T_t of ELRs has been studied by Cho et.al[26], showing the different behavior of kosmotropes and chaotropes (**Figure 7**)

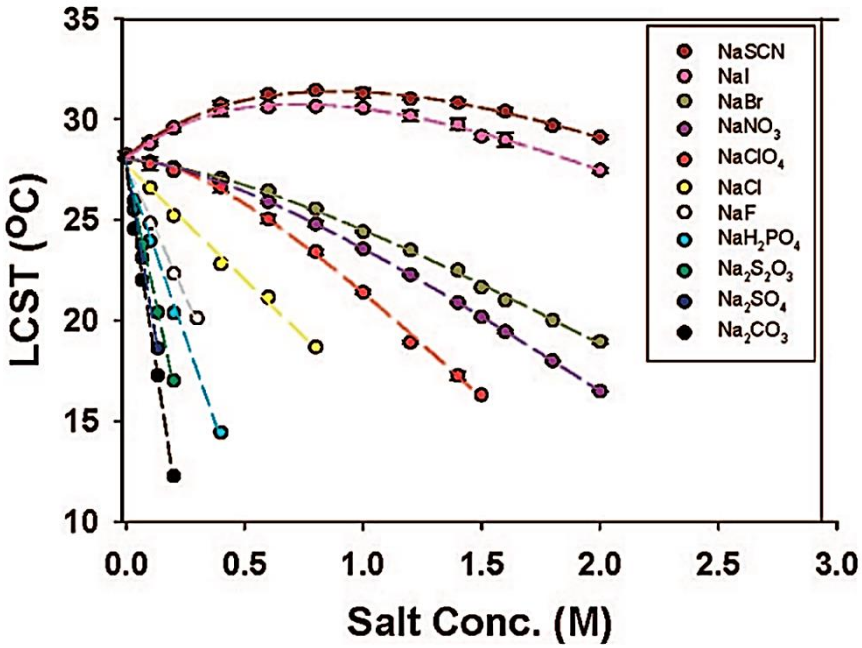

***Figure** 7: Effect of a series of sodium sal into the T_t of an ELR. Reproduced from [26]*

According to these authors, kosmotropic anions polarize the water molecules which are involved in hydrogen bonding to the amide group of the ELR employed, through direct interaction between the anions and the water molecules, resulting in a weakening of the hydrogen bonding of water to the ELR, causing a salting out effect. On the contrary, chaotropic anions interact directly to the amide moieties of the ELR studied by ion binding, causing a salting-in effect[26].

In a previous study Reguera et al[27]. studied the effect NaCl on the ITT of a model ELR. They determined that NaCl cause a significant concentration-dependent decrease in Tt and an increase in the transition

enthalpy[27]. The effect of an increase in NaCl concentration on the thermal behavior of the ELR is equivalent to an increase in the hydrophobicity of the recombinamer chain. In summary, the effect of NaCl can be interpreted in terms of causing a better organization of the recombinamer in the folded state and a more extensive and better structured corona of hydrophobic hydration surrounding the apolar moieties in the extended state of the recombinamer chain[27].

2.1.4.2.2. Other extrinsic factors.

Other extrinsic factors affecting the T_t could be the addition of organic molecules, such as surfactants, or pressure. Surfactants effects on the T_t strongly depends on the charge and concentration of the surfactant[28], as well as the ELR sequence (charge amino-acids)

In a pioneer study (chemical synthesized ELP) Urry et al. showed that an increment of pressure provokes, as a result, an increment of T_t for those ELP containing aromatic amino-acids such as Phe, Tyr or Trp[29]. In a posterior study, Tamura et al. showed for a recombinant polymer a duel behavior with pressure, an initial increment of T_t followed by a decrease of T_t once above a determined pressure[30] (**Figure 8**).

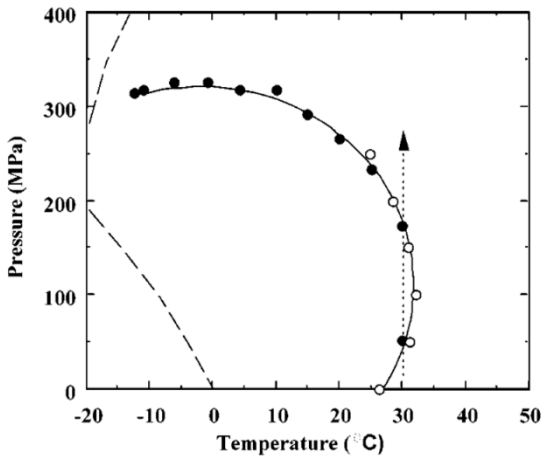

Figure 8: *T-P diagrams for the cloud-point of the0.05 w/v %(VPGIG)$_{40}$ solutions. Reproduced from* [30]

2.1.5. ΔT_t mechanism.

Previously, it has been shown the capacity of mechanical work creation as a result of the temperature increment above a certain transition temperature T_t. It consist on a transition from a state where the molecules are extended in solution, to a phase separated state where the molecules are ordered and aggregated, consequently a mechanical work is being done. Thus, the process is a thermo-mechanical transduction.

Different methods for modification of T_t have been described, most of them based on the modification of the polarity of certain functional groups, which can exist in two different states depending on a certain external stimulus. This change in the T_t, as result of different hydrophobicity, open up a working temperature window in which the polymer isothermally and reversibly switches between the folded and unfolded states in response to environmental changes (**Figure 9**).

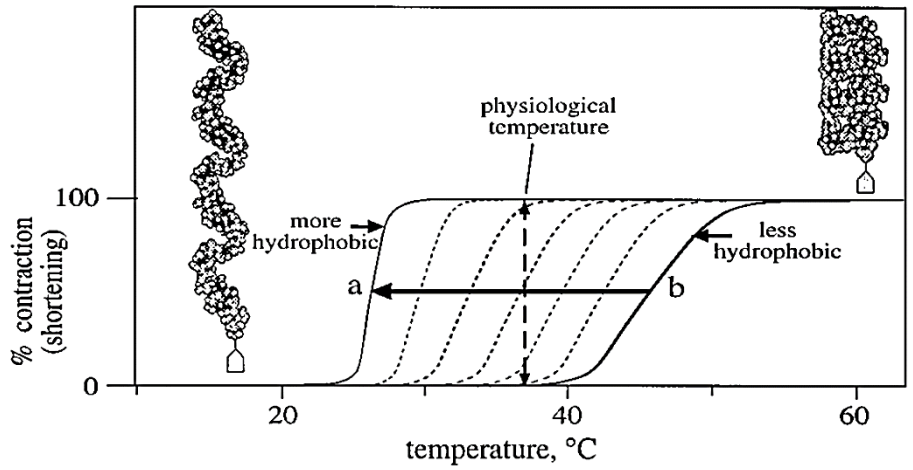

***Figure 9**: Plot as a function of temperature of the contraction of ELRs of different hydrophobicities. Reproduced from[31]*

This effect of changing the T_t is the basis of the ΔT_t mechanism and has been exploited to obtain pH, electric potential, light, chemical and other responsive interconvertible energy processes[31].

Experimental studies based on factors that control hydrophobic folding and assembly of ELRS resulted in a set of five phenomenological axioms for the engineering of protein based materials capable of inverse temperature transitions[31]

Axiom 1: The temperature intervals for the hydrophobic folding and assembly transition of a host protein or protein-based polymer with different guest substituents becomes a functional measure of their relative hydrophobicity.

Axiom 2: Heating to raise the temperature from below, to above, the temperature interval for hydrophobic folding and assembly of macromolecules can drive contraction with the performance of mechanical work.

Axiom 3: At constant temperature, an energy input that changes the temperature interval for thermally-driven folding and assembly in a macromolecule can itself, drive hydrophobic folding and self-assembly.

Axiom 4: Two or more different functional groups of a macromolecule, each of which can be acted upon by a different energy input that changes the temperature interval for hydrophobic folding and assembly, become coupled one to another by being part of the same hydrophobic folding and self-assembling domain, that is, the energy input acting on one functional constituent alters the property of another functional constituent as an energy output.

Axiom 5: More hydrophobic domains make more efficient the energy conversions involving constituents undergoing conversion between more and less hydrophobic states.

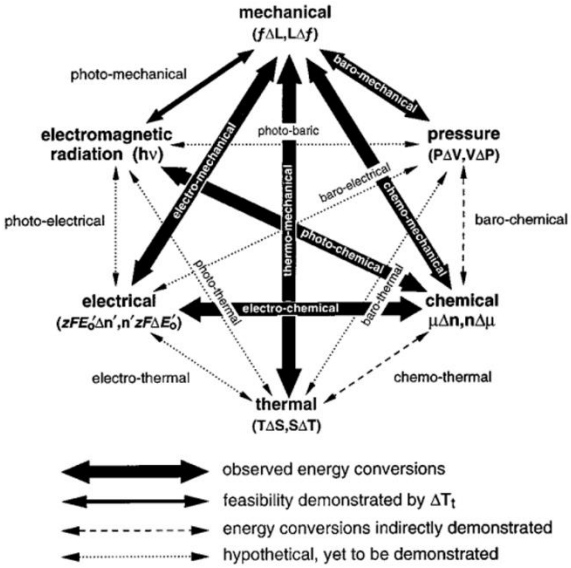

***Figure 10**: Representation of the pairwise interconversions of six different energies, which appear to be possible by means of inverse temperature transitions of specially designed protein based polymers.*[31]

2.1.6. Biosynthesis of ELRs.

Biosynthesis of ELRs is a step by step process, which starts with the design and construction of the gene which codified for the desired protein and its posterior cloning into a specific cloning vector (high control over transcription)(**Figure 13 A**). Several approaches can be used for the synthesis of the oligonucleotide monomer gene: annealing of two chemical synthesized complementary oligonucleotides[32, 33]; extension of two synthetic primers complementary on the 3' end, this approach is used for the obtention of bigger monomeric genes[34]; and last by Polymerase Chain Reaction (PCR)[35] .The obtaining of monomeric genes with the correct sequence and in sufficient length for the production of polypetides codifying genes requires some modifications of the strategy employed[32].

Once the monomeric gene has been cloned into the cloning vector, it has to be oligomerized. The oligomerization is carried out in a "head to tail" orientation, using one of the existing methods (concatenation and iterative and recursive method)[36, 37].

The first strategy to obtain the polymeric genes is the concatemerization method, a random, directional concatenation of the monomeric gene. This method allows multimeric genes with a defined distribution and discrete lengths to be obtained in a single cloning cycle. But, its creates uncontrolled oligomerization, resulting in a population of clones of different lengths.(**Figure 13**) During this work a complete control over the gene sequence was required and this method was not considered.

The iterative-recursive method consists of the sequential introduction of DNA segments, resulting in a one unit length growth of the monomer gene at each step. In order to this method been a success

is necessary a DNA segment with restriction sites for non-palindromic endonucleases at the gene ends[38]. This method allows total control over the length of the polymeric gene, but if the endonucleases employed are not type IIs restriction endonucleases, then superfluous base pairs will be introduce into the DNA sequence leading, once translated, to undesired amino-acids.

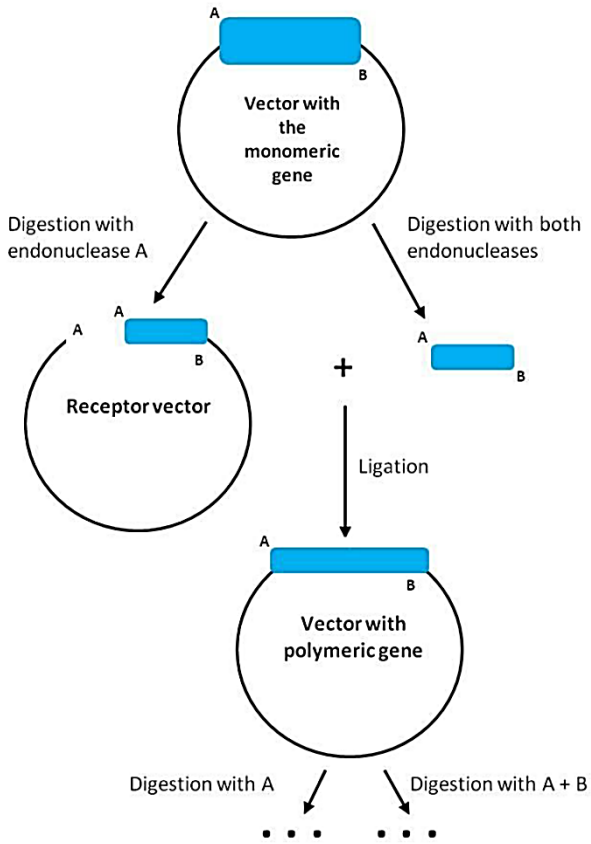

Figure 11: *Schematics of the recursive-iterative method. Reproduced from*[39]

The usage of type IIs restriction endonucleases is called Seamless cloning, which can be used in both concatenation and iterative-recursive methods[40]. An example of type IIs endonucleases are Ear I, which recognizes a specific non-palindromic sequences of six

nucleotides, and Sap I, which recognized a seven nucleotides sequence (**Figure 12**).

Figure 12: *Cleavage sequences of the restriction endonucleases Ear I and Sap I*

Both recognition sequences are identical with the exception of the extra nucleotide of the *Sap* I sequence. This analogy implies *Ear* I been able of recognize and cleavage also at *Sap* I places but not the other way around. Furthermore, the asymmetric three nucleotides ends generated by *Sap* I have the same size and orientation of those generated by *Ear*I.

Last but not least, *Ear* I and *Sap* I are type IIs restriction endonucleases, which implies the existence of a constant displacement between the recognized sequence and the exact cleavage place, which can be occupied by any type of nucleotide (N) (**Figure 12**)[40] This displacement is the origin of the *Seamless* terminology as none extra base pairs are introduced into the gene been oligomerize. This characteristic makes this type of endonucleases a perfect restriction enzymes for such oligomerization, both by concatenation and iterative-recursive method [41](**Figure 13**).

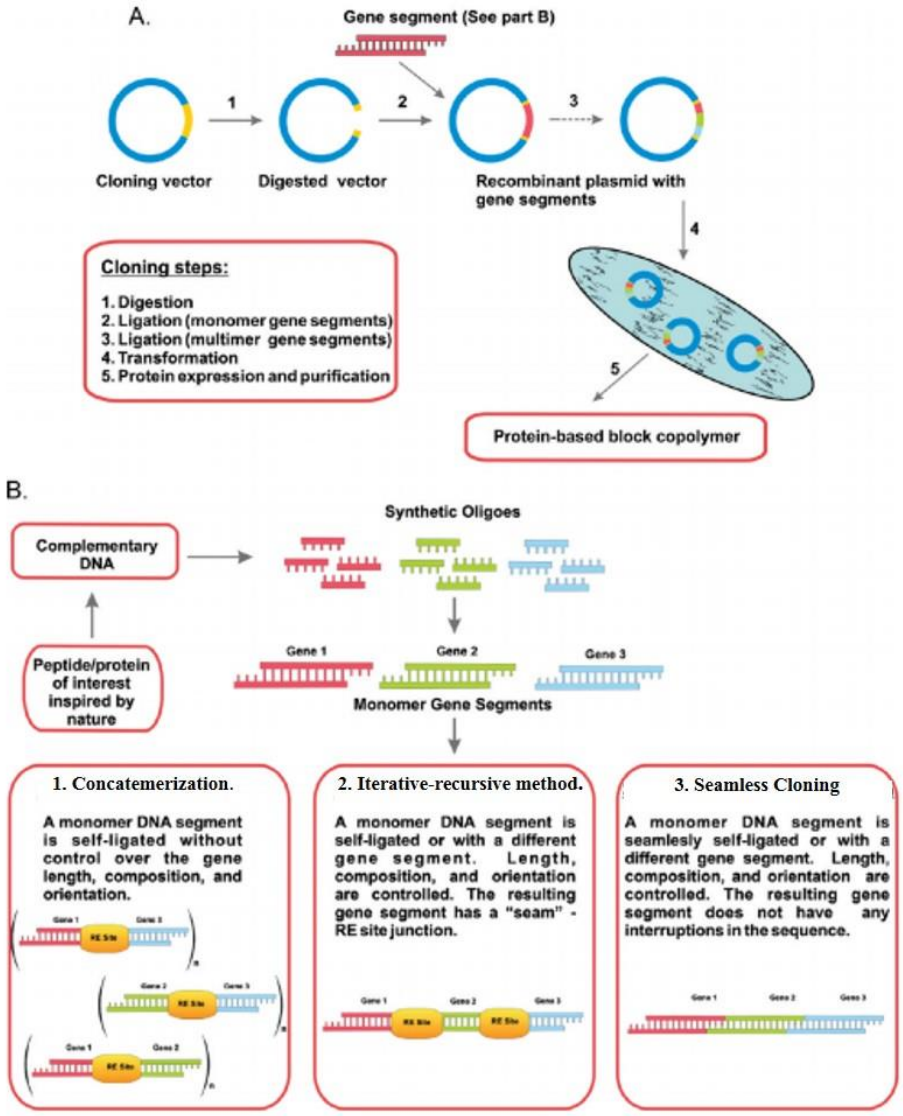

Figure 13: *A) Genetic engineering of polypeptides. B) Gene multimerization approaches. Adapted from*[42]

Once the final gene construction is achieved, it is cloned into an expression vector and a bacterial strain suitable for expression is transformed with it. The biosynthesis of an ELR end with the bioproduction of the recombinant protein followed by its purification (**Figure 13A**)

2.1.7. ELRs for biomedical applications.

Protein-based polymers have many advantages over conventional synthetic polymers because they are able to assemble hierarchically into stable, ordered conformations[43, 44]. This ability depends on the structures of protein chains as well as the microenvironment. Protein-based block copolymers have the ability to form varied nanostructures in aqueous solution that provides potential benefits for biomedical applications, such as therapeutic delivery, tissue engineering, and medical imaging[45]

ELRs are obtained by recombinant DNA technologies, which allow an extremely precise control over the amino acid composition. This technology opens up the possibility of designing ELRs with the specific properties required for a certain application. The degree of control and complexity attained by genetic engineering is clearly superior to that achieved by conventional chemical synthesis. ELRs are strictly monodisperse and can be obtained with molecular weights ranging from a few hundred Daltons to more than 200 kDa . Recent advances in recombinant DNA techniques have provided the tools needed to produce block copolymers (block corecombinamers) with the desired sequence, depending on the application, from simple amino acids with an absolute degree of control and complexity superior to those of synthetic polymers[42]

This design versatility, together with their high biocompatibility, bioactivity and self-assembling behavior, makes ELRs unmatchable materials for studies in the biomedical field. As a result, ELRs have been used in wide variety of applications, such as tissue engineering[46] or drug delivery[47]. Similarly, they have also been applied in the field of nanotechnology due to the range of

nanostructures, such as nanofibers[48] or nanoparticles[49], that can be formed from them (**Figure 14**).

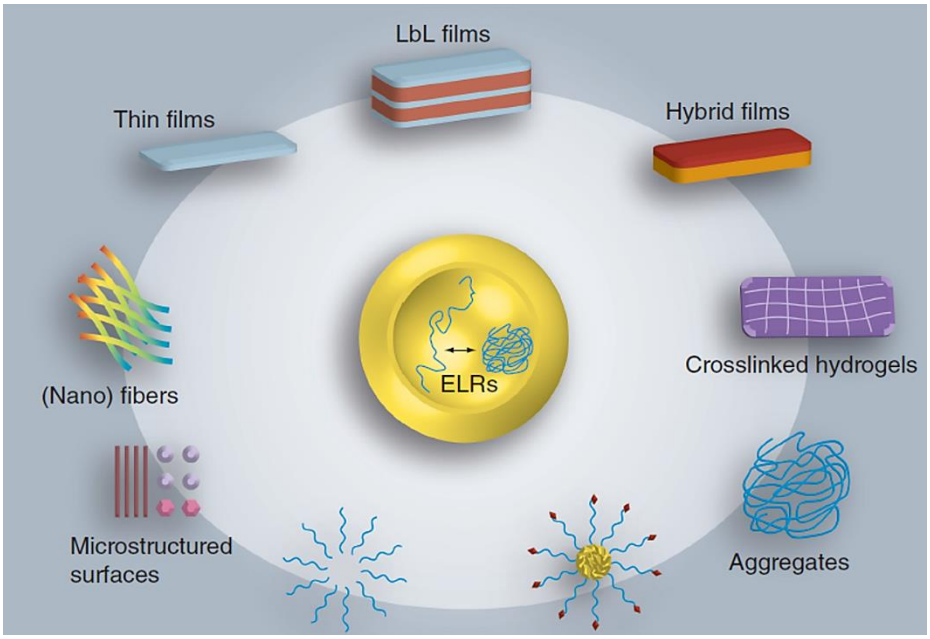

***Figure 14**: Summary of the different structures that ELR-based systems can adopt for its usage in biomedical applications. Reproduced from[50]*

The success of many of these biomedical applications hinges on the ability to control and manipulate the interface between them and the biological components, thus with their biocompatibility, which is clearly superior to that found in chemically produced polymers.

2.2. Block Copolymers.

Block copolymers have been the subject of numerous studies due to their ability to undergo self-assembled phase separation resulting in different complex morphologies. Self-assembly procedures have drawn attention over a number of years, with the self-assembly of nanoparticles being a particularly active field. Self-assembled polymer nanoparticles tend to be obtained from amphiphilic macromolecules. Generally speaking, a solution of these amphiphilic molecules in a

solvent that only specifically solvates one part of the molecule will result in aggregation due to interaction of the solvent with the solvophobic blocks of the molecule. The hydrophobic parts tend to form aggregates as this collapse is more entropically favorable than the ordination of water molecules around each hydrophobic segment. On the other hand, hydrophilic parts are dissolve in water as the formation of hydrogen bonds with water molecules is higher enthalpic compensated than the interaction between hydrophilic parts.

2.2.1. Physical properties of Block Copolymers.

Block copolymers are polymers composed of two or more covalently linked chemically distinct sequences (blocks).Thus, block copolymers can be designed as a hydrophobic block and a hydrophilic block, which can self-assemble into many different structures[51].

The degree of order and morphology of those aggregates are dependent on concentration and volume ratio between the hydrophobic blocks and the hydrophilic blocks, known as insoluble soluble ratio (ISR). Below a certain concentration, critical aggregation concentration (CAC), the hydrophobic blocks are capable of maintaining the molecules dissolved. On the contrary, once above the CAC block copolymers begins to self- assembly resulting from the separation from the solvent of the hydrophobic block. The CAC decreases as the ISR and the molecular mass increases[52].

The dimensionless packing parameter (p) is the ratio between the molecular volumes of the solvent-phobic chain and the volume occupied by the copolymer in the assembly, defined as[51]:

$$p = \frac{v}{a_0 d}$$

Where a_0 is the optimal surface area of the solvent-phobic segment at the interface of between both blocks resulting from the balance between solvophilic solvophobic interactions, *v* is the volume and *d* is the length of the solvophobic block. Generally speaking, if $p \leq 1/3$ the self-assembled structure result in spherical micelles, while $1/3 < p \leq ½$ correspond to cylindrical micelles and a p values between ½ and 1 are related to polymer membranes (**Figure 15**).

Theoretically speaking, the most stable assembly would be an infinity large membrane and an infinity long cylinder. Nevertheless, it goes without saying that the system is force to finite dimensions, thus a certain level of curvature (molecular frustration) is required in order to avoid the contact between the solvent and the insoluble parts[53].

Wormlike structures will come as a result of the stabilization by end-caps of cylindrical micelles if the molecular frustration is restricted to a specific part of the assembly. In the same way, under these local confinement of the molecular frustration, stabilization of membranes will consist on the curvature of the edges giving rise to disk-like micelles[54].

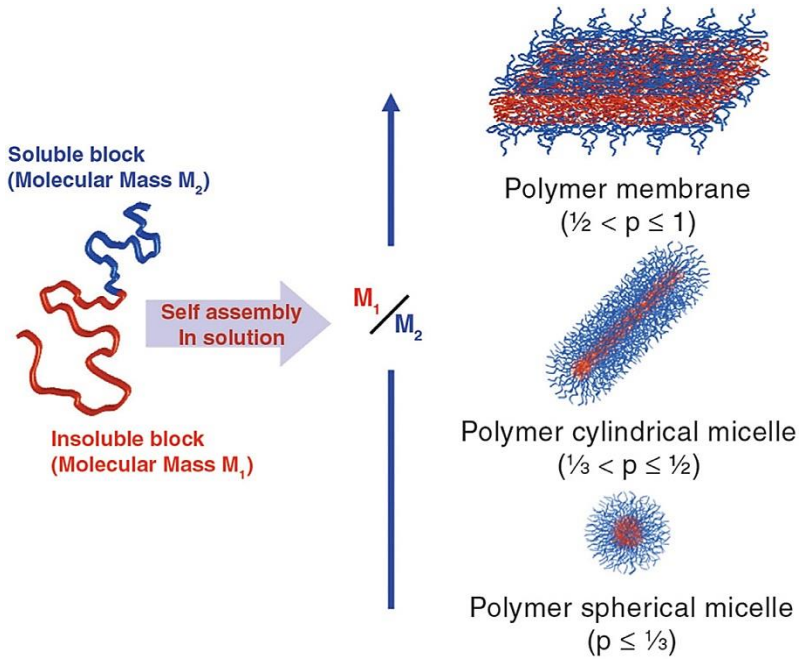

Figure 15: *Different geometries formed by block copolymers in selective solvent conditions. Reproduced from*[55]

On the other hand, if all the molecules share the molecular frustration then stabilization of cylinders and membranes will result in the formation of toroidal micelles (as cylinders bend) and vesicles (membranes closure)

Energetically speaking, the formation of vesicles and worm-like micelles is more favorable than disk-like and toroidal micelles. But, it has been demonstrated that those less likely structures can be stabilized by the increase of the molecular mass of the copolymer[56, 57], which will make the local frustration unfavorable, or by introducing extra interaction between block copolymers[58].

2.2.1.1. Multi-block copolymers:

The different structures obtained (micelles, vesicles..-) came as a result of the equilibrium interaction between both blocks (hydrophobic, hydrophilic) and the solvent. This rule is also applicable when the blocks are arranged as tri-blocks or multi-blocks. The overall ISR will determined whether spheres, cylinder or membranes are self-assembled by the block copolymers.

Despite the fact that the overall geometry of the assemblies formed by multi-blocks is the same, multi-blocks possess an extra level of control within the nanoparticles, which comes from the higher number of blocks and consequently an extra interaction between the blocks. Serve as an example ABC copolymers, if A and B are soluble and C insoluble it will lead to the formation of spherical core-shell micelles[59] (**Figure 16 b**). But, depending on the A/B ratio and the condition of the solvent, ABC copolymers have been shown in a cylindrical micelle shape[60].

On the other hand, if A and C are soluble while B is insoluble, ABC copolymers assembly will give rise to asymmetric "Janus" particles (half of the surface occupied by one block and the other by the other block), whose shape (spherical[61], cylindrical[62] or vesicular[63] **Figure 16 a**, **d** and **g** respectively) is dependent on the ISR. When B and C are insoluble and A soluble then the internal structure will depend on the B/C ratio, leading to the formation of spheres, cylinders[64] (**Figure 16 e**) or disk-like micelles[65], when B and C are equal in volume. If the volume of B and C is not the same, it has been demonstrated that the assemblies will present internal structures, which geometry is related to the B to C ratio. In this sense, raspberry-like micelles[66] (**Figure 16 c),** segmented cylindrical micelles[58] (**Figure 16**

f) or even vesicles containing hexagonally packed cylinders [67](**Figure 16 i**) have been reported.

Additionally, an ABCA tetra-block copolymer (A soluble, B and C insoluble) has been proven to self-assemble into vesicles with internal morphologies at the membrane, which varies from lamellar to cylindrical depending on the volume fraction between B and C[68] (**Figure 16 h**).

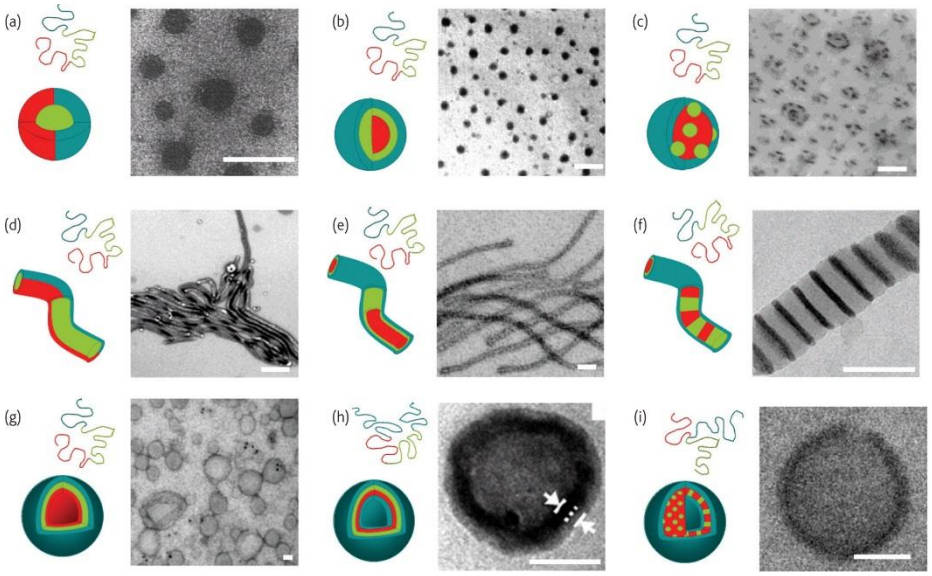

Figure 16: *Assemblies formed in selective solvents conditions by multi-block copolymers: a) Janus spheres, b) core-shell spheres, c) raspberry-like sphere, d) Janus cylinders, e) core-shell cylinders, f) segmented cylinders, g) asymmetric Janus membrane vesicles, h) double-layer membrane vesicles, and i) vesicles with hexagonally packed cylinders. Scale bar 50 nm. Reproduced from*[55]

2.2.1.2. Effect of concentration.

Should come as no surprise that the interaction between block-copolymers and solvent will be influence by concentration. As concentration is increased the above mentioned interaction becomes

more intense, resulting in an extra interaction between the isotropic phases. The formation of long range order mesophases come as a result of the minimization of free energy process. The local packing is also affected by the increase of concentration, resulting in a decrease of the local curvature. That is to say, generally speaking, those molecules which at low concentrations self-assembled into spherical micelles will turn into cubic phases packed micelles, followed by cylindrical hexagonally packed aggregates and finally membrane-like aggregates as the concentration increases[69, 70]

On the other hand, broadly speaking, those molecules assembling as cylinders at low concentrations did not pass thorough the stage of cubic phase packed micelles and form directly hexagonal phases at high concentrations[69, 70]. Vesicles assemble as lamellae at sufficiently high concentrations, going thorough vesicles hexagonally packed and bicontinuos phases at intermediate concentrations[71, 72] (**Figure 17**).

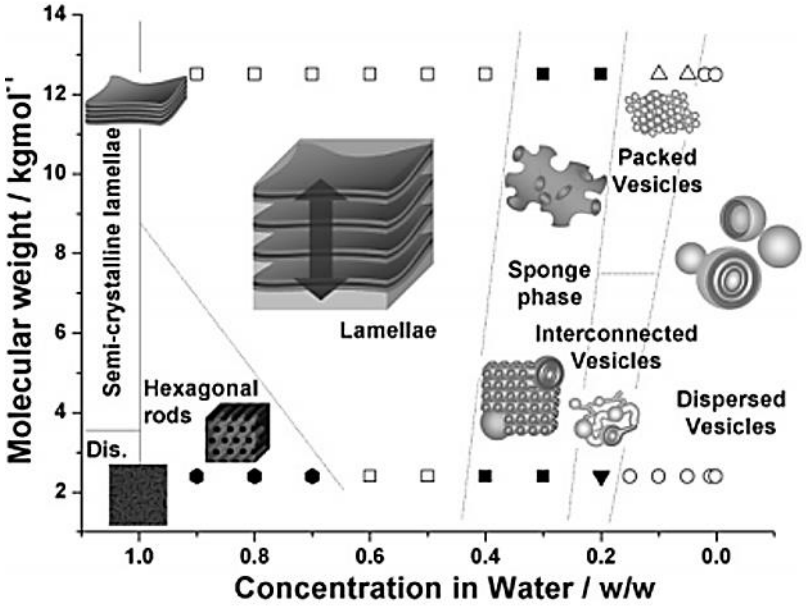

Figure 17 : *Phase diagram of PBO-b-PEO as a function of concentration and molecular weight. Reproduced from*[72]

Regarding those copolymer assembling as membranes at dilute conditions, they have been found to assemble as cubic[70] or hexagonal[72] inverse structures. These trend in morphologies are to be taken as a general and broad sequence of structures which are strongly affected by the copolymer molecular weight[57, 73].

2.2.1.3. Effect of salt.

The ratio between the hydrophilic and hydrophobic component blocks and the thermodynamics of the interactions between the two blocks and with solvent molecules are key aspects when it comes to determining the size and shape of the resulting aggregates[74]. This is of particular interest when one of the blocks contains a stimuli-sensitive compound as this block can show extraordinary changes in its polarity as a consequence of a change in the stimulus and, therefore, the self-assembly process is then governed by changes in this external stimulus.

One of the external stimuli known to govern self-assembly processes is a change in ionic strength. According to the literature data, it is clear that the presence of a salt presents two different effects, depending on the nature of the salt, in block copolymers such as Pluronic®. According to the Hofmeister series[75, 76], anions to the left of Cl^- have a strong tendency to salt out polymers/ proteins in the same way as cations to the right of Na^+, in other words causing a decrease in polymer/protein solubility in aqueous solution. "Salting in" ions provoke opposite effects.

$$CO_3^{2-} > SO_4^{2-} > S_3O_3^{2-} > H_2PO_4^- > F^- > Cl^- > Br^- > NO_3^- > I^- > SCN^-$$

$$NH_4^+ > Cs^+ > Rb^+ > K^+ > Na^+ > Li^+ > Ca^{2+} > Mg^{2+}$$

As a result, salt (NaCl, Na_2SO_4,Na_3PO_4) is responsible for lowering the temperatures at which micelles are formed[77] or change to rod-like micelles(KF, KCl, KSCN)[78] of chemical block copolymers. It also provokes the micellization of very hydrophilic linear block-copolymers[79] and has a strong influence on the structure of branched copolymers[80]. However, these effects are not exclusive for block copolymers, with the critical micelle concentration of ionic surfactants also being reduced by addition of salt ions due to charge screening of the hydrophilic heads[81]. The thermal stability of proteins is also affected by the presence of ions, also following the Hofmeister series[82, 83], and DNA strands are known to undergo conformational changes in the presence of multivalent cations[84, 85]. Self-assembling peptides are also known to undergo morphological changes under different saline conditions[86]. Thus, López de la Paz et al.[87] designed an amyloid fibril-forming heptapeptide that undergoes increased fibril formation at low NaCl concentrations, whereas only short filaments and amorphous aggregates are found at NaCl concentrations higher than 0.1M.

2.2.2. Copolymer-surfactant complexes.

Surfactants (Surface Active Agents) are amphiphilic molecules, which at low concentration are capable of adsorbing onto the surfaces or interfaces of the system and altering, usually reducing, the free energy of those surfaces or interfaces. An interface is understood to be a boundary between any two immiscible phases, whereas a surface denotes an interface where one phase is gas, normally air.

Surfactants can be divided into four groups depending on the nature of the hydrophilic group, which is an ionic or highly polar group:

- *Anionic*: The surfactant head group bears negative charge: i.e. Sodium dodecyl sulfate (SDS)
- *Cationic*: The surfactant head group bears positive charge: i.e: Cetrimonium bromide (CTAB
- *Zwitterionic*: Both positive and negative charges are present at the hydrophilic group. i.e.: Cocamidopropyl betain.
- *Nonionic*: The head group carries no apparent ionic charge. i.e.: Cetyl alcohol.

The hydrophobic group is normally a long hydrocarbon chain, which the longer it is the lower the solubility in water and the higher the solubility in organic solvents[88]. The increase in the length of the hydrophobic group also provokes a closer packing of the surfactant molecules at the interface together with an increase of the melting point of the surfactant and the sensitivity of the surfactant[88]. Last but not least, an increase in the length of the hydrophobic tail, result in an increase tendency of surfactants to adsorb at the interface or to form micelles[88]. Micelles are formed once the surfactant concentration is above a certain limit called critical micelle concentration (cmc). The

micelle formation is an entropically driven process, due to the entropy penalty of water (solvent) molecules isolating the hydrophobic part by hydrogen bonding is higher than the entropy penalty of surfactant molecules aggregating together, which result in the formation of micelles[88].

2.2.2.1. Copolymer-Surfactant interaction.

The interaction of amphiphilic copolymers with low molecular weight surfactants has attracted considerable attention in recent years because of the possibility of designing nano-objects with novel functionalities[89, 90] due to the fact that the addition of surfactants may induce aggregation of the copolymer or change the aggregation state of the pure polymeric micelles[91]. Copolymers and surfactants frequently carry opposite charges, thus meaning that the interaction between them is similar to the formation of polyelectrolyte complexes[92]. Surfactant-copolymer interactions are primarily governed by both electrostatic (between the surfactant head groups and the polyelectrolyte side groups) and hydrophobic interactions (between the hydrophobic backbone of the polyelectrolyte and the alkyl chains of the surfactant)[93-95]. The binding of ionic surfactants to oppositely charged polyelectrolytes occurs via two mechanisms: initially by ion-exchange and then, at higher surfactant concentrations, by cooperative binding[96]. The polyelectrolyte nature of these complexes and the fact that multi-component materials can enable better control of the aggregation properties compared to single surfactant complexes[97] make them promising candidates for a wide range of possible applications[98], for example a) in the controlled release of drugs, taking advantage of the specific binding properties of a copolymer with a very small amount of surfactant in the coating[99], b) in mimicking the cytoplasmic

organization of cellular microcompartments, or c) in the purification of proteins and the extraction of other biomolecules[100].

2.2.3. Protein-based block copolymers.

Protein-based block copolymers consist of a type block copolymer in which some or all of the building blocks are composed by protein inspired materials, peptide sequences. Throughout the careful and specific selection and positioning of amino acid residues it is possible the production of polymers with an absolute control over the hydrophobicity patterns or secondary structures, which give rise to a wide selection of tailor-made biomaterials[101, 102].

As it has been previously described, see 2.2.1, the microstructure formation of synthetic block copolymer is highly influence by the ISR, but the phase separation parameters are not the only factors influencing the structure formation when it comes to protein-based block copolymers. When dealing with protein inspired materials, intra and inter-molecular bonding, together with chain conformation, are to be taken also into account in the process of structures formation. Thus, a different phase behavior from that of synthetic block copolymers should be expected, mainly due to normally occurring interactions in protein, such as electrostatic interactions, peptide backbone rotational restrictions, high hydrogen bonding or hydrophobic interactions, are usually absent from the synthetic block copolymer systems. The supramolecular organization in proteins is mostly directed by two structural elements, α-helix and β-sheet. All in all, the conditions under which structures (microphase separation) self-assemble and subsequence phase diagram relationships is yet to be determine for most of protein-based copolymers.

Protein-based block copolymer can be divided into two main groups, 1) synthetic polymer-peptide block copolymer (hybrids) 2) protein/peptide block copolymers.

2.2.3.1. Block Copolymers Containing Coiled-Coil forming sequences: i.e. Leucine Zippers.

The α-helical coiled coil offers an attractive simplification of complex oligomeric protein interactions and constitutes one of the most important motifs underlying many of the functionalities found in natural proteins. In nature, the coiled-coil motif is found to be present in the 10 % of the eukaryotic proteins, such as keratins or chaperon proteins.

A coiled-coil consist of two or more right-handed helices bundling into a slightly left-handed superhelix[103](**Figure 18**).

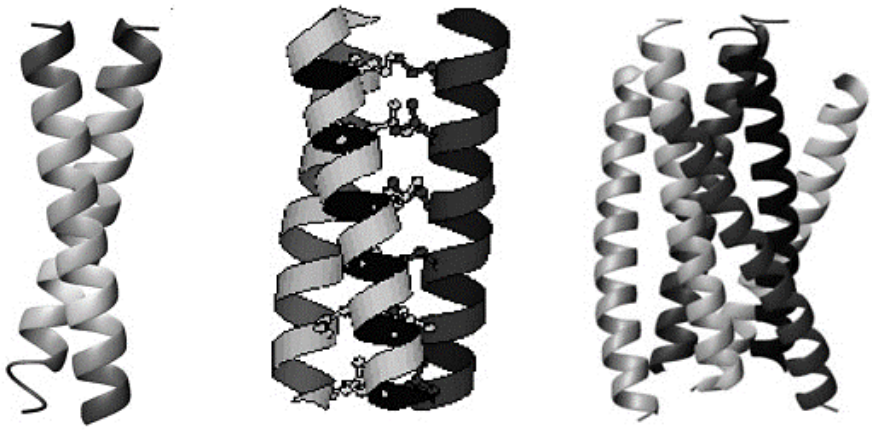

***Figure 18**: Schematic representation of a coiled coil dimer, trimer and hexamer. Reproduced from [104].*

The primary structure of coiled coil peptides is based on the repetition of seven amino acid residues (heptad repeats) denoted (**a-b-c-d-e-f-g**)$_n$, where n is the number of heptad repeats. Amino acids in the

a, and **d** positions are typically hydrophobic and interact with the complementary **a'** and **d'** amino acid positions in the opposite monomer creating a hydrophobic core essential for the dimer stability. The **e** and **g** positions typically contain charged amino acid which interact electrostatically with **e'** and **g'** regulating both homodimerization and heterodimerization determining the specificity of coiled coil recognition. Furthermore, Van der Waals between **g** and **e'** methylene groups and the underlying **a** and **d** amino acids contribute to stability[105, 106]. Residues at positions **b**, **c** and **f** are normally involved in hydrogen bonding due its exposure to the solvent.

In addition to coiled coil forming peptides, the coiled coil structure can also be achieved by Leucine Zippers, which are found in natural peptides. Leucine zippers consist of the repetition of Leucine at the seventh position over eight helical turns. The bonding between polypeptides containing Leucine zipper domains come as a result of the interaction between the side chains of the leucines at each α-helix, which give rise to coiled coil structures[107].

2.2.3.1.1. Characteristics of coiled coils.

The basic principles to be considered for the design, comparision and description of coiled coils are their stability, association number (number of helices in the superhelix), oligomerization selectivity (formation of homo-hetero dimers) and the orientation of the helices in the superhelix.

2.2.3.1.1.1. Stability.

Four major parameters are responsible for coiled coil stability, hydrophobicity of the core residues position a and d[108] , number of heptad repeats[109], electrostatic interactions between the residues in position e and g[110], and the helical predisposition of the remaining

amino acids[111]. It goes without saying that an increase in the number of heptad repeats will increase the possibilities of hydrophobic interactions in the core and more ionic interaction between **e** and **g** residues, which normally give rise to more stable coiled coil structures. The inclusion of residues with high helical propensity, such as Alanine, in position **b**, **c** or **f** will promote the formation of α-helices even at a low number of heptad repeat.

2.2.3.1.1.2. Association number.

The association number, also called oligomerization degree, is the number of helices forming the coiled coil superhelical bundle. This parameter is mainly influenced by the choice made regarding the amino acids at **a** and **d** positions (hydrophobic core). The side chain of these residues affects the packing geometry of the core, thus determining the association number. It has been proven that Leucine-zippers presenting combinations of amino acid residues, Isoleucine-Leucine, Isoleucine-Isoleucine, Leucine-Isoleucine, in the **a** and **d** positions, led exclusively to the formation of dimeric, trimeric and tetrametic coiled coils, respectively[112]. The only difference in the sequence were the **a** and **d** positions, the authors concluded that **a** and **d** amino acids were responsible for the switch in the association number of the helices. Other combinations of a and d positions, such as Val-Leu, have been also shown to result in the formation of dimeric coiled coils[113].

2.2.3.1.1.3. Oligomerization selectivity.

The formation of homodimers or heterodimers (oligomerization selectivity) is mainly determined by the electrostatic interactions between the charged amino acids placed at position **e** and **g**. Homodimers result from the presence of oppositely charged amino acids in these positions because of the attractive forces between the e

and g amino acids of the two strands. On the contrary, if **e** and **g** positions are occupied by amino acid of the same charge a repulsion between them will take place, resulting in the heterodimer formation if another peptide carrying oppositely charged **e'** and **g'** amino acids is available.

2.2.3.1.1.4. Orientation of helices.

The orientation of the helices is also determined by the electrostatic interaction between the amino acids residues in position **e** and **g**. Antiparallel heterodimers will result from the attractive forces between positions **e**:**e'** and **g**:**g'**, while parallel heterodimers will result from the attraction between residues in positions **e**:**g'** and **g**:**e'**.

2.2.3.2. Elastin-Like block co-Recombinamers (ELbcRs).

As it was said before in 2.1.7, recent advances in recombinant DNA techniques have provided the tools needed to produce block copolymers (block corecombinamers) with the desired sequence, depending on the application, from simple amino acids with an absolute degree of control and complexity superior to those of synthetic polymers

Amphiphilic elastin-like block co-recombinamers (ELbcRs) can form nano- or micro-sized structures[114-121] that can be directly injected into systemic circulation without the risk of blocking blood vessels[122-124]. To this end, ELR-based amphiphilic diblock and triblock copolymers have been synthesized in which the amphiphilicity[123, 156] of the component blocks is achieved by substituting the amino acid (X) in the guest position of the pentamer VPGXG by different hydrophilic (glutamic acid, aspartic acid or lysine) or hydrophobic (isoleucine or alanine, which is placed in the third position) amino acids. Nanoparticle formation occurs when the elastin-like block co-

recombinamer (ELbcRs) solution is heated above the characteristic Tt of the hydrophobic block, at which point the co-recombinamer chains organize themselves by hiding the hydrophobic blocks from the aqueous environment, thus reaching a minimum free energy situation (**Figure 19**).

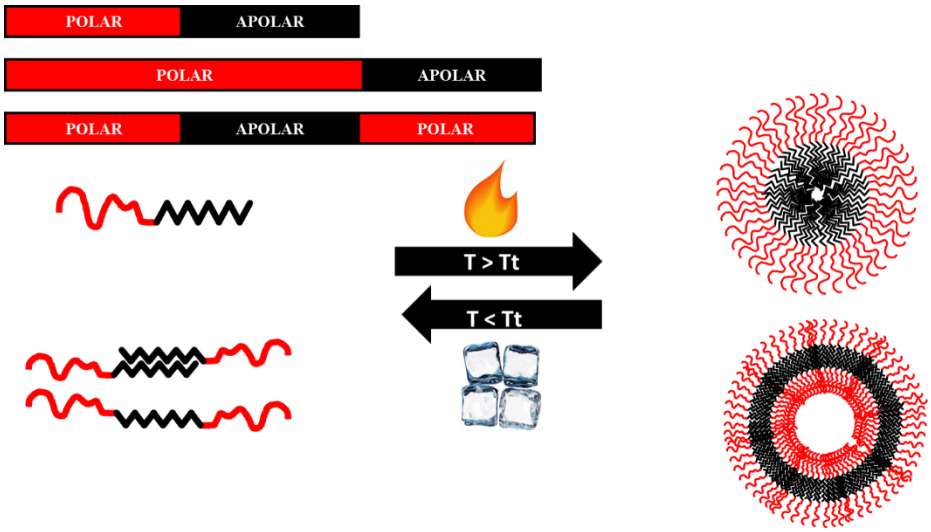

Figure 19: *Schematic representation of formation of self-assembled ELbcRs nanoparticles.*

Mean polarity, molecular weight, amino-acid sequence and molecular architecture are parameters influencing the final morphology and size of the final nano-assemblies, which have been demonstrated to assemble into micelles or hollow vesicles[119].

ELbcRs have also been reported as materials capable of forming physical hydrogels at a sufficiently high concentration. In this sense, both a tri-block (apolar-polar-apolar) and a tetra-block (polar-apolar-polar-apolar) have been reported to self-assemble into a physical

hydrogel once above the T_t. These materials are designed to be an injectable self-gelation systems with high applicability in biomedical applications, such as tissue repair or as drug delivery systems for local therapies. In order to fulfill the requirement of injectability the material is required to be a low viscosity liquid below the physiological temperature. In this sense, the monomers are completely unassociated in aqueous solution below the Tt and once above the Tt the hydrophobic elastin domains undergo a phase separation associating into micellar aggregates acting as virtual cross-links (**Figure 20**).

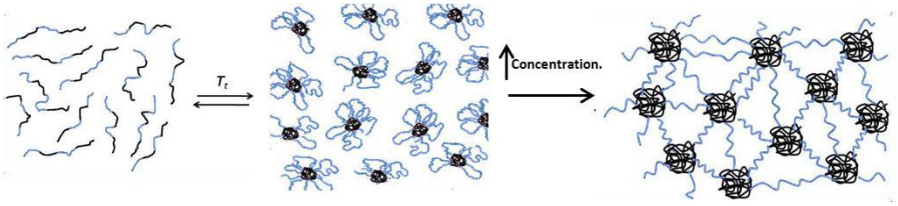

***Figure 20**: Schematic representation of the formation of a physical hydrogel through the micellation of a tetra-block ELbcR. Below Tt the monomers are extended, once above Tt the hydrophobic block (black) aggregates forming nanoparticles. If the concentration is increased that aggregation leads to the formation of a water swollen network resulting in the hydrogel formation.*

2.3. Polymer composite materials.

It is well known that composites materials are materials compose of two or more different constituent materials. These materials possess considerably different physical or chemical properties, that when both materials are combined, the resultant material present physic-chemical characteristics diverse from those of the individual components and both materials remains separate and distinct. The main difference between composites and blends is that the different component in the composite are still recognizable. Composite

materials are extensively used in a wide variety of field, such as space vehicle, home building or biomedicine.

A vast number of polymers are extensively used in biomedical applications, mainly due to its wide variety of compositions, forms and properties. Nevertheless, generally speaking, polymer tend to be either too weak or too flexible to meet the some mechanical demands of a certain application, such as orthopedic surgery. Polymer also are prone to absorb liquids and swell, which might be incompatible with certain applications[125] and their properties might be affect by the sterilization process[125]. On the other hand, metals present high strength, ductility and resistance to wear, but they present important drawbacks such as low biocompatibility in many cases, corrosion or the release of metal ions that might cause allergic reactions[126]. On the contrary, ceramic materials are known to be highly biocompatible but these materials present some drawback such a lack of resilience or brittleness[125]. Polymer composite materials are gaining attention because the combination of such materials are able to overcome some of the problems mention above. In this sense, polymer composites have been employed in a wide variety of applications. In the literature we can find different usages of polymer composites, as dental implants[125], cancer treatment[127] or complete knee replacement[125](**Figure 21**).

ELR have also been used as biocomposites and we can find examples of its usage as scaffold for bone tissue engineering when conjugated with collagen[128]. ELRs have been also conjugated with thiol-modified hyaluronan and used as treatment for early-stage disc degeneration[129]. Other ELRs composites (bioglass, carbon nosphere) have been employed in cell culture[130].

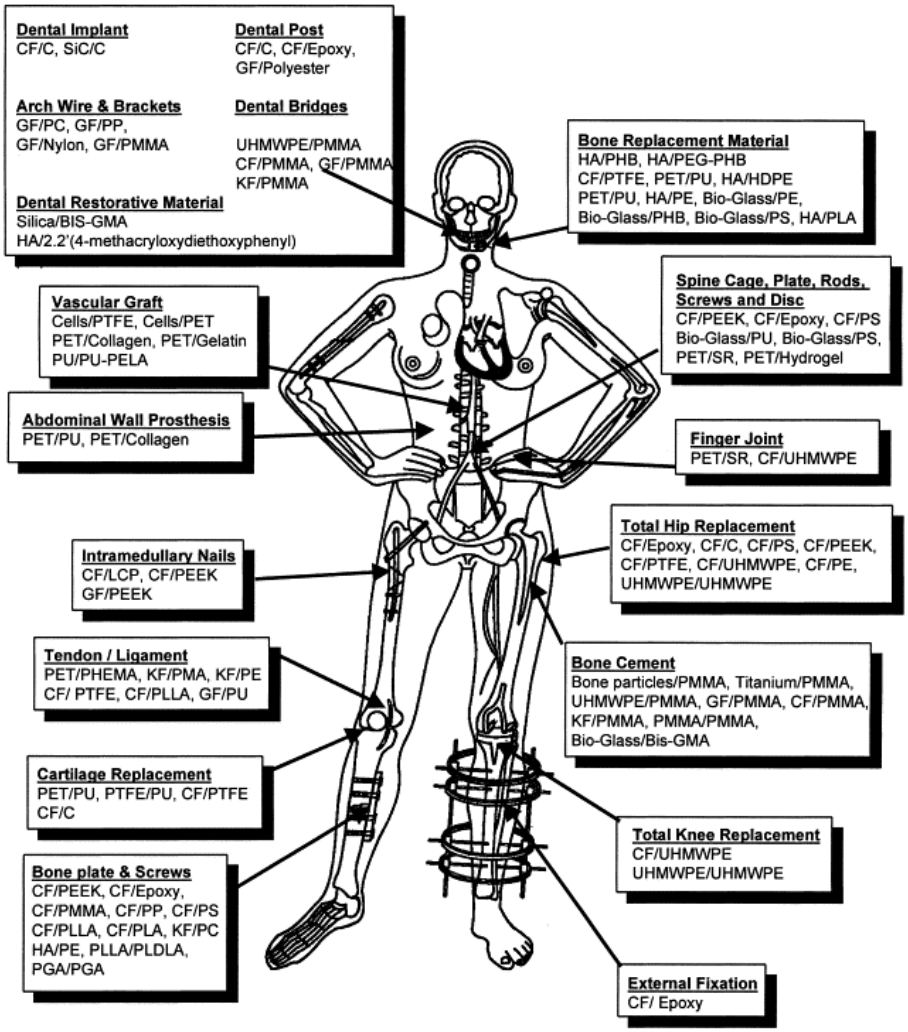

Figure 21: *Various applications of different polymer composite biomaterials. Reproduced from*[125]

2.3.1. Graphene based materials and its usefulness in biomedical applications.

In 2010, the Nobel Prize in Physics was awarded to Konstantin Novoselov and Andre Geim *"for groundbreaking experiments regarding the two-dimensional material graphene"*. Graphene, which contains a monolayer of carbon atoms organized into a highly packed 2D honeycomb structure, has emerged as the rising star of modern materials science due to its unique and outstanding properties, properties[131, 132], Some of these, such as its geometry and structure, provide graphene with high thermal and electrical conductivity or a high Young's modulus/fracture strength[133], all of which make graphene an ideal material for a wide variety of applications[134]. (**Figure 22**).

These properties include several which make graphene an interesting material for biomedical applications, namely high surface area, which, together with the π stacking of aromatic drugs, provides a higher loading capacity than is possible with other nanomaterials[135], near-infrared energy absorption, which is useful, amongst others, for thermal cancer treatment[136], or highly sensitive electrical properties, which can be applied in nanosensors or neural scaffolds[137]. All in all, polymer/ graphene nanocomposites find usefulness in the biomedical field mainly in drug delivery (which comes from graphene's high surface area, π-π stacking and electrostatic or hydrophobic interactions which gives graphene the capacity of loading poorly soluble drugs without compromising potency or efficiency) and tissue engineering, due to graphene's high elasticity, strength and flexibility which can be used as a reinforcement in tissue engineering scaffolds, such as hydrogels or electrospun fibers. Functionalized GO has also been used for gene transfection[138] and bioimaging applications[139].

However, as we have seen previously for other materials, graphene, or graphene oxide, present two mayor drawbacks for biomedical applications, namely their poor solubility and toxicity. To overcome this problem, graphene is being conjugated to other molecules, mainly biocompatible polymers, to increase its solubility and confer biocompatibility, thus forming polymer-graphene composites.

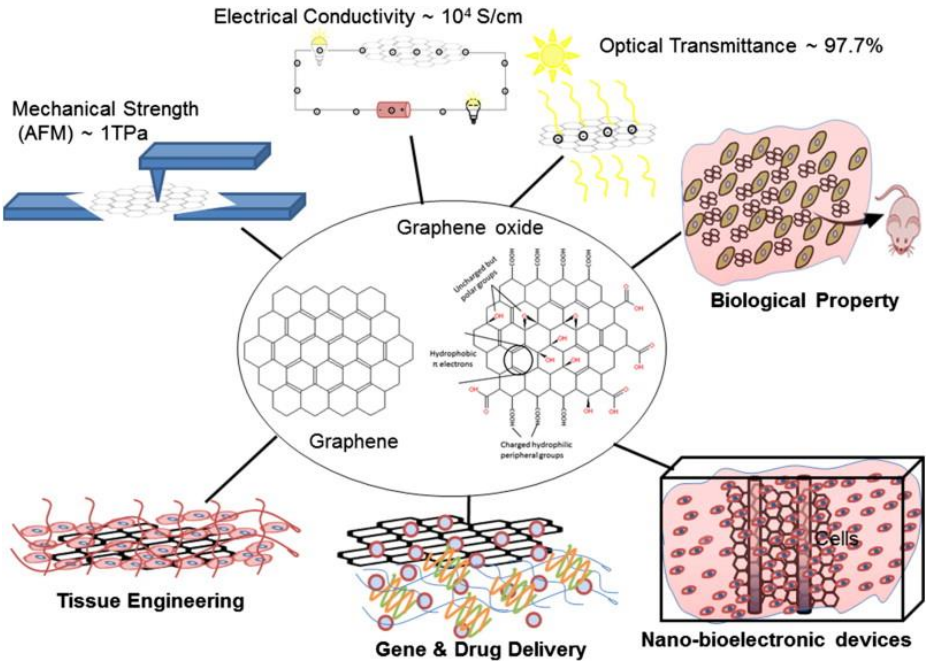

***Figure 22**: Schematic representation of possible applications of graphene-based nanomaterials in non-medical and biomedical field. Reproduced from*[140].

Graphene based nanomaterials can be divided depending on either the number or layers (single layer graphene, multilayer graphene) or the chemical modifications (graphene oxide, reduce graphne oxide). Single layer graphene is synthesized by repeated mechanical exfoliation[131], another possibility is an exceptionally controlled growth on silicon substrates by chemical vapor deposition[141]. The complicated proper

production in bulk of single layer graphene, together with its low solubility has become multilayer graphene or graphene oxide into more widely used materials for biomedical purposes.

Graphene oxide (GO) (**Figure 22**) is a highly oxidize form of chemically modified graphene consisting of graphene sheets with carboxylic acid, epoxide and hydroxyl groups in the plane. The presence of the carboxylic groups confer GO with a negative surface charge at neutral pH, while the epoxy and hydroxyl groups are uncharged but polar. The polarity of those groups allows GO to form weak interactions, such as hydrogen bonding or other surface reaction[142]. Additionally, GO possess free π electrons from unmodified graphene areas. The presence of this areas, which ate hydrophobic, allows the π-π interactions which are useful for the encapsulation of drugs or for a non-covalent functionalization of GO. Thus, GO is an amphiphilic molecule useful for the stabilization[143] of hydrophobic molecules in aqueous solutions.

2.3.1.1. Preparation of polymer/graphene nanocomposites.

Graphene and graphene oxide present two major drawbacks as a biomedical material, namely their poor solubility (although graphene oxide can be dispersed in water it collapses in saline conditions[144]), which is critical for such applications, and toxicity. It is commonly accepted that the in vitro cellular toxicity of this material is correlated with its surface coating, becoming more biocompatible as the biocompatibility of the material used in the coating increases[145-147]. There are, therefore, two main strategies to functionalize graphene based materials with polymers, namely, non-covalent interactions or covalent interactions.

Non-covalent production of polymer/graphene nanocompistes has been carried out mainly by three different strategies, which are described below:

- *Mixing*: Polymer-GO (or other graphene based material) have been prepared by simply mixing a suspension of GO with the desired polymer[148]. The mixture is precipitated using a non-solvent for the polymer, which will encapsulate the GO during precipitation.
- *In situ polymerization*: In this method the graphene based material is mixed with the desired monomer, followed by a polymerization in the presence of the graphene based material. Through this method, graphene has been functionalized covalently[149] and non-covalently[150] with a variety of polymers, such as PMMA[151].
- *Π stacking interaction*: This method takes advantage of the presence of aromatic rings in graphene based materials, which allows the π stack to take place. It goes without saying that it is also required the presence of such aromatic ring at the desired polymer[152].

Pure carbon materials have a lack of useful functionalities which make its covalent linkage with polymers challenging. On the contraty, graphene oxide present a surface rich in functional groups, which opens up its covalent functionalization with polymers through a variety of methods, such as click-chemistry[153] or diimide activation amidation[154].

HYPOTHESIS

3.0. HYPOTHESIS.

3.1. The thermal properties of ELbcRs are highly affected by salt addition. This work aims to analyze the effect of the presence of salts on the self-assembly behavior of ELbcRs, Hence, it is hypothesized that topographical features of self-assembled ELbcR nanostructures can be controlled by the simple addition of salts.

3.2. The interaction of amphiphilic copolymers with low molecular weight surfactants may induce aggregation of the copolymer or change the aggregation state of the pure polymeric micelles. Thus, it is hypothesized that the conjugation of amphiphilic ELbcRs with surfactants of different head polarity will give rise to nano-objects with novel structures and functionalities, which may find usefulness in purification processes or drug delivery applications.

3.3. Graphene oxide have outstanding properties, which are highly interesting in the biomedical field, but, they have two major drawbacks for its usage in this field, low solubility in aqueous media and high toxicity. Hence, it is hypothesized that specifically designed ELRs can be covalently attached to graphene oxide giving rise to composite functional materials with high solubility and biocompatibility.

3.4. As synthetic polypeptides, ELRs can be produced by recombinant methods and specifically designed to contain specific sequences and tailored molecular designs of interest. Thus, it is hypothesized that by means of genetic engineering, it can be designed and produced ELRs containing leucine zipper domains in their sequences, which may lead to the obtaining of brunched recombinamers as a result of coiled-coil aggregations by simple mixing different ELR-Zippers.

MATERIALS & METHODS

4.0. MATERIALS AND METHODS.

4.1. MATERIALS

4.1.1. Chemical Reagents.

All the reagents employed on this work are listed on **Table 1**

***Table 1**: Reagents employed and suppliers.*

Reactive and Abbreviation	Brand
4-Dimethylaminopyridine (DMAP)	Sigma Aldrich.
Acetic acid	Merck.
Acetone	Sigma Aldrich.
Acrylamide/Bis-acrylamide	Amresco.
Agarose seakem.	Cambrex.
Ammonium persulphate (APS).	Sigma Aldrich.
Ampicilin	Apollo Scientific.
Bromophenol blue	Sigma Aldrich
Calcium chloride ($CaCl_2$)	Sigma Aldrich.
Chloridric acid	Merck.
Coomassie Brillant-blue R-250	Sigma Aldrich
Decaline	Sigma Aldrich
Diethyl ether	Scharlau.
Dimethyl sulfoxide (DMSO)	Carlo Erba
Disodium hydrogen phosphate (Na_2HPO_4)	Fluka
Dodecyltrimethylammonium bromide (DTAB)	Sigma Aldrich.
Ethanol	Merck
Ethylenediaminetetraacetic acid(EDTA)	Sigma Aldrich

Glicerol.	Sigma Aldrich
Graphene oxide	Nanoinnova technologies.
Hexamethylene diisocyanate (HDI)	Sigma Aldrich.
Isopropanol	Invitrogen.
Kanamycin	Apollo.
Methanol.	Sigma Aldrich.
Mineral oil	Sigma Aldrich.
N,N'-Dicyclohexylcarbodiimide (DCC)	Sigma Aldrich.
N,N-Dimethylformamide (DMF).	Sigma Aldrich.
Octyl-β-D-Glucopyranoside	Sigma Aldrich.
Phenylmethylsulfonyl fluoride (PMSF).	Apollo.
Phosphate buffered saline (PBS)	Gibco.
Polydimethylsiloxanes (PDMS)	Dow Corning.
Potassium chloride (KCl).	Sigma Aldrich.
Sodium chloride (NaCl)-	Sigma Aldrich
Sodium dodecyl sulfate (SDS)	Sigma Aldrich.
Sodium hydroxide	Sigma Aldrich.
Sodium sulfate (Na_2SO_4)	Fluka
Tetracycline	Apollo.
Tetramethylethylenediamine (TEMED).	Sigma Aldrich.
Toluene.	Sigma Aldrich.
Tris(hydroxymethyl)aminomethane (Tris).	Sigma Aldrich.
Type I water	Millipore
Urea.	Fluka.
β-Mercaptoethanol.	Sigma Aldrich.

4.1.2. Glass material & other materials.

During the realization of this doctoral thesis light scattering techniques have been employed, where glass test tubes were used. The contamination of such tubes with organic residues, dust or grease may interfere with the results obtained, being necessary to pay special attention to the cleaning of the tubes employed. An optimum cleaning is achieved by rinsing the tubes out with distilled water followed by a wash with a mixture soap-water (Hellmanex ®II special for optical cleaning). To remove soap traces the tubes are extensively washed with water. Finally, the tubes are rinsed with water type I and allowed to dry in an oven at 60 ° C for at least 4 hours.

Other glass materials after washing and rinsing several times with distilled water were sterilized on an autoclave (Autester E-75). Other laboratory materials like tips, conical tubes, Eppendorf tubes, etc…, are bought sterile or are sterilized when needed on an autoclave (Autotester E-75, 20 minutes 120°C one atmosphere).

4.1.3. Molecular biology materials.

4.1.3.1. Restriction enzymes.

The restriction enzymes used in this work are listed below:

BamHI, DpnI, EarI, EcoRI, SapI,XhoI (New England Biolabs).

Eam1 104I (Fermentas).

All enzymes are used according to the manufacturer instructions.

4.1.3.2. Other enzymes.

During the realization of this work the following enzymes have been employed, being all of them purchased to New England Biolabs.

T4 DNA Ligase.

Shrimp alkaline phosphatase (S.A.P.).

Antartic alkaline phosphatase.

4.1.3.3. Cloning and expressing vectors.

The DNA fragments employed were cloned in pDrive cloning vector (Qiagen), **Figure 23**.

pDrive Cloning Vector

Positions of various elements

Vector size (bp)	3851
Multiple cloning site	266–393
LacZ α-peptide	216–593
T7 RNA polymerase promoter	239–258
T7 transcription start	256
SP6 RNA polymerase promoter	398–417
SP6 transcription start	400
Ampicillin resistance gene	1175–2032
Kanamycin resistance gene	2181–2993
pUC origin	3668
Phage f1 origin	588–1043
Primer binding sites:*	
M13 forward (–20)	431–447
M13 forward (–40)	451–467
M13 reverse	209–224
T7 promoter primer	239–258
SP6 promoter primer	400–418

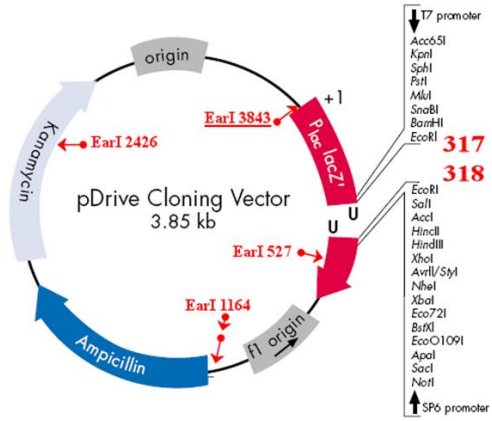

Figure 23: *Scheme of pDrive cloning vector.*

For the expression of the different recombinant polimers a p7 expression vector has been employed **Figure 24**. The p7 expression vector was constructed in our laboratory from Novagen's pET-25b (+) vector, by Dr. A. Girotti.

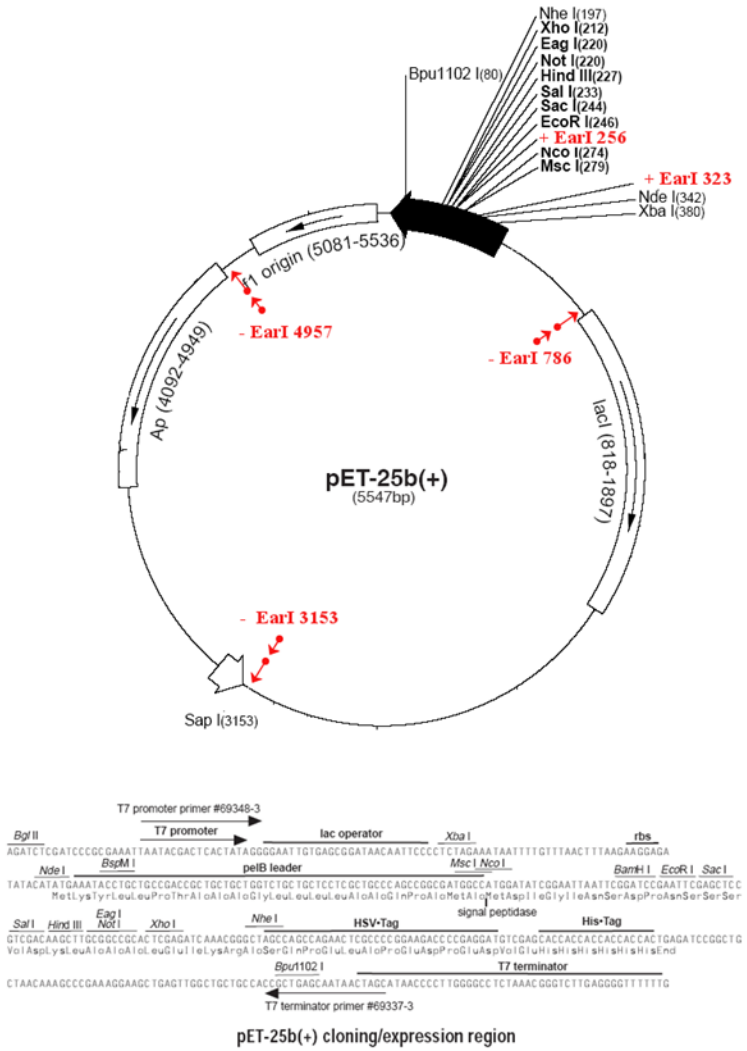

Figure 24: *Scheme of p7expression vector based on Navagen's pET-25b(+) vector.*

4.1.3.4. Other reagents.

Quantm Prep Plasmid Miniprep Kit (Biorad).

QIAquick Gel Extraction Kit Protocol (Qiagen).

4.1.4. Bacterial Strain.

During the realization of this work different strains of *Escherichia Coli* have been employed and are listed below:

XL1-Blue (Stratagene).

BL21(DE3)Star (Invitrogen).

BLR(DE3) (Novagen).

4.1.5. Culture media.

The culture media used for bacteria growth and transformation are listed below:

Luria-Broth (LB) (Pronadisa): Concentration 25g/l.

Terrific Broth (TB)(Formedium): 55.85 g/l + 8ml/l Glicerol.

LB-Agar: LB 25 g/l + 1.5 % (p/v). Agar (Fluka).

SOC I. (Sigma Aldrich)

4.1.6. Buffers.

During the performance of the work presented on this thesis different buffers were employed:

PBS (pH=7,4): 5mM Na2HPO4 pH=7,4, NaCl 140 mM

TAE: 40 mM Tris-acetate, 1mM pH=8 EDTA

TE (sonication buffer): 10 mM pH 8 Tris-base, 1 mM pH=8 EDTA, 1mM PMSF.

TBS (washing buffer) :20 mM pH 8 Tris-base, 140 mM NaCl.

Running buffer: Tris-base 25 mM pH=8,3, glicina 192 mM y SDS 0,1% (w/v).

DNA loading buffer: 30% (v/v) glycerol, 0.1% (w/v) SDS, 0.05% (w/v) bromophenol blue (BPB), 50mM Tris pH 8, 0.05mM EDTA

Protein loading buffer: Tris 1MpH 6.5 312.5 mM, SDS 10%(w/v), Glycerol (v/v), β-Mercaptoethanol 25%(v/v), bromophenol blue (BPB) 2% (v/v).

All the solutions were prepared using ultrapure type I water (Millipore).

4.1.7. Elastin-like recombinamers.

All the elastin-like recombinamers (ELRs) and elastin-like block co-recombinamers (ELbcRs) employed in the development of this work have been synthesized in our laboratory (Grupo Bioforge) by DNA recombinant techniques. Those recombinamers listed in **bold** at **Table 2** were specifically designed and produced for the realization of this thesis. It are produce by *Escherichia Coli* fermentation and purified taking advantage of both the smart nature and the reversible thermo-dependent segregation showed by this kind of materials, by inverse transition cycling (ITC)[3]

The recombinamers employed, the abbreviation, molecular weight (Mw), and amino acid sequence are shown in **Table 2**.

Table 2: *Composition and molecular weight of the ELbcRs and ELRs employed.*

Abbreviation	Amino-acid sequence	M_W(Da)
E50A40	$[(VPGVG)_2(VPGEG)(VPGVG)_2]_{10}$-$(VPAVG)_{40}$	38513
E1000A40	$[(VPGVG)_2(VPGEG)(VPGVG)_2]_{20}$-$(VPAVG)_{40}$	59290
E50A40E50	$[(VPGVG)_2(VPGEG)(VPGVG)_2]_{10}$-$(VPAVG)_{40}$-$[(VPGVG)_2(VPGEG)(VPGVG)_2]_{10}$	59288
IKx24	$[(VPGIG)_2(VPGKG)(VPGIG)_2]_{24}$	51979
HRGD6	$\{[(VPGIG)_2(VPGKG)(VPGIG)_2]_2$-(AVTGRGDSPASS)-$[(VPGIG)_2(VPGKG)(VPGIG)_2]_2\}_6$	60661
9K-EI2RGD	3K-$[(VPGVG)_2(VPGEG)(VPGVG)_2]_{10}$-$(VGIPG)_{60}$-3K-$[(VPGVG)_2(VPGEG)(VPGVG)_2]_{10}$-$(VGIPG)_{60}$-$[(VPGIG)_{10}$-(AVTGRGDSPASS)- $(VPGIG)_{10}$-$]_2$-3K	113552
E10Z3	$[(VPGVG)_2(VPGEG)(VPGVG)_2]_{10}$-VGGGGGVAQLEEEVQALEEEVAQCEEEVQALEEEVAQLEEEVGGGGG	26221
E20Z6	$[(VPGVG)_2(VPGEG)(VPGVG)_2]_{20}$-VGGGGGVAQLRSRVQARARVAQCRSRVQALRNRVAQLRSRVGGGGG	46645

E15Z5	$[(VPGVG)_2(VPGEG)(VPGVG)_2]_{15}$-VGGGGGVAQFKKKVQAFKKKVAQCKKKVQALEEEVAQLEEEVGGGGG	36670
E20Z2	$[(VPGVG)_2(VPGEG)(VPGVG)_2]_{20}$ -VGGGGGVAQFEEEVQAFEEEVAQCEEEVQALKKKVAQLKKKVGGGGG	46749
(E10Z3)x3	$\{[(VPGVG)_2(VPGEG)(VPGVG)_2]_{10}$-VGGGGGVAQLEEEVQALEEEVAQCEEEVQALEEEVAQLEEEVGGGGG$\}_3$	77087
E10Z3E10Z2E10Z3	$[(VPGVG)_2(VPGEG)(VPGVG)_2]_{10}$-VGGGGGVAQLEEEVQALEEEVAQCEEEVQALEEEVAQLEEEVGGGGG - $[(VPGVG)_2(VPGEG)(VPGVG)_2]_{10}$-GGGGGVAQFEEEVQAFEEEVAQCEEEVQALKKKVAQLKKKVGGGGG- $[(VPGVG)_2(VPGEG)(VPGVG)_2]_{10}$-VGGGGGVAQLEEEVQALEEEVAQCEEEVQALEEEVAQLEEEVGGGGG	77347
E10Z5E20Z6E10Z5	$[(VPGVG)_2(VPGEG)(VPGVG)_2]_{10}$-VGGGGGVAQFKKKVQAFKKKVAQCKKKVQALEEEVAQLEEEVGGGGG -$[(VPGVG)_2(VPGEG)(VPGVG)_2]_{20}$-VGGGGGVAQLRSRVQARARVAQCRSRVQALRNRVAQLRSRVGGGGG- $[(VPGVG)_2(VPGEG)(VPGVG)_2]_{10}$-VGGGGGVAQFKKKVQAFKKKVAQCKKKVQALEEEVAQLEEEVGGGGG	98141

4.2. METHODS.

4.2.1. DNA agarose gel electrophoresis.

DNA agarose gel electrophoresis are used to separate and check the appearance and size of DNA fragments form either a plasmid or from an enzymatic digestion with endonucleases. Different concentrations (in 1x TAE), are applied according the sizes of the DNA fragments and the kind of gel, analytical or preparative (**Table 3**)

Table 3: *Optimal resolution for linear DNA.*

Fragment size (bp)	Agorese final % 1x TAE.
800-10000	0.8
400-8000	1
300-7000	1.2
200-4000	1.5
100-2000	2

The gels are prepared in an Erlenmeyer by adding the quantity of Agarose and volume of TAE required for each concentration. The agarose is melted on a microwave. Once melted the flask is weighted and type I water is added until reaching the initial weight, thus maintaining the initial concentration and gel uniformity. After cooling down to 60°C the gel is casted in a horizontal tray with the desired comb.

0.20 volumes of 5x loading buffer are added to the samples. A fixed voltage, between 2 and 7 V/cm – according to each sample, is

then applied. The electrophoresis is run having as references the color markers (**Table 4**).Last, the gel is stained for 10 to 30 minutes in a 1x GelRed solution, and the DNA bands are visualized by exposition to UV light in a Viber Lourmat, TFX-20M transilluminator.

Table 4: *Relation of linear DNA migration with the bromophenol blue (BFB)*

TAE 1x –BPB	% Agarose
2900	0.30
1650	0.50
1000	0.75
500	1
370	1.25
200	1.75
150	2

4.2.2. Plasmid purification.

The plasmids employed in this work were purified using the commercial system "Quantum Prep Plasmid Mini, Midi o Maxiprep Kit" (Biorad) following the manufacturer's instructions. DNA was eluted with type I water. For applications were higher DNA concentration is required only half of the recommended elution volume is used and the elution water is used at 65°C.

4.2.3. DNA digestion with restriction enzymes.

Reaction conditions (temperature, concentration, time of reaction, buffer) for the digestion are supplied by the enzyme manufacturer. The rate of digestion is controlled by DNA agarose gel electrophoresis

4.2.4. DNA dephosphorylation.

Dephosphorylation reaction conditions (temperature, time of reaction, buffer) are supplied by the phosphatase manufacturer. For the p7 expression vector two different consecutive phosphatases were used and the incubation time was enlarged until one hour.

4.2.5. DNA fragments purification from an agarose gel.

The target DNA band is first separated and visualized in an agarose gel of an appropriated concentration and stained with RedGel (as indicated in 4.2.1), secondly, the band is extracted from the gel with the help of a scalpel. Minimum quantity of agarose should be cut during band extraction.

The purification of the fragment is carried out using the commercial system “QIAquick Gel Extraction Kit Protocol” (Qiagen), following the protocol indicated by the manufacturer.

4.2.6. Ligation reaction: Cloning.

The reaction ligation is carried out in a final volume of 10-12µL by mixing the insert with the vector, in a molar relation from 1:1 to 5:1, and T4 DNA ligase as enzyme with its corresponding buffer following the specifications indicated by the supplier. The reaction is conducted during 1 hour at room temperature or during 24 hours at 4°C.

4.2.7. Cloning on the pDrive/ p7 vector.

The ligation reaction is interrupted by the inactivation of the T4 DNA ligase by incubation during 10 minutes at 70°C. Once the ligation reaction is concluded, a certain quantity of it is used to transform competent cell as specified below.

4.2.8. Transformation of competent cells.

4.2.8.1. Transformation of XL1 blue subcloning grade competent cells.

This bacterial strain has an efficiency ≥ 106 transformants per microgram of DNA. Plasmid DNA to be amplified by cloning is transformed in this bacterial strain following the protocol specified by the supplier.

4.2.8.2. Transformation of XL1 blue competent cells.

This bacterial strain has an efficiency ≥ 108 transformants per microgram of DNA. Ligation products were transformed into this bacterial strain following the protocol specified by the supplier.

4.2.8.3. Transformation of BLR (DE3) competent cells.

This bacterial strain is transformed with the expression plasmid p7 following the method TSS reagent ("Transformation and Storage Solution")

A single colony, isolated and grown in a LB-agar plate, is used to inoculate 10mL of LB medium and is grown at 37ºC with shaking (250rpm), until reach a OD_{600}=0.3-0.4. At this point the metabolism and cell growth is stopped by incubation on ice for 5 minutes. The cell suspension is centrifuged at 3000rpm (1100Gx) for 10minutes at 4ºC. The supernatant is discarded and the pellet is re-suspended in 1mL of cold x1TSS solution. About 1-10ng of plasmid in final volume of 1-10µL are added to the mix. The cellular suspension plus the plasmidic DNA are kept on ice one hour followed by a heat shock, exposition at

42ºC for 2 minutes. The heat shock is stopped by immersion on ice for 2 minutes. 1mL of warm LB is added and the suspension is incubated one hour at 37ºC with shaking (250rpm).Finally, 50-200µL of the transformation mix is plated in LB-agar plus the antibiotic plates that are incubated for 16-20 hours at 37ºC.

4.2.9. Glycerol stock preparation.

Positive clones, which are of special interest, are store in glycerol stocks. The selected colonies were grown at 37°C with shacking (250rpm.) on LB or LB with 0.5% of glucose (for the expression strains), until reaching an OD_{600}= 0.6-0.8. At this point 0.1 volumes of 80% sterile glycerol are added and the cells are kept on cryovials at -80°C.

4.2.10. Production and purification of recombinant polymers.

4.2.10.1. Recombinant polymer's expression.

During the biosynthesis of the ELRs employed in this work the expression vector p7 has been employed. p7 has been obtained in our laboratory by mutagenesis of pET25b (+) by Dr. Alessandra Girotti. The final constructions were transformed on the bacterial strain BLR (DE3) following the above mention protocol (see 4.2.8.3).

ELRs expression starts inoculating the desired colony in liquid LB medium plus antibiotic at 37 ° C with orbital shaking (250 rpm.) during approximately 6 hours. This culture is used as inoculum for a fresh TB medium (plus antibiotic), in a volume ratio of 1:500, not exceeding the 25% of the capacity of the Erlenmeyer used.

This culture is grown for 14-16 hours at 37 ° C with orbital shaking (250rpm.)

4.2.10.2. Bacteria disruption.

Once the induction is finished, the bacteria's metabolism and growth are stopped by cooling it down to 4ºC. After spinning down, by ten minutes cold centrifugation at 5000xg, and eliminate the supernatant, the cells are washed and re-suspended with 100mL of washing buffer (see 4.1.6) per liter of culture. A new centrifugation, same conditions as before, is made and the supernatant is discarded. The pellet is then re-suspended in 25mL of TE (see 4.1.6) per liter of culture. Cell suspension is kept at 4ºC and 10µg/mL of PMSF protease inhibitor is added.

Bacteria are disrupted (lysated) by changing pressure disruption employing a Constant Cell Disruption System (Model TS 0.75KW, Constant System) Finally, the lysate is centrifuged at 4ºC for 60 minutes at 15000xg;.The supernatant contains the recombinant polymer biosynthesized.

4.2.10.3. Purification of the recombinant protein-based polymer.

The purification of ELRs starts from the supernatant obtained at the end of the lysis process (see 4.2.10.2), taking advantage of the ELRs' smart nature and inverse temperature transition[15]. Therefore, the purification process is based on successive cycles of precipitation (heating) and resuspension (cooling) of the supernatant. The ELRs biosynthesized in this work had glutamic acid residues in their sequence (see **Table 2**), which at a pH above its pKa are depronated and therefore negatively charged what increase significantly their T_t.[155] In order to reduce the Tt and in this sense, facilitate the precipitation of the ELRs, NaCl is added during the purification process until a 2M concentration is achieved. Likewise, β-mercaptoethanol (50 mM) is

added in order to break the disulfide bond likely formed between the cysteines present in some the ELRs employed (see **Table 2**)

Finally, after the last purification cycle, the re-suspended polymer is dialyzed against cold type I water, with several water changes. The suspension is then lyophilized and stored at -20°C. Purification steps, as well as the final product, are checked by polyacrylamide gel electrophoresis. (See 4.2.11)

4.2.11. Denaturing polyacrylamide gel electrophoresis.

The protein polyacrylamide gel electrophoresis in the presence of sodium dodecyl sulfate – SDS-PAGE – is made following the protocol for discontinuous systems described by Laemmli[156]. In such gels, it exist a directly proportional relation between the protein migration velocity (V) both a directly proportional relation, to the product of the effective charge (q) and the electrical potential gradient (E) , and an inversely proportional relation to the friction coefficient, **Equation 1.**

$$V = q.E/f \quad \textbf{(1)}$$

The proteins' effective charge almost doesn't differs because the SDS strongly interacts with proteins providing them with approximately one negative charge per each amino acid residue The SDS completely denatures the proteins by breaking the non-covalent interactions responsible for the quaternary and tertiary structure. Besides, a reducing agent (β-mercaptoethanol) is added to the samples in order to break the disulfide bonds that might existents. The reducing and denaturing process is facilitated with the heating of the samples during 5 minutes near boiling temperature.

A "MiniVE vertical electrophoresis system" from Hoefer (Amersham Pharmacia Biotech, Pittsburg, USA) electrophoretic system

was employed to perform the polyacrylamide electrophoresis. The total percentage of acrylamide (%T) in the resolving gel varies according to the molecular weight of the polypeptide we want to separate. The optimal %T for a determined size range is presented in **Table 5**

Table 5: *Optimal %T according to the polypeptide target size range.*

Target size range (kDa)	%T in resolving gel.
24-205	7.5%
14-205	7.5%
14-66	12.5%
14-45	15%

The composition of a resolving and stacking for a gel X%T is detail in **Table 6**.

Table 6: *Composition of the resolving and stacking gel in a gel 15%T*

	Resolving gel.	Stacking gel.
Acrylamide 40%	X % (w/v)	4% (w/v)
Tris -HCL pH 8.8	375 mM	-------
Tris –HCL pH 6.8	-------	125 mM
SDS 10%	0.1% (w/v)	0.1% (w/v)
APS 10 %	0.05% (w/v)	0.05% (w/v)
TEMED	0.05% (w/v)	0.08% (w/v)

*Both gels are prepared in type I water.

4.2.12. Native Polyacrylamide gel electrophoresis.

Under native PAGE conditions, polypeptides retain their higher-order structure, the ability of interact with other polypeptides and it is often retain enzymatic activity[157]. Thus, the migration of proteins depends on many factors, including size, shape and native charge.

Therefore, native PAGE is a useful technique when it comes to assaying native structures of proteins[157]. In this work it has been used to study the interaction between the different leucine zippers domains present at the ELRs employed.

In order to prepare a native polyacrylamide gel, the same components than those used in 4.2.11 are employed, with the exception of the reducing agent β-mercaptoethanol and SDS. Heating the samples must also be avoided and the running time should double than SDS-PAGE.

Native polyacrylamide gels, owing to the lack of SDS, cannot be copper stained and they have to be stained by Coomassie Brilliant Blue.

4.2.13. Preparation of ELbcRs aqueous solutions for the obtaining nano-objects.

Aqueous solutions of the amphiphilic ELbcRs were prepared from lyophilized specimens of the purified polymers dissolved to appropriated concentration for each experimental technique (no higher than 25 μM) in NaCl solution of the appropriate concentration (3.9, 7.8, 15.625, 31.25, 62.5 mM and 0.125, 0.25M) for the study of the effect of salts on the ELbcR self-assembling procedure.

Ultrapure type I water was used as solvent for the study regarding the effect of surfactants on the ELbcR self-assembling process. DTAB, SDS and Octyl were dissolved at the appropriate concentration in type I water. The E50A40/surfactant solutions were prepared by mixing the individual aqueous solutions.

In both studies, solutions were filtered using a 0.45 µm PVDF syringe filter and a neutral pH was achieved by adding small amounts of HCl or NaOH.

The solutions prepared for light scattering experiments were likely to suffer solvent evaporation during the experiment, in order to avoid the possible experimental error associated to concentration variation, mineral oil was added to those solution to prevent from evaporation.

4.2.14. Preparation of the ELR leucine zipper aqueous solutions.

In order to assure the deprotonation of the glutamic acids, which are present at the sequences of those ELRs that contain leucine zipper domains (see 4.1.7), the pH was adjusted to 7 prior the lyophilization.

The individual solutions were prepared using type I water as solvent. The ELR mixtures were made by simply mixing equal-molar solutions of the individual ELRs. The final mixture concentration was 1 mg/ml. This concentration was selected due to the requirements of the experimental techniques.

4.2.15. Obtaining of ELR-graphene oxide composites.

The ELRs IKx24, HRGD6 and 9KEI2RGD were chosen to be conjugated with GO. In this work we have chosen a covalent linkage, due to its higher stability and stronger attachment compared with a non-covalent bond, for the obtaining of ELR-GO composites. Due to the presence of carboxyl groups on the graphene oxide, ELRs bearing amino groups (IKx24, HRGD6 and 9KEI2RGD) present in lysines (see **Table 2**) were employed to perform an amidation reaction between the two groups, this reaction being mediated by carboxyl group activation using the carbodiimide methodology(**Figure 25**).

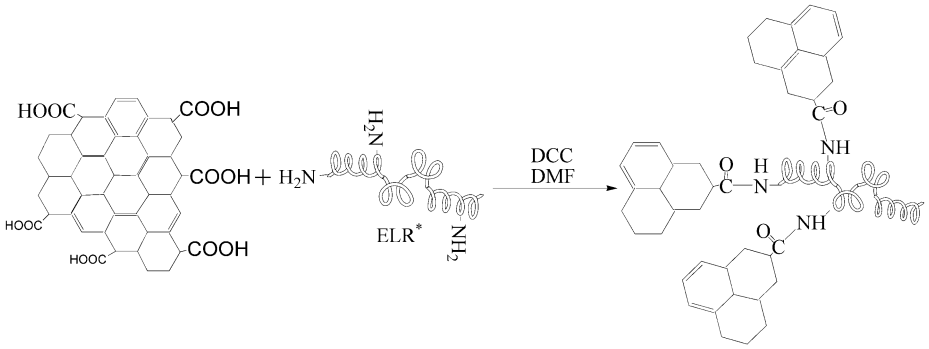

***Figure 25**: Synthesis of ELR-GO composites.*

A detailed reaction protocol is described below:

20 mg of GO was dispersed in 2mL of DMF and sonicated for 1 h. Later, a 70 μM solution of DCC in 1 mL of DMF is added to the GO suspension and transferred to a round bottom flask where is allowed to react, with stirring, for 2 h to ensure carboxyl activation.

Once the carboxyl activation is finished, 600 mg of ELR are dissolved in 20 mL of DMF (90 mmol of DMAP was added to the 9K-EI2RGD to confer a basic environment).Both solutions were mixed and allowed to react for 48 hours while stirring under a nitrogen atmosphere.

Once the reaction was complete, the mixture was centrifuged (10,000 rpm, 5 min) to eliminate unreacted GO and reaction by-products.The supernatant was extensively diluted in diethyl ether to precipitate the ELR-GO composite.

After centrifugation at 10,000 rpm for 5 min, the supernatant was discarded. The resulting pellet was re-suspended in acetone and centrifuged. This acetone cycle was repeated three times.

The final pellet was dried on a rotary evaporator to remove acetone.The dry pellet was re-suspended in type I water and dialyzed

against type I water. Finally, the composites are frozen, lyophilized and kept at -20°C until its usage.

4.2.16. Preparation of electrospun ELR-GO nanofibers.

In the electrospinning process, fibers ranging from 50 nm to 1000 nm or greater can be produced by applying an electric potential to a polymeric solution. The electrical potential applied provides a charge to the polymer solution so that, when it overcomes the surface tension, causes the formation of a jet that is ejected from the tip, which is known as Taylor cone. The charged jet undergoes instabilities and gradually thins in air, primarily due to elongation and solvent evaporation. The charged jet eventually forms randomly oriented nanofibers that can be collected on a stationary or rotating grounded metallic collector.

Solution properties like solution viscosity, surface tension and conductivity affect the process of electrospinning. The other important factors include the flow rate of the liquid solution in the capillary, electric potential applied, tip-metal screen distance, humidity and air properties of the process surroundings. Another important factor is the proper grounding of the metal screen. Changing the factors appropriately, different fibers and nanofibers could be effectively electrospun.

Aqueous HRGD6-GO solutions (25 wt%) were used for the electrospinning process. These solutions were infused through an 18G x 1” needle at a constant voltage and flow rate of 38 kV and 0.25 mL/h, respectively. HRGD6-GO nanofibers were directed to a grounded, circular indium tin oxide (ITO) collector with a diameter of 12 mm over a collector distance of 15 cm. Electrospun surfaces were cross-

linked by immersion in 10% HMDI/acetone solution overnight and then exhaustively washed with ultrapure deionized water.

4.2.17. Preparation of micropaterned ELR-GO hydrogels.

Surface micropatterned HRGD6-GO chemical hydrogels were obtained by replica moulding on polydimethylsiloxane (PDMS) micropatterned substrates as moulds. The PDMS prepolymer and curing agent were mixed at a 10:1 (wt/wt) ratio and degassed for 1 hour. The mixture was subsequently deposited onto previously fluorosilanized patterned silicon masters and cured at 65°C for 1 h. The PDMS replicas were carefully removed from the silicon wafer and used without any further surface treatment.

Two different silicon masters were used, one presenting grooves with a width of 20 μm and separated by 50 μm, and one with 50 μm hexagons.

The hydrogels were obtained by chemical crosslinking. An HRGD6-GO solution was prepared at a concentration of 100 mg/mL in DMF at room temperature and a solution of HDI was prepared at 20°C in DMF. The polymer: HDI molar ratio was 1:4. The HRGD6-GO solution was cast onto the PDMS mold covering all the surface, then the HDI solution was deposited on it and allowed to react overnight at room temperature. The hydrogels were peeled off and immersed in ultra-pure water. They were thoroughly washed in ultrapure water to remove remaining unreacted chemical reagents and solvent.

4.2.18. Experimental techniques.

4.2.18.1. Dynamic light scattering.

Dynamic light scattering (DLS), also called Quasi-Elastic light scattering (QELS) or Photon correlation spectroscopy (PCS), is a technique for measuring the size of particles normally in the sub-

micron region. Typically, DLS is concerned with measurements of dispersed particles or suspended macromolecules in a liquid medium, measuring the particles Brownian motion and relating it to the particles' size.

Brownian motion is the random movement of particles suspended in a fluid due to their collision with the solvent molecules that surround them. Thus, the random motion will be affected by different factors, mainly the size of the molecules (the bigger the molecules, the slower they move), the viscosity of the solvent (the more viscous the solvent, the slower the molecules move) and temperature. Temperature is a crucial parameter, both temperature stability and temperature accurate knowledge are required, due to its influence on the solvent viscosity and owing to, temperature instability will lead to convection currents in the sample, thus non- random motion, resulting in incorrect size interpretation.

The velocity of the Brownian motion is defined by the translational diffusion coefficient (D), which is used to calculate the size of the particles by using the Stokes-Einstein equation:

$$D_h = \frac{k_B T}{3\pi\eta D} \quad \textbf{(2)}$$

Where k_B is the Boltzmann constant, T is the temperature and η is the viscosity. It is worth noting, that DLS refers to how a particle diffuse within a fluid so the calculated diameter is a hydrodynamic diameter (D_h), (effective molecule diameter + hydration layer, **Figure 26**)

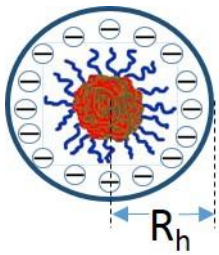

Figure 26: *Schematic representation of particle with its hydration layer, hydrodynamic radius.*

The particles diffusion speed, due to Brownian motion, is measured by measuring the rate at which the intensity of the scattered light fluctuates using a digital auto correlator.

A correlator is a signal comparator, thus it measures the degree of similarity between two signal, or one signal with itself at varying time intervals. If the particles are large the signal will be changing slowly and the correlation will persist for a long time. On the other hand, if the particles are small and moving quickly then correlation will reduce faster. (**Figure 27**)

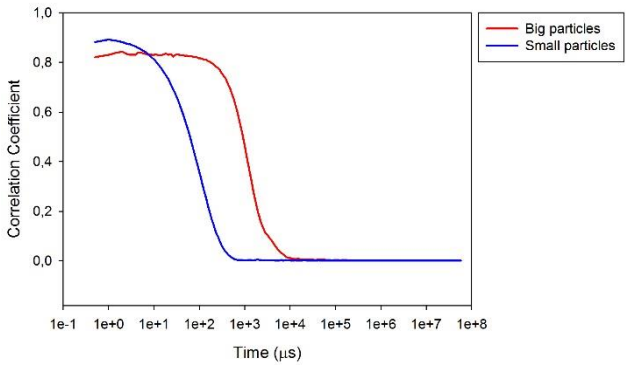

Figure 27: *Typical correlogram from samples containing large particles (red, long decay time) or small particles (blue, short decay time) Perfect correlation is indicated by unity and no correlation is indicated by zero.*

The correlation function G(τ) of the scattered intensity is as follows (**Equation 3**):

$$G(\tau) = < I(t).I(t+\tau) > = \lim_{T\to\infty} \frac{1}{T} \int_{t_0}^{t_0+T} I(t).I(t+\tau)\,dt \quad \textbf{(3)}$$

T is the integration time, t_0 is the initial time and τ is the time difference of the correlator.

For a large number of monodisperse particles in Brownian motion the correlation function is an exponential decaying function of the correlator time delay τ:

$$G(\tau) = A[1 + B\exp(-2\Gamma\tau)] \quad \textbf{(4)}$$

where A is the baseline of the correlation function, B is the intercept of the correlation function and Γ is the decay rate:

$$\Gamma = D.q^2 \quad \textbf{(5)}$$

where D is translational diffusion coefficient and q is the wave vector:

$$q = \frac{4\pi n}{\lambda}\sin\left(\frac{\theta}{2}\right) \quad \textbf{(6)}$$

Where n is the refractive index of the dispersant, λ is the wavelength of the laser and θ is the scattering angle.

Size is obtained from the correlation functions by using various algorithm. In this work we have used two of them, a Cumulants[158] analysis and a CONTIN[159, 160] analysis.

Light scattering measurements were performed using a BI-200SM multiangle goniometer (Brookhaven Instrument, Holtsville, NY) with a 33 mW He−Ne vertically polarized laser at a wavelength of 632.8 nm and a digital correlator (BI-9000AT) and a Zetasizer nano ZSP (Malvern instruments) equipped with a 10 mW He-Ne laser at a wavelength of 633 nm..

For the Brookhaven apparatus. DLS measurements were monitored at a scattering angle of 90°, filtered recombinamer solutions at a concentration of 25 μM were introduced into glass cells and stabilized for 10 min at the desired temperature.The hydrodynamic diameter of the ELbcR nanoparticles in the presence of salt were determined. For the zetasizer apparatus samples (25 μM, filtered) were introduced into polystyrene cuvettes and stabilized for 10 min at a desired temperature. The hydrodynamic diameter of the ELbcR nanoparticles in the presence of surfactants were determined

Mineral oil was added to the sample cells, to prevent water evaporation during the measurements; no interference between this mineral oil and the ELbcR was observed.

4.2.18.2. Static light scattering.

Static light scattering (SLS) measures the dependence of the average scattered intensity on the scattering angle. The static properties of the particles in solution are not time dependent, and structural information, including Molecular weight (Mw), second osmotic viral coefficient (A2) and the root mean square radius, also called the radius of gyration (Rg), can be obtained. SLS data obtained from solutions at different angles as well as different concentrations can be analyzed by several algorithms firstly reported in a classical article by Zimm:

$$\frac{K_c}{R_\theta} = \frac{1}{M_w}\left(1 + \frac{1}{3}q^2\langle R_g^2\rangle_z + 2A_2c + \cdots\right) \quad \textbf{(7)}$$

where the optical constant K is defined as $(2\pi^2 n_0^2/\lambda^4 N_A)(dn/dc)^2$, n_0 is the refractive index of the solvent, dn/dc (see 4.2.18.3) is the specific refractive index increment, N_A is Avogadro's number, θ is the scattering angle, λ is the wavelength, c is the nanoparticle concentration and q is the scattering vector (see 4.2.18.1)

By plotting K_c/R_θ against q^2 + kc (where k is the scattering center) and extrapolating the experimental data to zero concentration and zero angle, the molecular weight of the aggregates (Mw,agg), the gyration radius (Rg), and the second virial coefficient (A2) can be obtained.

In some cases the conventional Zimm plot showed a curvature on the angular dependence. The data were linearized using the Berry equation:

$$\sqrt{\frac{Kc}{R_\theta}} = \sqrt{\frac{1}{M_W}}\left(1 + \frac{16\pi^2}{6\lambda^2}\left(R_g\right)^2 Sin^2\left(\frac{\theta}{2}\right) + \cdots\right)(1 + A_2 M_W c) \qquad \textbf{(8)}$$

$(Kc/\Delta R_\theta)^{1/2}$ was plotted against (sin2(θ/2) + kc), Berry plots, and the same extrapolations (zero angel and zero concentration) were carried out in order to calculate the Rg, Mw,agg and A2

SLS measurements were performed in order to determine the gyration radio and the molecual weight of the ELbcR nanoparticles in the presence of salt. ELbcR solutions were filtered adn equilibrated at the desired temperature, with concentrations ranging from 1.0 to 8.0 mg/mL and for scattering angles of between 50° and 130°. The elastic (static) intensity was measured using toluene as standard with a known absolute scattering intensity

The aggregation number (Nagg) (i.e., number of ELR chains per nanoparticle) was also calculated from previous data by dividing the Mw,app by the Mw of the ELbcRs. The structure of the self-assembled nanoparticles was further characterized by calculation the ρ ratio (ρ = Rg/ Rh)[161].

4.2.18.3. *Determination of the specific refractive index increment, dn/dc.*

The refractive index (nD) was determined experimentally for the ELbcRs over a wide range of concentrations (1-8 mg/mL) using a digital refractometer (Mettler Toledo RE50, 589.3 nm (Sodium D-.line) Mettler-Toledo, Greifensee, Switzerland) equipped with a Peltier thermostat that kept the samples at working temperature within an accuracy of 0.02°C. The value of the specific refractive index increment (dn/dc) was deduced from the slope of plots of refractive index versus ELbcR concentration at the corresponding temperature. All measurements were carried out in triplicate

4.2.18.4. *Zeta potential.*

ζ-potential analysis is a technique for determining the surface charge of nanoparticles in solution. The ζ-potential of the ELbcR/surfactants complexes was monitored at 65 °C using a Zetasizer nano ZSP apparatus (Malvern instruments). Measurements were carried out in a range of different surfactant concentrations (from 0 to 16 mM) mixed with 25 μM of the ELbcR solution. The ζ-potential values, which were determined using the Smolukowski equation relating ionic mobility to surface charge, were plotted as the average of 10 repeated measurements.

4.2.18.5. *Differential scanning calorimetry.*

Differential scanning calorimetry (DSC) is a technique in which the difference in the amount of heat required to increase the temperature of a sample and reference is measured as a function of temperature.

DSC experiments were performed using a Mettler Toledo 822e with a liquid-nitrogen cooler. The solutions were prepared at 50 mg/mL

in milliQ water. For analysis, 20 µL of the solution was placed in a standard 40 µL aluminum pan and sealed hermetically. The same volume of milliQ was placed in the reference pan.

This technique is employed in order to determine the effect of the presence of GO in the T_t of the ELRs.Thermal procedure isotherm at 0 °C for 5 min, ramp 5.0 °C·min^{-1} from 0 to 55 °C

4.2.18.6. Cell Viability.

The experiment was carried out in order to check the cell viability on ELR-GO composites. First, a 20 mg.mL^{-1} solution of ELR-GO (IK-GO, HRGD6-GO and 9K-EI2RGD) was placed on the wells and it was left to absorb during 1 hour at 4ºC. Later, the excess of ELR-GO solution was removed and BSA was added in order to block those possible unspecific interactions. Later, the surfaces were washed with sterile PBS. The plates with the absorbed ELR-GO were sterilized with UV light during 30 minutes. Once the sterilization was completed, HFF-1 cells suspended in serum-free medium were seed at a density of 10^4 cells per cm^2. Loosely adhere or unbound cells were removed by changing the medium 60 minutes after seeding and then maintained for 2 days. Cells were also seeded on surfaces containing ELR without graphene oxide and in surfaces only with BSA.

4.2.18.7. Optical microscopy.

Optical microcopy was performed in order to visualize the micropatterned surfaces of the ELR-GO hydrogels and to visualize the cell of the viability experiment.

The hydrogels were visualized with an optical microscope Nikon eclipse 80i while cells were visualized with a fluorescence microscope Nikon eclipse Ti-SR, Japan

4.2.18.8. Rheology.

Rheology is the study of flow and deformation of materials under applied forces. In this sense, it was used to analyze the thermogelification process of an ELR-GO composite, by studying its mechanical properties in order to obtain the storage and loss moduli of the hydrogel.

The thermogelification process of a 15 wt% 9K-EI2RGD-GO solution were evaluated as a function of temperature using a controlled stress rheometer (AR-2000ex, TA Instruments) at a constant strain of 0.1% and a frequency of 1 Hz. The heating rate was 5.0 °C/min and mineral oil was placed around the sample in order to prevent evaporation. A frequency of 1 Hz and a strain of 0.1% were selected.

4.2.19. Experimental techniques performed by external services.

4.2.19.1. Amino-acid analysis

The amino acid composition of the ELRs employed during this work was determined by *Laboratorio de Técnicas Instrumentales (University of Valladolid)*.

After addition of a known quantity of α-aminobutyric acid as internal pattern the samples were hydrolyzed (6M HCl, 1% Phenol and 2.5 hours at 155°C) and evaporated. The powder was resuspended in 1mL of 20mM HCl and a 1/10 dissolution was prepared. The quantification of the less represented amino acids was made from the most concentrated sample and the quantification of the most represented amino acids from the 1/10 dissolution. One aliquot of each dissolution was derivatizated according to the AccQ-Tag Waters method and analyzed by HPLC with UV detection, using a WATERS600 HPLC gradient system with a WATERS2487 detector..

4.2.19.2. MALDI-TOF.

Determination of the ELRs molecular weight was made by MALDI TOF at the *Laboratorio de Técnicas Instrumentales (University of Valladolid).*

4.2.19.3. Circular dichroism.

Circular dichroism CD was performed in the *Servicios Centrales de Investigación University of Almeria*, as well as in the University della Basilicata (Italy), in order to determine the secondary structure of ELR-Zippers. In both places, the apparatus employed was a spectropolarimeter Jasco J-810.

The experimental parameter employed were as follows:

Scan speed: 50 nm/min

Cell length: 0.1 mm

Spectra were recorded at room temperature collecting data from 250 nm to 190 nm. Ellipticity is reported as the mean residue ellipticity [θ] in deg cm^2 $dmol^{-1}$, which is calculated according to the following equation:

$$[\theta]=[\theta]_{obs}\ (10/n_a dc)$$

Where $[\theta]_{obs}$ is the measured ellipticity (in milideg), n_a is the number of amide groups, c is concentration (mol/L), and d is the path length of the cell in centimeters.

4.2.19.4. Transmission electron microscopy (TEM).

TEM measurements were conducted using a JEOL JEM-1230 electron microscope (cicBiogune, Bilbao) operating at 120 kV, in order to visualize the structures formed by ELbcR/salt and ELbcR/surfactant solutions. Specimens were prepared by placing a drop of the stabilized heated solution (25 μM) at the corresponding temperature on a preheated plasma-treated carbon-coated copper grid, followed by water

evaporation at the same temperature. Samples were stained with uranyl acetate solution (1.0 wt %) to enhance the contrast of the nanoparticles.

4.2.19.5. *Scanning electron microscopy (SEM).*

Scanning electron microscopy measurements were carried out to visualize both ELbcRs/surfactatns and electrospun ELR-GO fibers. Stabilized solutions of E50A40/surfactant solutions (25 μM/2 mM) heated to 65 °C were placed on a preheated silicon wafer grid, followed by water evaporation and then observed with a FEI Quanta 200FEG environmental scanning electron microscope (ESEM) operating at an accelerating voltage of 30 kV.

Electrospun ELR-GO fibers were observed directly from the ITO surfaces, where were deposited, without further treatment.

4.2.19.6. *Cryo-Transmission electron microscope (Cryo-TEM)*

Cryo-TEM measurements were conducted on a JEOL JEM-FS2200 electron microscope (Unidad de microscopía avanzada, Parque científico Universidad de Valladolid) operating at 200 kV, in order to visualize the structures formed by ELbcR/salt and ELbcR/surfactant solutions. Stabilized solutions of E50A40/surfactant (25 μM/2 mM) and ELbcR/NaCl solutions heated to 65°C were placed on a preheated plasma-treated carbon-coated copper grid, followed by cryo-vitrification of the sample using a Cryoplunge CP3 Gatan

4.2.19.7. *Analytical ultracentrifugation.*

During the realization of this work sedimentation velocity experiments were carried out to study the interaction between the different ELR-leucine zippers.

At a sedimentation velocity experiment, the macromolecules are subjected to a high centrifugal field such that the force of centrifugation is greater than diffusion, so that there is a net transport of material

towards the bottom of the cell. It is a hydrodynamic transport method which allows fractionating macromolecules, based on the differences in the sedimentation coefficient (a function of the mass, density and macromolecular form)

Sedimentation velocity experiments were carried out in Centro de Investigaciones Biológicas, CSIC, Madrid with a XL-I model ultracentrifuge.

4.2.19.8. Thermogravimetric analysis.

Thermogravimetric analysis (TGA) were performed in order to determine the weight percentage of graphene oxide on the ELR-GO composites. TGA was performed at Leical, Departamento de Física de la Materia Condensada. Universidad de Valladolid. Using a TGA 1 Mettler Toledo. The method employed constist on two stages:

- From 50°C to 650°C, 20°C/min under 60 ml/min of N_2.
- From 650°C to 850°C, 20°C/min under 60 ml/min of Air.

RESULTS & DISCUSSION

5.0. RESULTS AND DISCUSSION.

5.1. Chapter 1: The effect of NaCl on the self-assembly of elastin-like block co-recombinamers: Tuning size of micelles and vesicles

Abstract: Elastin-like block co-recombinamers (ELbcRs) are able to reversibly self-assemble into different structures depending on their molecular architecture. ELbcRs are sensitive to environmental changes and their self-assembly is driven by a change in their environment, typically a temperature change. Herein we present a study of the effect of the addition of NaCl on the size and shape of thermally driven self-assembled nano-objects. The presence of salts increases the effective hydrophobicity of recombinamers and our results show how this could induce changes in the size of the aggregates formed upon heating, such as micelles and hollow vesicles. Additionally, many researchers are currently using NaCl to tune the transition temperature of ELRs. However, this method is used without a complete understanding of the potential changes in the self-assembly process that might result. Therefore, although salts other than NaCl are used for comparison in this study, the main effort is directed towards the effect of NaCl as this salt is widely and routinely used to control the transition temperature, Tt, in ELR purification protocols and their applications. Dynamic light scattering (DLS) was used to follow the formation, and determine the size, of the nano-objects assembled, whereas static light scattering (SLS) was performed to study the molecular weight and gyration radius of the aggregates. This work suggests the possibility of being able to control dimensions of ELbcR-based self-assembled nanoparticles by NaCl addition.

Self-assembly procedures have been the subject of numerous studies over a number of years, with the self-assembly of nanoparticles being a particularly active field. Self-assembled polymer nanoparticles tend to be obtained from amphiphilic macromolecules. Generally speaking, a solution of these amphiphilic molecules in a solvent that only specifically solvates one part of the molecule will result in aggregation due to interaction of the solvent with the solvophobic blocks of the molecule. Thus, micelles are the most common structure reported as they can be obtained using many different molecular interactions, whereas more complex morphologies, such as hollow or tubular structures, require specific molecular interactions, such as hydrogen bonding, to drive the self-assembly procedure towards formation of the desired morphology[162, 163]. Nanoparticles are highly interesting systems in biomedical applications because of their versatility and their multiple potential uses, such as drug carriers[114, 164] or gene delivery[165, 166]

Additionally, it has been demonstrated that both the size and shape of nanoparticles have a great impact on drug delivery efficiency[167]. As such, an ability to tune and control this parameter is crucial when designing drug-delivery systems.

The ratio between the hydrophilic and hydrophobic building blocks and the thermodynamics of the interactions between the two blocks and with solvent molecules are key aspects when it comes to determining the size and shape of the resulting aggregates[74]. This is of particular interest when one of the blocks contains a stimuli-sensitive compound as this block can show extraordinary changes in its polarity as a consequence of a change in the stimulus and, therefore, the self-assembly process is then governed by changes in this external stimulus.

Amphiphilic elastin-like block co-recombinamers (ELbcRs) can form nano- or micro-sized structures[114-121] that can be directly injected into systemic circulation without the risk of blocking blood vessels[122-124]. The study presented herein is based on our previous study[119], which demonstrated that di-triblock recombinamers consisting of two or three different ELR blocks can self-assemble into micelles or hollow vesicles upon varying the length and block arrangements in the ELbcRs.

It is well known that salts cause a significant concentration-dependent decrease in Tt and an increase in the transition enthalpy[27]. The effect of an increase in NaCl concentration on the thermal behavior of the ELR is equivalent to an increase in the hydrophobicity of the recombinamer chain. In summary, the effect of NaCl can be interpreted in terms of causing a better organization of the recombinamer in the folded state and a more extensive and better structured corona of hydrophobic hydration surrounding the apolar moieties in the extended state of the recombinamer chain[27].

As a consequence of the aforementioned reduction in Tt, NaCl has been extensively employed during the ELR purification process, as well as in different buffers used for different applications, without taking into consideration the possible morphological effects induced. On some occasions NaCl addition is also used to tune the Tt of different ELRs during use. However, in such cases only the change in Tt is studied without taking into account that salt addition could also result in substantial changes in the way that these recombinamers self-assemble.

In this work we have tried to shed light on the effect of the presence of NaCl on the self-assembly behavior of ELbcRs, and whether the change in thermal properties of the ELbcRs caused by salt

addition has any significant effect on the size and shape of the nanostructures formed. This study explore the possibility of adding NaCl as a simple means of controlling the topographical features of self-assembled ELbcR nanostructures.

5.1.1. Influence of the addition of NaCl into the T_t of ELbcRs.

The recombinant technology employed in the ELbcR production gives us absolute control over their composition at a gene level, thereby allowing total control of block length and composition with a single amino acid precision. All the different ELbcRs used herein were monodisperse and with a totally defined composition. The ELbcRs selected for this study comprises two different building blocks, namely a fixed-size block containing L-alanine (A-block, (VPAVG)) and a variable-length block containing L-glutamic acid (E-block, $[(VPGVG)_2(VPGEG)(VPGVG)_2]$.The E block is no longer temperature sensitive and remains soluble at any temperature[119, 155] at neutral pH, whereas the A block retains its thermal sensitivity and a T_t can easily be identified. The two blocks are in a random conformation and in solution below the T_t of the A block. On the contrary, they are in an aggregated state above the T_t due to the collapsed state of the A block, which give rise to self-assembled nanoparticles. The self-assembly behavior of these ElbcRs was investigated in pure water solutions in a previous study, which determined its ability to form micelles and vesicles[119]. Herein, the effect of the presence of ions on the aggregation process of those ELbcRs will be evaluated.

Table 7: *ELbcRs evaluated in this chapter.*

ELbcR Nomenclature	Amino acid sequence
E50A40	$[(VPGVG)_2(VPGEG)(VPGVG)_2]_{10}$-$(VPAVG)_{40}$
E100A40	$[(VPGVG)_2(VPGEG)(VPGVG)_2]_{20}$-$(VPAVG)_{40}$
E50A40E50	$[(VPGVG)_2(VPGEG)(VPGVG)_2]_{10}$-$(VPAVG)_{40}$-$[(VPGVG)_2(VPGEG)(VPGVG)_2]_{10}$

A good understanding of T_t is crucial when working with ELbcRs, DLS measurements were carried out at a ELbcR concentration of 25 μM as a function of temperature in order to determine the corresponding T_t and to evaluate the stability of the particles formed in order to establish the appropriate working temperature. The thermally driven aggregation monitored by DLS (**Figure 28**) revealed, as expected, that the presence of salts decreases T_t[27]. NaCl concentrations lower than 31.25 mM were not evaluated in this case as those concentrations are too low in order to have a noticeable effect on the T_t. The transition temperature, $T_{t,}$, is taken to be the temperature at which the change in the scattered intensity reaches a value of 50% . A summary of the T_t observed by DLS is presented in **Table 8**.

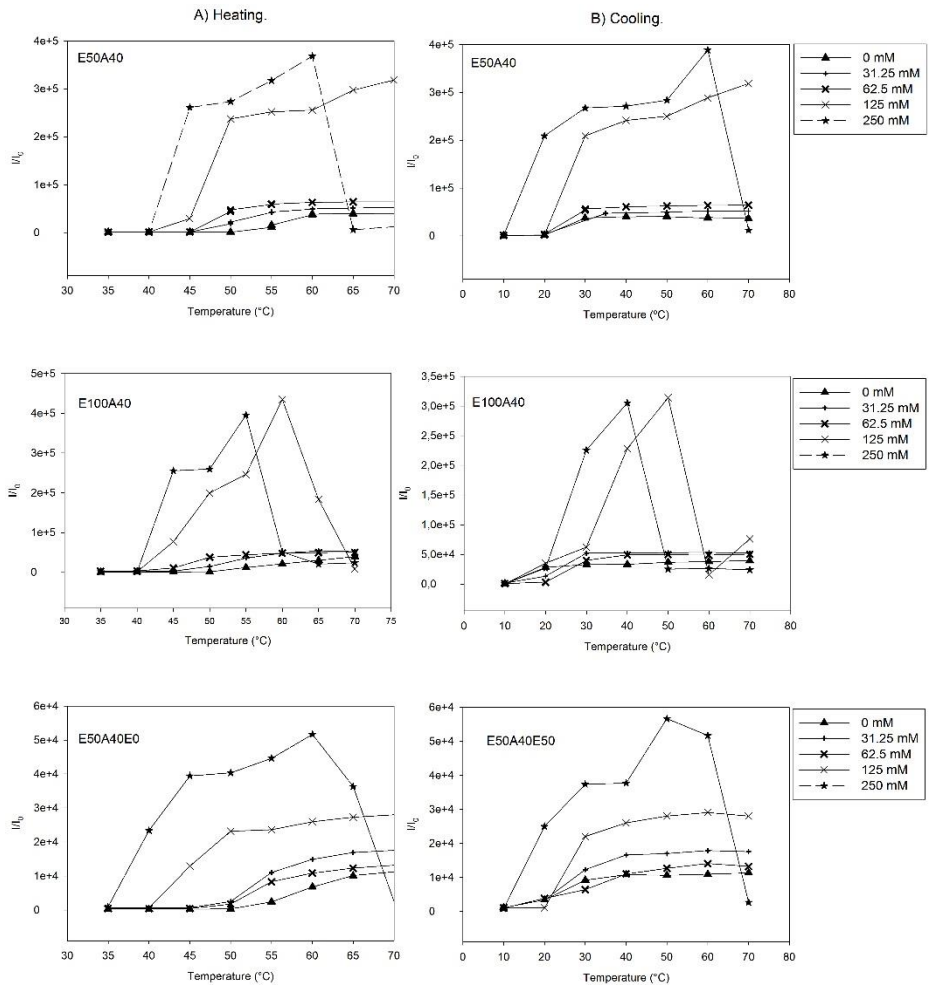

***Figure 28**: Plots of the scattered light intensity vs. temperature A) heating stage B) cooling stage for E50A40, E100A40 and E50A40E50 at different NaCl concentrations.*

Table 8: *T_t of the different ELbcR as function of NaCl concentration*

NaCl concentration [mM]	E50A40 T_t [°C]	E100A40 T_t [°C]	E50A40E50 T_t [°C]
0	56	59	59
31.25	51	53	54
62.5	49	51	54
125	48	48	45
250	43	44	41

Aggregates were readily formed once the T_t was exceeded, as deduced by the increased intensity of scattered light above the T_t. Once the nanoparticles are formed no difference in intensity was observed with further temperature increases for concentrations up to 125.0 mM (E50A40 and E50A40E50) or 62.25 mM (E100A40). In all cases, for a 250.0 mM NaCl solution, an increase in scattering intensity was followed by a marked decrease in intensity as the temperature was further increased. This is attributed to micro-aggregation and subsequent sedimentation due to the phase transition underwent by the E-block as a consequence of the marked decrease in T_t induced by the addition of NaCl. Thus, the E50A40 and E50A40E50 nanoparticles showed high thermal stability for concentrations of up to 125.0 mM, although a slight increase in intensity was observed for 125.0 mM for E50A40 at 65 and 70ºC. In the case of E100A40, this stability is observed up to a NaCl concentration of 62.5mM. All ELbcRs

underwent micro-aggregation and sedimentation in 250.0 mM NaCl solution (E100A40 also at 125.0 mM) when increasing the temperature far above their Tt.

The well-known hysteresis in self-assembly of the A-block[168], together with the reversibility of the nanoparticles, were investigated with a cooling stage (**Figure 28B**). C Complete dissolution of the nanoparticles only occurred under strong undercooling (below 20°C).Similar intensities and sizes were obtained after a new heating process in all cases, thereby confirming the reversibility of the system. In order to observe the stability of the nano-objects formed, samples of the three ELbcRs dissolved in NaCl solutions above 31.25 mM were kept at their corresponding temperature, taken from DLS results, for two weeks. After that time, DLS measurements were again carried out, with comparable light scattering intensity and size values being obtained in all cases (including the sample in absence of NaCl). This stability over time, together with the above-mentioned thermal stability, suggests that these self-assembled ELbcR nano-objects are stable systems.

5.1.2. Dynamic light scattering characterization of NaCl effect on ELbcRs nanoparticles.

Dynamic light scattering measurements were performed in order to shed further light on the part played by NaCl in the self-assembly of ELbcRs. The autocorrelation functions obtained by DLS experiments at 90° were analyzed using the CONTIN algorithm[160]. The large decreases in Tt observed with increasing NaCl concentration made it difficult to establish a single working temperature. As a result, samples up to 31.25 mM NaCl were studied at a temperature of 65°C, whereas

NaCl concentrations of 62.5, 125.0 and 250.0 mM were studied at temperatures of 60, 50 and 45°C, respectively.

The size distributions obtained from this analysis are shown in **Figure 29**. When dissolved in water, the hydrodynamic diameters (Dh) were 140, 205, and 215 nm for E50A40, E100A40 and E50A40E50, respectively, thus agreeing well with previously reported data[119].

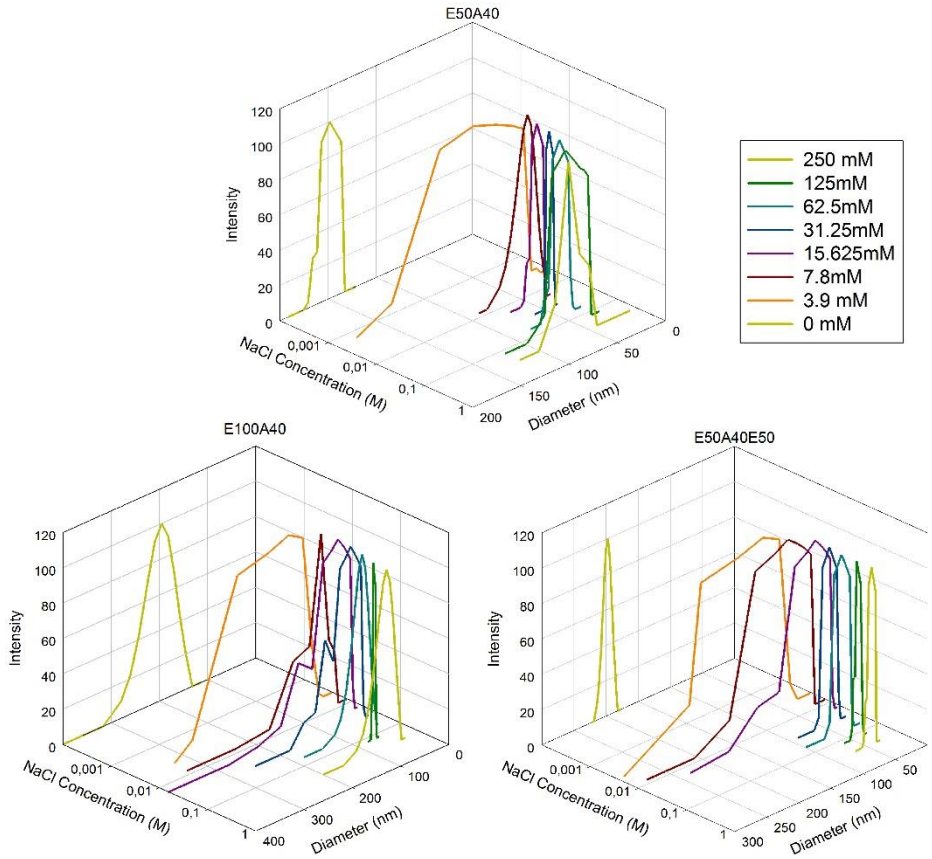

Figure 29: *Size distributions as measured by DLS for E50A40, E100A40 and E50A40E50 at different NaCl concentrations*

Interestingly, the Dh (hydrodynamic diameter) obtained in the presence of NaCl was significantly smaller, especially at the highest concentrations. Moreover, samples of E50A40 and E50A40E50/E100AA40 can be seen to behave differently. The

polydispersity index increased significantly (up to 0.26) for E50A40 at 3.9 mM NaCl with a broad size distribution centered at approximately 80 nm, whereas from this concentration up to 250.0 mM, the size distribution and polydispersity index decreased markedly to approximately 56 nm and 0.05 respectively which represents a 60% size reduction compared with the value obtained in the absence of NaCl (140 nm). E50A40 has been reported to self-assemble into core-shell micelles[119], and although a clear size reduction was still observed, it was not as marked as for E50A40E50 and E100AA40. In contrast, the size reduction for the other two ELbcRs was progressive up to a NaCl concentration of 15.625 mM, after which further addition of NaCl had no significant effect on the size of the nano-objects formed. As can be seen, the size reduction is higher for E100A40 and E50A40E50, which were previously reported to form vesicles when dissolved in water above their Tt[119]. The Dh value for E100A40 shifts from 205 to 66 nm (a 77% reduction), and E50A40E50 exhibits the most marked reduction, decreasing by approximately 80% from 215 to 42 nm. This size reduction is consistent with the idea that the presence of NaCl results in better organization of the recombinamer chains in the folded state, thus leading to more closely packed structures. However, the higher decrease observed for E50A40E50 and E100A40 could also indicate a change of particle morphology.

Interestingly, this reduction in size, together with the populations observed in pure water, was also observed when dissolving the ELbcRs in water, heating the mixture above the T_t and subsequently adding a NaCl solution until the desired concentration was achieved (**Figure 30**).

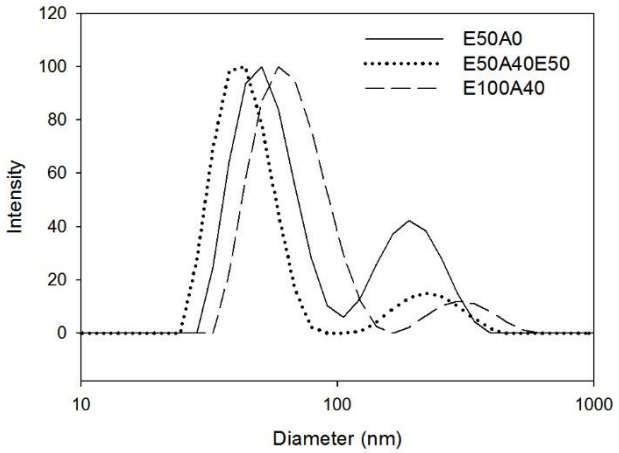

Figure 30: *Size distributions of the ELbcR nano-particles self-assembled in water followed by the addition of NaCl solution up to a NaCl concentration of 62.5mM.*

Although both populations were found, the majority of the nanoparticles correspond to the small size distribution found when dissolved in NaCl solution; no variation was observed within 24 hours. This result suggests that even though the addition of ions is subsequent to nano-object formation, the higher ionic strength of the environment forces the already folded hydrophobic parts to adopt a different, more compacted, conformation. In contrast, a mono-disperse particle distribution is achieved if the self-assembly procedure occurs under sufficiently concentrated saline conditions, with no trace of the assembled sizes found in water.

5.1.3. Static light scattering characterization of NaCl effect on ELbcRs nanoparticles.

In order to shed light on the morphology of the nanoparticles formed, SLS measurements were performed over the ELbcRs concentration range 1.0-8.0 $mg.mL^{-1}$ for scattering angles of between

50° and 130°. The specific refractive index increment (dn/dc) for the three ELbcRs tested showed a minimal dependence on temperature, molecular weight, and NaCl concentration. As such, a dn/dc of 0.160 $mL.g^{-1}$ was used for all three ELbcRs in all cases.

The nD was studied experimentally for the three amphiphilic ELbcRs in a wide range of concentrations (1-8 mg/ mL) and NaCl concentrations (0-0.25M). **Figure 31** shows the linear dependence of nD with concentration for E100A40 solutions at different NaCl concentrations.

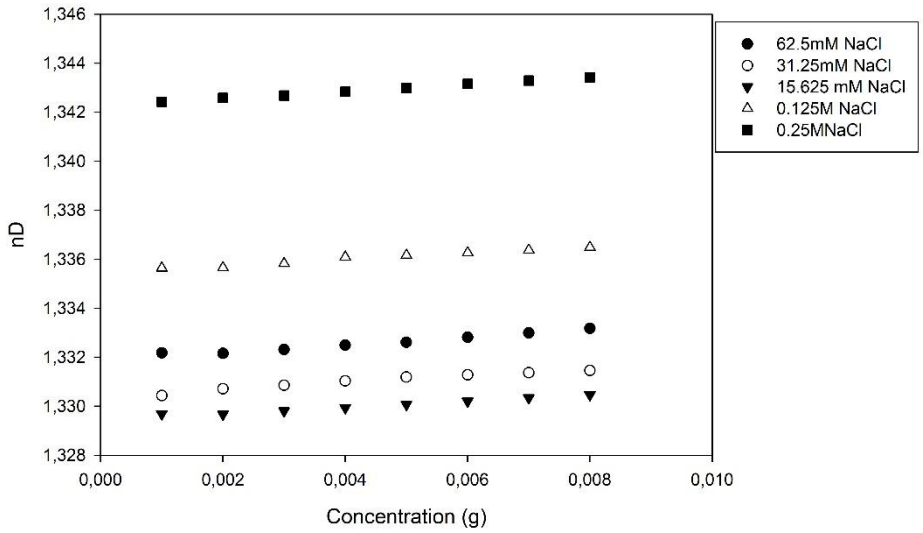

Figure 31: *NaCl concentration dependence of nD for E100A40.*

The value of the specific refractive index increment (dn/dc) was deduced from the slope of plots of the refractive index versus concentration for each ELbcR .The results are listed in **Table 9**.

Table 9: *Specific refractive index increments, dn/dc, for E50A40, E100A40 and E50A40E50 in aqueous solution at NaCl concentrations.*

ELbcR\[NaCl]	***250 mM***	***125mM***	***62.5mM***	***31.25mM***	***15.625mM***
E50A40	0.161	0.158	0.158	0.162	0.159
E100A40	0.165	0.160	0.164	0.164	0.162
E50A40E50	0.162	0.159	0.158	0.160	0.160

A Berry plot was used for the calculation of the gyration radius (Rg) and the molecular weight of the aggregates (MWagg)[169, 170]. **Figure 32** shows the angular (θ) and concentration (c) dependence (Berry plot) for the ELbcRs in 62.5 mM aqueous NaCl solution at 60°C. The apparent molecular weight values for the nanoparticles were estimated by extrapolating c and θ to zero, and the radius of gyration was obtained from the slope of the angular dependence of the Berry plots.

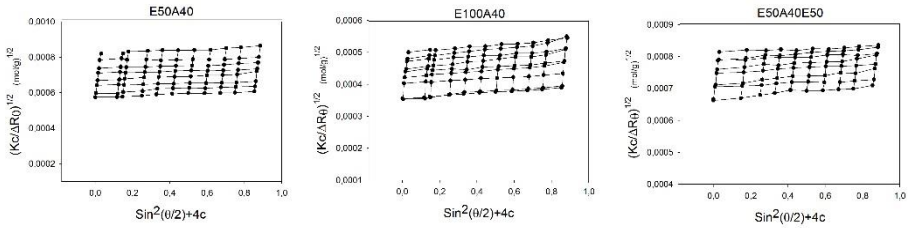

Figure 32: *Berry plots for E50A40, E100A40 and E50A40E50 in 62.5 mM aqueous NaCl solution.*

The average number of aggregation (Nagg), which can be understood as the number of ELbcR chains per nanoparticle, was also calculated by simply dividing Mwagg by the Mw of a single recombinamer chain.

A summary of the light-scattering properties for the different nanoparticles dissolved in the NaCl solutions at which their size is stabilized (above 31.25 mM, lower concentrations presented higher polydispersity, which made the SLS data unreliable) are shown in **Table 10**.

Table 10: *Summary of the light-scattering properties for ELbcRs*

ELbcR	**NaCl[a]**	**$R_h=(D_h/2)$ [nm]**	**R_g [nm]**	**$M_w/10^7$ [g.mol^{-1}]**	**N_{agg}**	**$\rho(R_g/R_h)$**
E50A40	-	74 ± 1	58 ± 2	1.2 ± 0.10	312±26	0.78 ± 0.04
E50A40	+	28 ± 3	23 ± 3	0.7 ± 0.10	200±29	0.82 ± 0.20
E100A40	-	100 ± 3	83 ± 3	2.0 ± 0.20	337±34	0.83 ± 0.05
E100A40	+	33 ± 2	34 ± 4	0.8 ± 0.10	137±22	1.03 ± 0.18
E50A40E50	-	96 ± 2	87 ± 2	1.1 ± 0.10	185±17	0.91 ± 0.04
E50A40E50	+	21 ± 2	26 ± 1	0.2 ± 0.03	38 ± 07	1.24 ± 0.17

[a]- data obtained in pure water, + average values obtained in NaCl solutions

A reduction in N_{agg} with an increase in hydrophilic block length has been reported previously for amphiphilic block copolymers in a given solvent [171, 172]. As the values of R_g, which is related to mass distribution, for both E50A40E50 and E50A40 are essentially the same, and the hydrodynamic ratio (R_h) value for E50A40E50 is significantly smaller than that for E50A40, the higher value of N_{agg} found for E50A40 compared with that for E50A40E50 suggests a completely different molecular arrangement within the nanoparticles. In agreement with the higher size reduction observed, the decrease in N_{agg} for E50A40E50 and E100A40 is significantly greater than that for E50A40. The R_h and R_g values obtained for E50A40E50 and E100A40

in water were similar, and both recombinamers were found to self-assemble into a vesicular structure[119]. However, in the presence of NaCl, the Rh and Rg values for these recombinamers are no longer similar and therefore they cannot be assumed to still self-assemble into the same morphology. These results agree with the previous assumption whereby the nanoparticles are closely packed, thus resulting in a better organization of the chains and suggesting three different morphologies for the three recombinamers.

In order to gain a better insight into the structures formed, we combined the data obtained by DLS and SLS to calculate the ρ ratio, which is a structure-sensitive parameter that provides information regarding the density distribution of the particles and therefore particle morphology. Theoretically, a ρ ratio close to 1 is attributed to a vesicle type morphology, ρ values around 0.77 are generally considered to indicate spherical micelles, whereas a random coil has a ρ value of 1.5[161, 173]. Thus, this parameter is crucial in order to understand the conformation of the nanoparticles in solution.

The ρ ratios previously reported for E50A40, E100A40 and E50A40E50 in water were 0.78, 0.83, and 0.91, respectively. E50A40 was considered to be micellar in nature whereas the other two correspond to vesicles[119]. A combination of light scattering and microscopy techniques were used to determine E100A40 as a vesicle when its ρ value in water (0.83) is closer to the micellar one. A clear discussion about it can be found elsewhere[119].

The ρ values shown in **Table 10** suggest, once again, the different self-assembly behaviors shown by the three different recombinamers. Thus, whereas E50A40 underwent only a slight increase in ρ value (from 0.78 to 0.82 ± 0.2), thereby indicating that

addition of NaCl should not promote a significant change in morphology, the other two exhibited a marked increase in this parameter, thereby indicating a substantial change in morphology. In light of those results, we can hypothesize that, in the presence of NaCl, E50A40 retains the micellar structure found in pure water. The small size reduction is attributed to a slightly better organization of the self-assembling blocks, which results in a stronger hydrophobic interaction and a reduction in the amount of water present in the self-assembled hydrophobic blocks, and therefore a more closely packed structure of the hydrophobic core. Both these proposals are consistent with the higher apparent hydrophobicity of the apolar block caused by the presence of salts, as described elsewhere[27] for different ELRs.

Although the above mentioned size reduction is more marked in the case of E100A40 and E50A40E50, major differences are also found between them, thereby indicating that both the recombinamer sequence, molecular weight and polarity as well as the way in which the distinct blocks are arranged within the chain have a crucial impact on the self-assembly procedure, as discussed elsewhere[42]. Although both ELbcRs experienced an increase in the ρ value, E100A40 appears to retain the vesicle morphology exhibited in water (ρ ~ 1 in NaCl) whereas E50A40E50 shows a ρ value (1.24 ± 0.17) half way between vesicles and a random coil conformation (ρ = 1.5)[161, 173], thereby suggesting that the nanoparticles formed by this ELbcR could be vesicles with some degree of structural instability as they are approaching, but have not yet reached, the conditions required for a transition from a vesicular arrangement to a different structure, such as micellar or nanofibrillar.

A schematic representation of this thermally driven nanoparticle formation is presented in **Figure 33**.

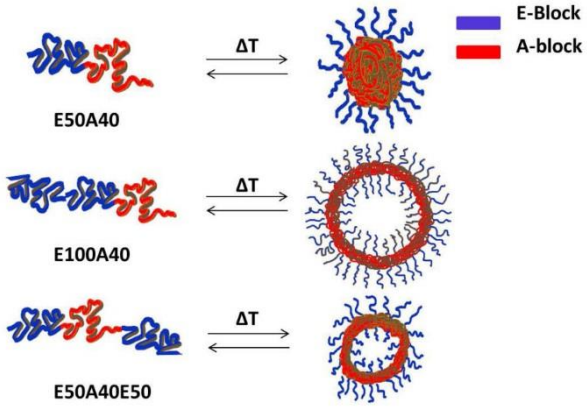

Figure 33: *Schematic representation of micelles and vesicles obtained by self-assembly of the ELbcRs in saline solutions.*

5.1.4. Cryo-TEM characterization of ELbcRs in NaCl solutions.

In order to shed light on this working hypothesis, TEM experiments were carried out at a mid-range NaCl concentration of 62.5 mM.(**Figure 34**).

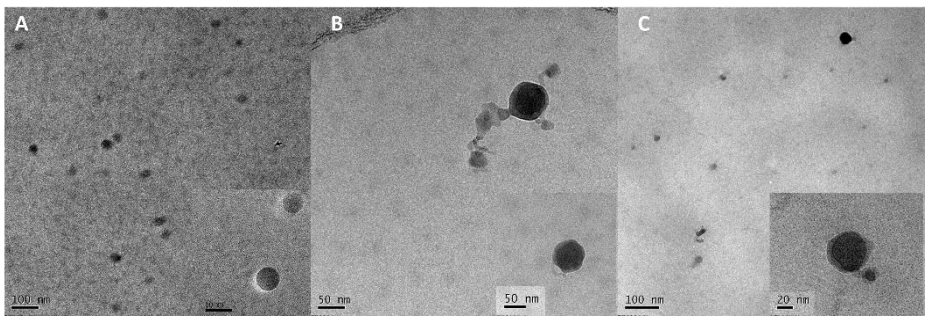

Figure 34: *Cryo-TEM images of the self-assembled nanoparticles: A) E50A40, B) E100A40, C) E50A40E50 in a 62.5 mM NaCl solution.*

Image analysis and particle-size measurements showed good agreement between the sizes obtained by Cryo-TEM and DLS. From a morphological point of view, it is possible to perceive the difference in morphology between the vesicle shape of E100A40/ E50A40E50 and

the micelle conformation of the E50A40 in agreement with the diverse ρ values found.

5.1.5. Effect of other salts into the ELbcRs self-assembly.

As a simple test of the potential effect of other anions/cations in the self-assembly of these ELbcRs, DLS experiments were carried out with a selected set of different salts (KCl, $CaCl_2$, Na_2HPO_4 and Na_2SO_4).

According to the Hofmeister series[75, 76], the ability of anions and cations to salt proteins out of solutions is as follows[174]:

$$CO_3^{2-} > SO_4^{2-} > S_3O_3^{2-} > H_2PO_4^{-} > F^{-} > Cl^{-} > Br^{-} > NO_3^{-} > I^{-} > SCN^{-}$$

$$NH_4^{+} > Cs^{+} > Rb^{+} > K^{+} > Na^{+} > Li^{+} > Ca^{2+} > Mg^{2+}$$

A salt concentration of 62.5 mM was employed in all cases. As expected, the reduction in Tt provoked by $CaCl_2$ and Na_2SO_4[175] was too high and therefore it proved impossible to analyze all samples at the same temperature. As a result, scattered-light intensity versus temperature and DLS experiments (data not shown) were performed to determine the working temperature (60ºC for NaCl, KCl and Na_2HPO_4, and 40ºC and 45ºC for Na_2SO_4 and $CaCl_2$ respectively).

Interestingly, two different behaviors were observed. Thus, whereas KCl and Na_2HPO_4 affected the size of the nano-objects in an essentially identical manner to NaCl (**Table 11**), the other two salts resulted in completely different self-assembled structures.

Table 11: *Hydrodynamic diameter measured by DLS for ELbcRs dissolved in different 62.5 mM salt solutions.*

ELbcR	Salt	Dh(nm)
E50A40	KCl	53.50 ± 4.30
	NaCl	55.68 ± 6.86
	Na_2HPO_4	54.15 ± 5.24
E100A40	KCl	64.90 ± 5.20
	NaCl	66.52 ± 4.82
	Na_2HPO_4	70.15 ± 4.73
E50A40E50	KCl	41.55 ± 2.87
	NaCl	42.10 ± 3.00
	Na_2HPO_4	37.40 ± 3.41

The addition of Na_2SO_4 and $CaCl_2$ induced clearly different behavior in the ELbcRs, with E100A40 and E50A40E50 self-assembling into two completely different particle distributions in solutions of these two salts. Thus, although the majority of nanoparticles were found in a narrow distribution centered at approximately 20 nm, a significant group containing aggregates of approximately 350 nm was also observed.

In contrast, E50A40 showed a single broad peak, thereby indicating highly polydisperse nanoparticle distributions centered at 95

nm for the $CaCl_2$ solution and at 68 nm for the Na_2SO_4 solution. Surprisingly, despite the polydyspersity of the distribution, the sizes were bigger than those observed in NaCl in both cases.

According to Tomé et al.[176], interaction of the cation with amino acids is masked by the strong interaction between the anion and the system when the anion is a sulfate. Divalent cations (such as Ca^{2+}) are also able to form strong charged complexes with the carboxylate groups, thereby somehow reducing the effect of the anion. Although further studies are still required, it appears that a balance between the competitive interactions of cations and anions with the ELbcRs is a key parameter as regards the stability and monodispersity of ELbcR self-assemblies.

5.1.6. Final remarks.

The effects of co-dissolution of NaCl on the geometry and size of thermoresponsive elastin-like block co-recombinamers has been investigated. The study principally relied on the use of different light-scattering techniques and image confirmation by transmission electron microscopy. It can be concluded that, for a given composition, the ability of these ELbcRs to self-assemble into micelles or vesicles is highly affected by the presence of co-dissolved Na^+ or Cl^- ions. Interestingly, the presence of NaCl, and the concomitant changes in the apparent hydrophobicity of the apolar blocks and their interaction in the segregated hydrophobic domains, does not appear to change the morphology of the self-assembled nano-objects. Thus, in the compounds studied, those recombinamers that self-assemble into vesicles when dissolved in neat water remain as vesicles in the presence of NaCl. Similarly, those compounds that form micelles in water retain their micellar structure in the presence of salts. However, NaCl addition

has an extraordinary effect on the size of these aggregates, with NaCl causing a substantial decrease in nanoparticle size in all cases. Interestingly, there is no linear dependence between particle size and NaCl concentration. In contrast, there is a two-state dependence in all cases in which, for a small range of low NaCl concentrations, the self-assembled nanostructures (either micelles or vesicles) switch quite abruptly to a lower diameter, with further NaCl addition having no further effect on either size or shape. This is relevant from the viewpoint of potential applications, especially for the ELbcRs E100A40 and E50A40E50, since they do not lose their vesicular structure. Vesicle formation is relatively rare in self-assembled ELRs and is highly interesting due to the potential use of such structures for drug and gene delivery, particularly for both hydrophobic and hydrophilic drugs. In summary, NaCl addition is a simple and additional means of controlling nanoparticle size.

Additionally, the effect caused by NaCl is not exclusive as other salts containing different cations and anions also have a profound effect on the self-assembly behavior of these ELbcRs. Interestingly, these effects are different in some cases within the set of salts studied, thereby suggesting variations in the effect caused by different cations and anions.

5.2. Chapter 2: The effect of surfactants on the self-assembly of a model elastin-like block co-recombinamer: From micelles to an aqueous two-phase system

Abstract: Recent advances in genetic engineering now allow the synthesis of protein-based block co-recombinamers derived from elastin-like peptide sequences with complete control of chemistry and molecular weight, thereby resulting in unique physical and biological properties. The individual blocks of the elastin-like block co-recombinamers (ELbcRs) display different phase behaviours in aqueous solution, which leads to the thermally triggered self-assembly of nano objects ranging from micelles to vesicles. Herein, interaction of the cationic surfactant dodecyl trimethylammonium bromide (DTAB), the anionic surfactant dodecyl sodium sulfate (SDS) and the non-ionic surfactant octyl-β-glucopyranoside (OG) with an ELbcR has been investigated by dynamic light scattering (DLS), ζ-potential and cryo-transmission electron microscopy (Cryo-TEM). At 65 ºC and neutral pH in aqueous solution, the ELbcR (E50A40) is associated into micelles with a diameter of 150 nm comprising a hydrophobic (A) core and a hydrophilic (E) anionic (from the glutamic acid residues) corona. The size of these self-assemblies can be controlled by adjusting co-surfactant concentrations. Although the effects of surfactants on the self-assembly behavior of ELbcRs depends on the hydrocarbon chain length and head group of the surfactants, a general tendency to increase in size, which in some cases leads to flocculation and a phase-separated state, is observed. These results support the use of surfactants as a highly interesting means of controlling the self-assembly of ELbcRs in aqueous solution, as well as their use in drug delivery or purification processes

The interaction of amphiphilic copolymers with low molecular weight surfactants has attracted considerable attention in recent years because of the possibility of designing nano-objects with novel functionalities[89, 90] due to the fact that the addition of surfactants may induce aggregation of the copolymer or change the aggregation state of the pure polymeric micelles[91]. Copolymers and surfactants frequently carry opposite charges, thus meaning that the interaction between them is similar to the formation of polyelectrolyte complexes[92]. Surfactant-copolymer interactions are primarily governed by both electrostatic (between the surfactant head groups and the polyelectrolyte side groups) and hydrophobic interactions (between the hydrophobic backbone of the polyelectrolyte and the alkyl chains of the surfactant)[93-95]. The binding of ionic surfactants to oppositely charged polyelectrolytes occurs via two mechanisms: initially by ion-exchange and then, at higher surfactant concentrations, by cooperative binding[96]. The polyelectrolyte nature of these complexes and the fact that multi-component materials can enable better control of the aggregation properties compared to single surfactant complexes[97] make them promising candidates for a wide range of possible applications[98], for example a) in the controlled release of drugs, taking advantage of the specific binding properties of a copolymer with a very small amount of surfactant in the coating[99], b) in mimicking the cytoplasmic organization of cellular microcompartments, or c) in the purification of proteins and the extraction of other biomolecules[100].

In this work we synthesized an ELbcR containing two different building blocks that has previously been well described[155]. The first block comprises 10 pentaicosapeptide repeats of $[(VPGVG)_2(VPGEG)(VPGVG)_2]$ (E50), a well-known pH-responsive

recombinamer, and the second comprises 40 pentapeptide repeats of (VPAVG) (A40), a thermoresponsive recombinamer with no pH responsiveness. In general, the blocks that form part of the co-recombinamer structure were found to be in a soluble extended state when cooled below their T_t and in an aggregated nanoparticle-type state above T_t[119]. In addition, the T_t values are only directly affected by pH for the block with glutamic acid (E) in its composition due to the presence of side chains sensitive to pH changes.

Surprisingly, the effect of low molecular weight surfactants on the aggregation behavior of ELRs has received relatively little attention[177-180]. Ionic surfactants, especially anionic surfactants such as sodium dodecyl sulfate (SDS), are known to be able to modify the thermosensitive behavior of ELRs as a result of intensive polymer-surfactant interactions and the formation of charged polymer/surfactant complexes[181].Thus, while the most common pattern of ELR/surfactant interaction results in destabilization of the polymeric micelles, there is an increasing amount of evidence in the literature pointing to the fact that the presence of ionic surfactants could induce additional effects[98]. Cationic surfactants, especially dodecyl trimethylammonium bromide (DTAB) and cetyl trimethylammonium bromide (CTAB), are often introduced as oppositely charged surfactants to form complexes with block copolymers containing anionic polyelectrolyte segments, thus allowing the solubility and thermosensitivity of the polymer to be modified. However, to the best of our knowledge, there are no studies concerning the influence of cationic surfactants on the aggregation behavior of ELRs. This is most probably because cationic surfactants interact more weakly with polar polymers than anionic surfactants. Nevertheless, the interaction with cationic surfactants has been found to

be of interest[91, 182]. Non-ionic surfactants (e.g. Triton X-100) do not alter the phase transition of elastin-like recombinamers[28]. Within this framework, we examined the effect of the addition of surfactants on the temperature-dependent critical phenomena of E50A40 in aqueous solution as well as on the resulting self-assembled nanostructures using several physicochemical methods, such as dynamic light scattering, zeta potential, and cryo-transmission electronic microscopy, in order to study the phase-transition mechanism and nanostructures of ELbcR/surfactant systems in aqueous solution. In order to isolate the effects of the polar head of the surfactant on the aggregation properties, and the role played by the hydrophobic interaction between the hydrophobic block of the ELbcR and the alkyl chains of the surfactant, three surfactants with similar hydrophobic tails, namely anionic SDS, cationic DTAB and non-ionic OG, were chosen (**Figure 35**). The pH of the ELbcR was neutralized to 7.0 in all experiments to avoid including this variable in the study of the properties of E50A40 in the presence of surfactants.

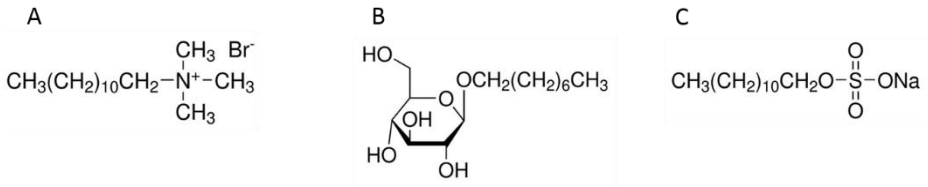

***Figure 35**: Chemical structure of the different surfactants employed in this work, A) DTAB, B) OG, and C) SDS.*

5.2.1. Determination of E50A40/surfactant complexes T_t

The temperature sensitivity conferred by the A-block in the ELbcR (E50A40) has been studied. The production of ELbcRs using recombinant technology provides us with absolute control over their composition, which is mainly monodisperse. The ELbcR selected for

this study comprises two different building blocks, one containing L-alanine [(VPAVG)] (A-block) and one containing L-glutamic acid [$(VPGVG)_2(VPGEG)(VPGVG)_2$] (E-block). The A-block possesses a hydrophobic character and has previously been reported in the literature to be a more "plastic" than "elastic" pentapetide[183, 184], presenting a hysteretic self-assembly behavior. The E block loses its thermal sensitivity at neutral pH due to deprotonation of the carboxylic groups of the glutamic acid, which therefore become negatively charged with a more hydrophilic character than the A block, thereby conferring an amphiphilic nature on ELbcRs. The ELbcR used in this study was purified by ITC and its purity confirmed by SDS-PAGE and MALDI-TOF, as described previously[155].

When working with ELbcRs, a good understanding of T_t is essential. In the case of ELbcRs, the presence of one block has an impact on the T_t of the other. Thus, even at pH values above the pK_a of the γ-carboxylic group, at which the E block is unable to show an LCST transition, it nevertheless still has an influence on the LCST behavior of the A block[155].

In order to evaluate the effect of the addition of different charged surfactants on the T_t of the ELbcRs, dynamic light scattering measurements were carried out using aqueous surfactant solutions with concentrations ranging from 0 to 16 mM. The temperature dependence of the intensity of scattered light when heating ELbcR/surfactant solutions is shown in.**Figure 36**.

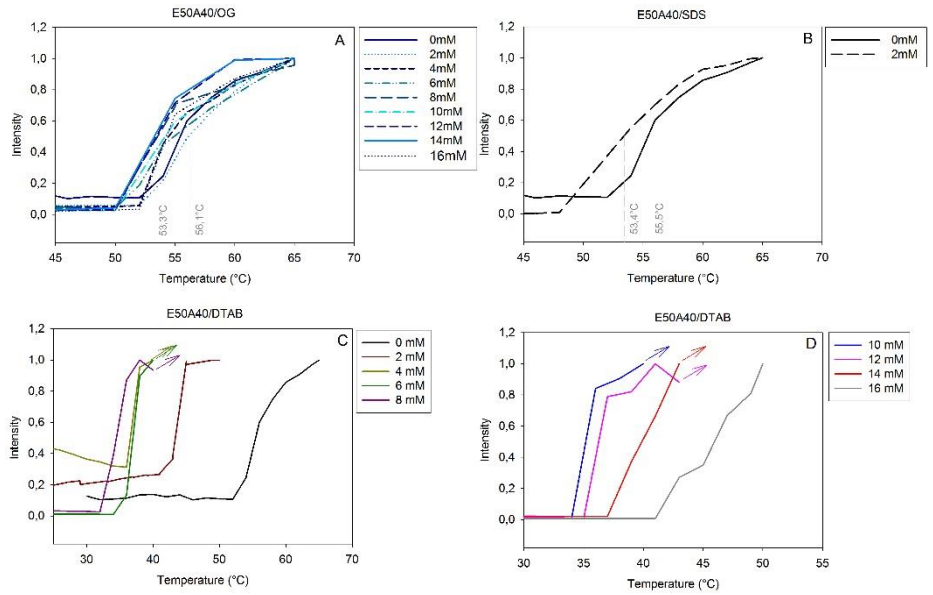

Figure 36: *Normalized intensity profile of scattered light as a function of temperature for E50A40 and different concentrations of surfactant solutions. A) E50A40/OG, B) E50A40/SDS, C & D) E50A40/DTAB. Arrows represent the fluctuation of the scattered light intensity as a result of flocculation of the ELbcR/DTAB complex. Representation of these points would make visualization of the T_t impossible.*

The transition temperature (T_t) is taken to be the temperature at which the change in the scattered intensity reaches a value of 50%. As expected, the addition of octyl-β-glucopyranoside had no significant effect on the T_t (**Figure 36A**), with temperatures ranging from 53.3 to 56.1 °C being obtained for the ELbcRs.

Previous studies have shown that SDS can increase or decrease the T_t of ELRs depending on its concentration and the molecular weight of the ELR[178, 179]. Indeed, Yamaoka *et al.* have shown that SDS strongly interferes with the aggregation of ELRs[178] and that addition of 0.17 mM SDS to a dilute peptide solution (0.002%) suppresses the aggregation process completely. Similarly, Ghoorghian *et al.* have

shown that the addition of SDS to an ELR solution leads to an overall decrease in micelle stability[180], with micelles being stable at up to 0.02% SDS. As a result, there appears to be a limit to the range of SDS concentrations in which micelles can form. In our case, negatively charged SDS suppresses self-assembly at concentrations higher than 2 mM. Surprisingly, this concentration of SDS had no significant effect on T_t (**Figure 36B**).

The addition of positively charged DTAB had a very striking effect. Thus, for concentrations up to 8 mM (**Figure 36C**), T_t decreased in an almost linear manner, whereas further addition resulted in an increase in T_t (**Figure 36D**). We propose that this behavior is probably due to charge screening between the E-block and the polar head of the surfactant, which increases the hydrophobicity of the ELbcR in a similar manner to NaCl[27], thus provoking a decrease in T_t. Once all the glutamic acid residues have been neutralized, the entire ELbcR/surfactant complex becomes positively charged and therefore less hydrophobic, thus resulting in an increase in T_t.

A summary of the T_t values for different ELbcR/surfactant solutions is shown in **Table 12**..

Table 12: *T_t values for the different ELbcR/surfactant solutions.*

Concentration (mM)	E50A40/ Surfactant T_t (°C)		
	SDS	**DTAB**	**OG**
0	55.5	55.5	55.5
2	54	43.5	56.1
4	-	36.5	54.5
6	-	36.5	55.2
8	-	34	53.6
10	-	35	54.1
12	-	36	53.6
14	-	39.6	53.3
16	-	46	54.2

5.2.2. Dynamic light scattering characterization of E50A40/surfactant complexes.

Dynamic light scattering measurements were performed in order to shed further light on the part played by surfactants in the self-assembly of ELbcRs. The DLS results for the ELbcR without surfactant above T_t suggest the presence of nano-objects with a narrow size distribution centered at 150 nm and a very low polydispersity index (0.005), thus indicating the uniformity of the nanoparticles formed, as reported previously[119].

The effect of the different surfactants can already be appreciated from the correlation functions obtained by DLS (**Figure 37**). In contrast, once DTAB is added, this uniformity in the objects formed

upon self-assembly disappears, with a clear increase in the polydispersity index.

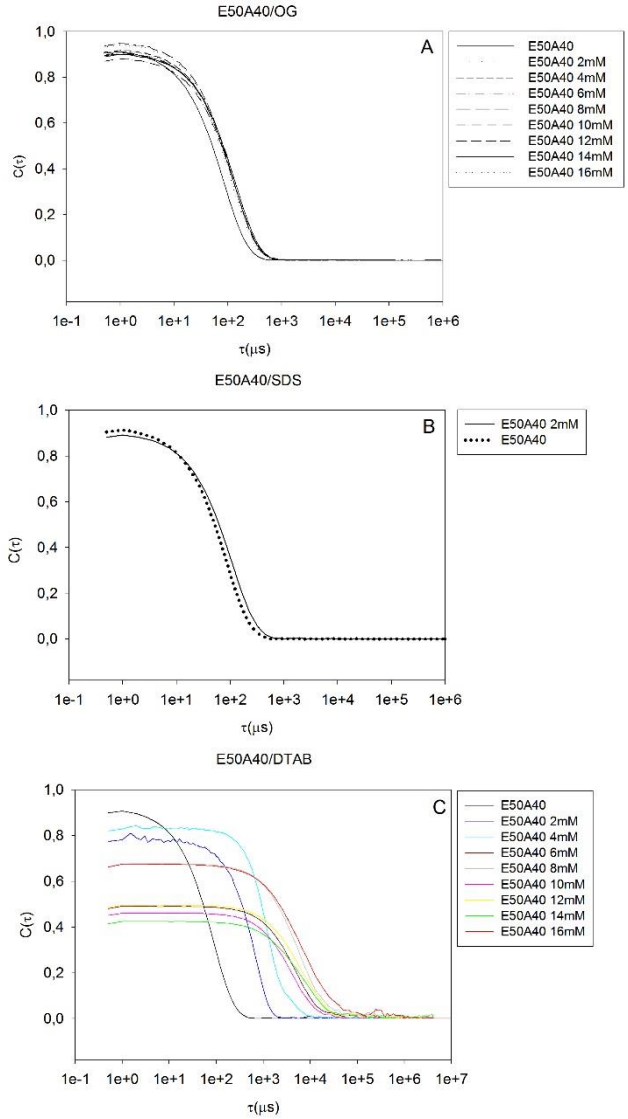

Figure 37: *Autocorrelation functions obtained by DLS for A) E50A40/OG, B) E50A40/SDS, C) E50A40/DTAB.*

The correlation functions showed a completely different behavior for the complex depending on the surfactant employed. Thus, OG and SDS complexes showed a very similar, concentration-

independent correlation function to that obtained for E50A40 (**Figure 37A**, **Figure 37B**), thus indicating similar assemblies to those found for E50A40. In contrast, the effect of DTAB on the delay time can readily be seen even at concentrations as low as 2 mM (**Figure 37C**). This increase in delay time suggests the presence of large particles or aggregates and would appear to indicate that the principal association between E50A40 and the surfactant is due to charge interaction. Similarly, the hydrophobic interaction between the hydrophobic block of the ELbcR and the alkyl chains of the surfactants would appear to have little influence on the self-assembly process, even at high surfactant concentrations, as can be seen from the correlation functions for octyl β-glucopyranoside.

The correlation functions were integrated using the CONTIN algorithm[160] in order to obtain the self-assembly size distributions (**Figure 38**).

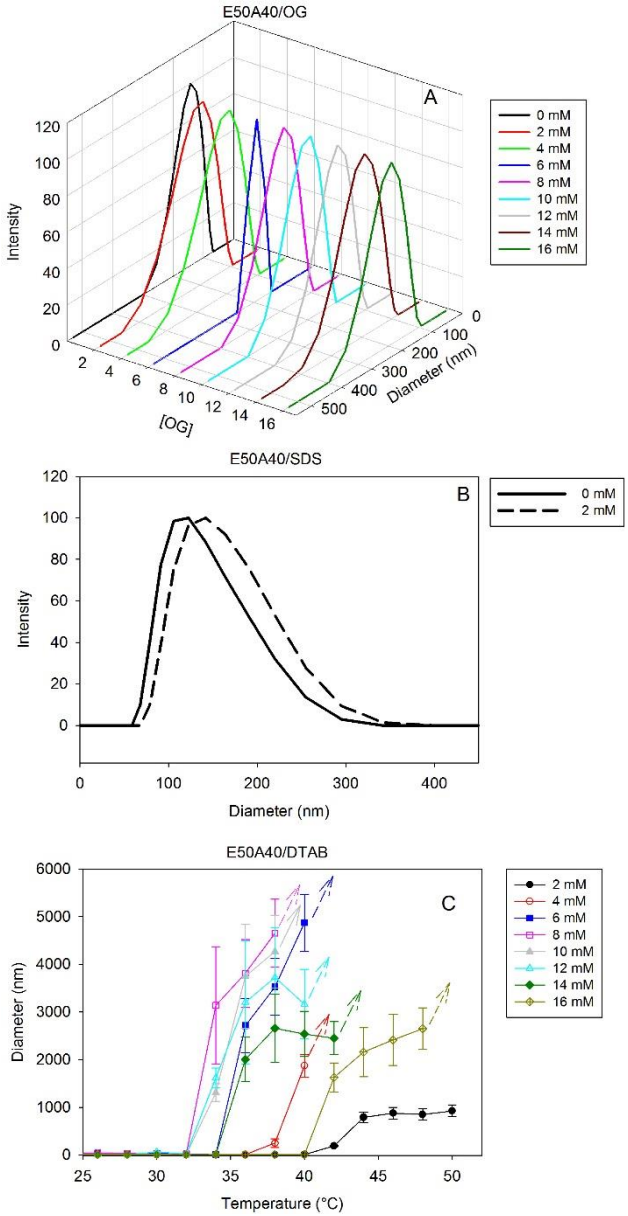

***Figure 38**: A) Temperature-dependent size distribution of E50A40/OG, B) Size distribution of E50A40/SDS as measured by DLS at 65°C, C) Evolution of mean E50A40/DTAB diameter with temperature.*

Interestingly, despite the apparently limited role played by the hydrophobic interaction between the hydrophobic parts of both the ELbcRs and the surfactants, the addition of OG had a non-negligible, concentration-independent effect on the size of the nanoparticles that resulted in a 24% increase in the average hydrodynamic diameter from 150 to 186 nm (**Figure 38A**), probably due to hydrophobic interactions between the A block of the ELbcR and the alkyl chains of the surfactant. This small increase and the concentration independence seem to indicate that, at this ELbcR concentration, the hydrophobic interaction between the two molecules is limited, reaching saturation at OG concentrations as low as 2 mM. This limited association between ELbcRs and OG suggests use of the latter as an effective surfactant for purification purposes.

The size distributions showed very little effect of the addition of negatively charged surfactants (SDS) (**Figure 38B**), exhibiting a slight increase in both the average hydrodynamic diameter (7% increase) and polydispersity index. Kim *et al.* have suggested that charge repulsion may limit the association of ELbcRs with a high density of glutamic acid units[124]. It seems plausible that a similar repulsion effect between SDS and the glutamic acid residues, which hampers the hydrophobic interaction, is taking place here and is responsible for the smaller size increase observed in comparison with that observed for E50A40/OG.

DLS measurements were performed for SDS and OG at 65 °C as further temperature increases had no effect on either the nanoparticles or the thermal stability shown by this ELbcR[119].

DTAB solutions did not exhibit this thermal stability at all concentrations, thereby suggesting a two-step aggregation process. Figure 3C shows the evolution of the hydrodynamic diameter with

temperature. Lower DTAB concentrations (<2 mM) did not lead to flocculation of the complexes, as can be seen from the similarity of the diameters (<1000 nm) observed above T_t. For concentrations higher than 2 mM, the self-assembly process begins with the formation of aggregates a few micrometres in diameter followed by aggregation of these aggregates and subsequent flocculation over a short time period. These large aggregates are represented by upwards arrows in **Figure 38C**. The addition of small quantities of DTAB has a marked impact on the self-assembled structures formed by E50A40, changing from a monodisperse 150 nm size distribution (micelles) to a polydisperse distribution (microaggregates), thereby suggesting that possible charge interactions lead to a hydrophobic "tri-block" that aggregates due to the temperature responsiveness of the ELbcR.

The reversibility of the process observed for the three ELbcR/surfactant complexes is noteworthy. Complete dissolution of the assemblies only occurred under strong undercooling, thus indicating that the presence of surfactants has no effect on the well-known hysteresis behavior in the self-assembly behavior of the A-block[168]. Comparable intensities and sizes were obtained after a new heating process in all three cases, thus confirming the reversibility of the system.

A summary of the DLS data is presented in **Table 13**.

Table 13: Summary of DLS data.

Concentration (mM)	Surfactant	D_h (nm)	PDI
0	-	148 ± 2	0.005 ± 0.002
2	DTAB	860 ± 117	0.228 ± 0.048
	OG	174 ± 10	0.112 ± 0.042
	SDS	159 ± 6	0.168 ± 0.048
4	DTAB	1872 ± 242	0.319 ± 0.142
	OG	189 ± 8	0.108 ± 0.018
6	DTAB	4874 ± 597	0.438 ± 0.199
	OG	191 ± 15	0.113 ± 0.041
8	DTAB	4655 ± 710	0.378 ± 0.120
	OG	189 ± 6	0.028 ± 0.015
10	DTAB	4268 ± 761	0.299 ± 0.104
	OG	186 ± 6	0.069 ± 0.010
12	DTAB	3164 ± 730	0.449 ± 0.138
	OG	193 ± 5	0.071 ± 0.022
14	DTAB	2451 ± 348	0.325 ± 0.037
	OG	182 ± 4	0.058 ± 0.012
16	DTAB	2652 ± 436	0.215 ± 0.109
	OG	186 ± 6	0.070 ± 0.024

The hydrodynamic diameter values obtained for the DTAB solutions should be treated with caution as the polydispersity indexes are very high and the CONTIN analysis is less accurate under such

conditions. Despite this, these results indicate the formation of micro-aggregates prior to flocculation of the complex.

5.2.2.1. E50A40/ DTAB kinetic stability.

The diameters observed for the ELbcR/DTAB complex are much larger than those expected for an amphiphilic ELbcR in which the more hydrophobic block collapses above Tt while the other block remains soluble, thus resulting in self-assembled nanoparticles a few hundred nanometers in size[119]. Micron-sized aggregates are characteristic of ELbcRs in which both blocks have collapsed. This situation is encountered when the glutamic acid residue of the hydrophilic block are uncharged, thereby resulting in a double transition corresponding to the transition of each individual block with increasing temperature[155]. In order to shed some light on the aggregation process of these ELbcR/DTAB complexes, their kinetic stability was evaluated. Thus, different concentrated DTAB samples were kept at their corresponding transition temperature, which was measured previously (**Table 12**), for 90 min. Aggregate size and scattered light intensity were then determined (**Table 14**).

Table 14: Summary of the scattered light intensity for ELbcR/DTAB over a period of time at a fixed temperature.

DTAB Concentration (mM)	Temperature (°C)	Time (min)	Intensity (kcps)
2	43.5	5	4586 ± 92
		90	4931 ± 104
	65		10534 ± 636
4	36.5	5	1179 ± 77
		90	1586 ± 18
	65		324796 ± 20225
6	36.5	5	1791 ± 11
		90	3541 ± 30
	65		66390 ± 14564
8	34	5	2315 ± 15
		90	2273 ± 107
	65		502094 ± 11375
10	35	5	3410 ± 326
		90	3365 ± 243
	65		151565 ± 13064
12	36	5	5207 ± 421
		90	13491 ± 4283
	65		97581 ± 19275
14	39.6	5	5473 ± 728
		90	11,386 ± 5809
	65		360425 ± 31230
16	46	5	33158 ± 18,284
		90	46087 ± 15361
	65		425331 ± 28429

As can be seen for **Table 14**, the scattered light intensity remains constant as long as the temperature is kept invariable. Once the temperature is increased to 65 °C a sharp increase in intensity is found for all concentrations studied. The size of the aggregates was found to remain constant at the T_t, subsequently increasing with a further increase in temperature, as can be seen from **Figure 38C**. The size distributions are shown in **Figure 39**.

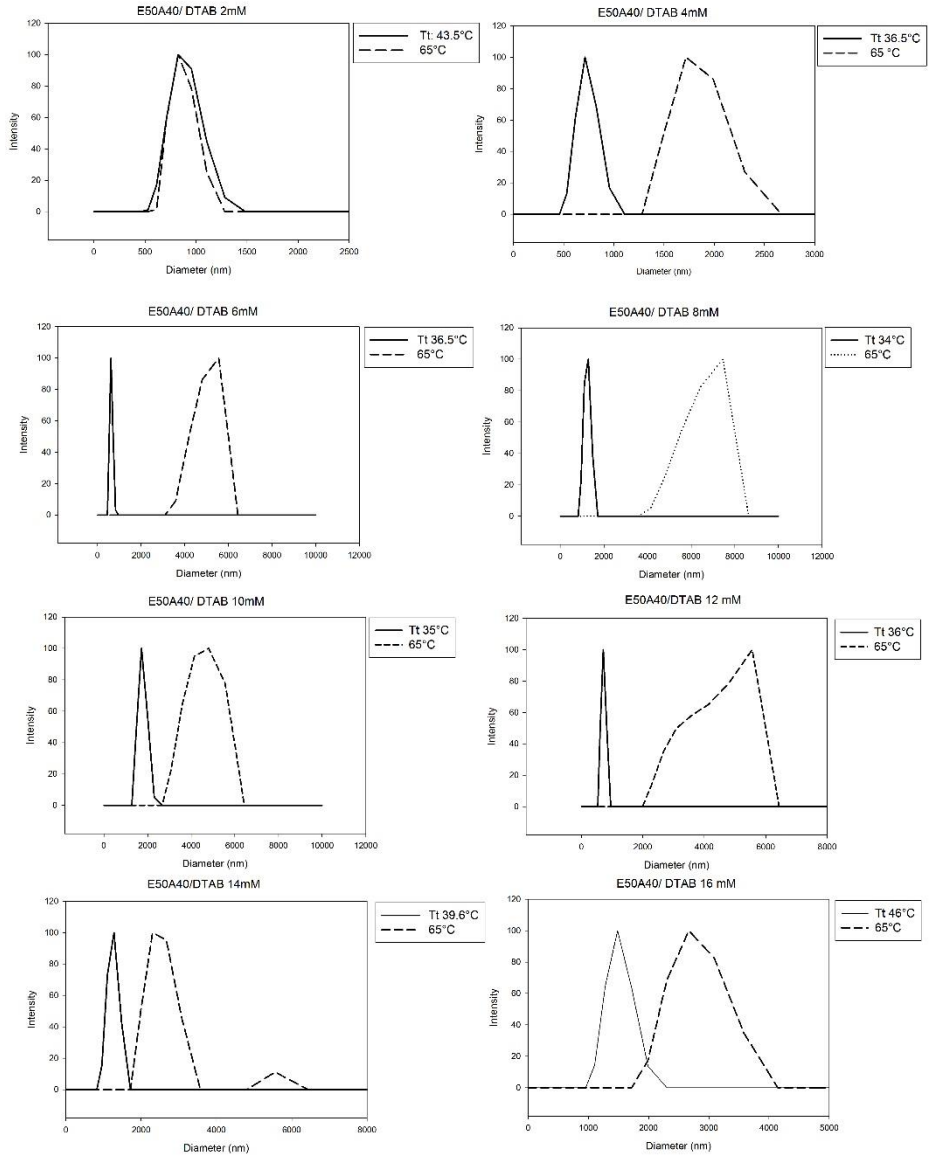

Figure 39: *Size distribution of ELbcR/DTAB as measured by DLS after 90 min at their corresponding T_t and at 65°C*

In light of these results, it can be concluded that the ELbcR/DTAB complexes are kinetically stable and, therefore, that the flocculates form as a result of aggregation of smaller aggregates due to the collapse of both blocks of the ELbcR as the temperature increases.

5.2.2.2. Influence of the formulation route in E50A40/surfactant complexes.

Recent studies have suggested that mixing strongly interacting nanosystems provides out-of-equilibrium structures, thus meaning that the formulation route (mixing order, speed, etc.) has a crucial effect on the final assemblies[185, 186]. In order to test whether the way in which ELbcRs and surfactants are mixed has an effect on the resulting self-assembled structures or not, four different mixing routes were tested. The present study was carried out by adding the corresponding surfactant solution to the ELbcR solution at 4 °C. Inverting the mixing order (adding the ELbcR to the surfactant solution) at 4 °C, and mixing the two components at 65°C, at which the self-assembled ELbcR nanoparticles have already formed, were therefore evaluated. A surfactant concentration of 8mM was selected for DTAB and OG, whereas 2mM was chosen for SDS.

The mixing order did not have a relevant effect at either temperature. Interestingly, however, mixing the two components at a temperature above the Tt of the ELbcR, at which the nanoparticles had already formed, did have a marked effect on the resulting aggregates, with the exception of DTAB, for which the same flocculation of the complexes observed previously was observed. As far as SDS and OG are concerned, exactly the same results were obtained with or without addition of the surfactant (**Figure 40A**). In light of these results, the SDS concentration was increased to 4mM as this concentration was previously found to prevent micelle formation. Surprisingly, this did not result in disassembly of the ELbcR nanoparticles (**Figure 40A**). As such, SDS and OG were cooled to 4 °C and then heated again to 65 °C. This resulted in the same 24% and 7% size increase previously found for the OG solution and the 2 mM SDS solution, respectively.

Inhibition of micelle formation for the 4 mM SDS solution was also observed (**Figure 40B**). It can therefore be concluded that ELbcRs must be below their T_t for OG and SDS to have any effect on the self-assembled nanoparticles. In contrast, DTAB interacts strongly with the negatively charged glutamic acids, thus leading to flocculation of the complexes irrespective of the mixing route.

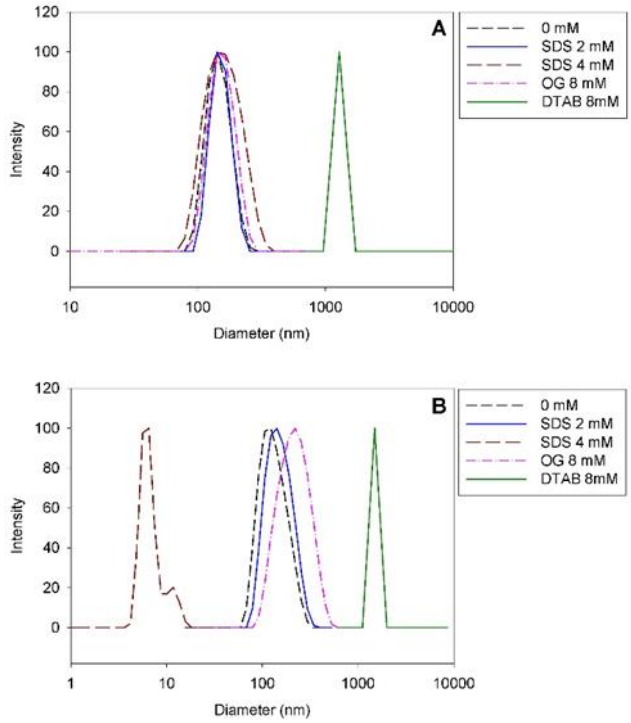

Figure 40: *A) Size distribution of ELbcR/surfactant complexes as measured by DLS at 65 °C when mixing the different components at 65 °C, B) Size distribution of ELbcR/surfactant complexes as measured by DLS at 65 °C when mixing the samples at 65°C, cooling to 4°C and then heating to 65 °C.*

5.2.2.3. Effect of ELbcR concentration on E50A40/surfactant complexes.

Additionally, the influence of ELbcR concentration was studied by varying the concentration up to sixfold (50 μM, 100 μM, 150 μM) while keeping the surfactant concentration constant (8 mM for DTAB and OG, 2 mM for SDS). The ELbcR concentration cannot be increased much further due to the dilute conditions required for light scattering. Under these dilute conditions the only relevant effect of varying the ELbcR concentration was a reduction in T_t (**Figure 41**), as the sizes remained invariable (**Figure 42**). A decrease in the T_t of an ELR with concentration has been reported previously [17].

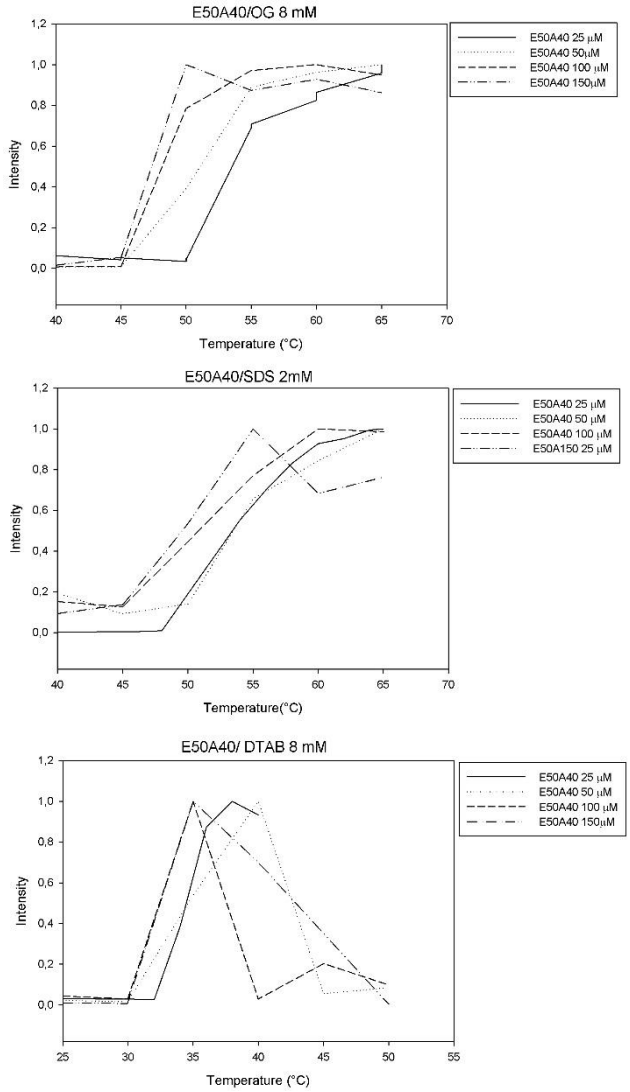

Figure 41: *Normalized intensity profile of scattered light as a function of temperature for different concentrations of ELbcR at a fixed surfactant concentration. T_t.is taken to be taken to be the temperature at which the change in the scattered intensity reaches a value of 50%.*

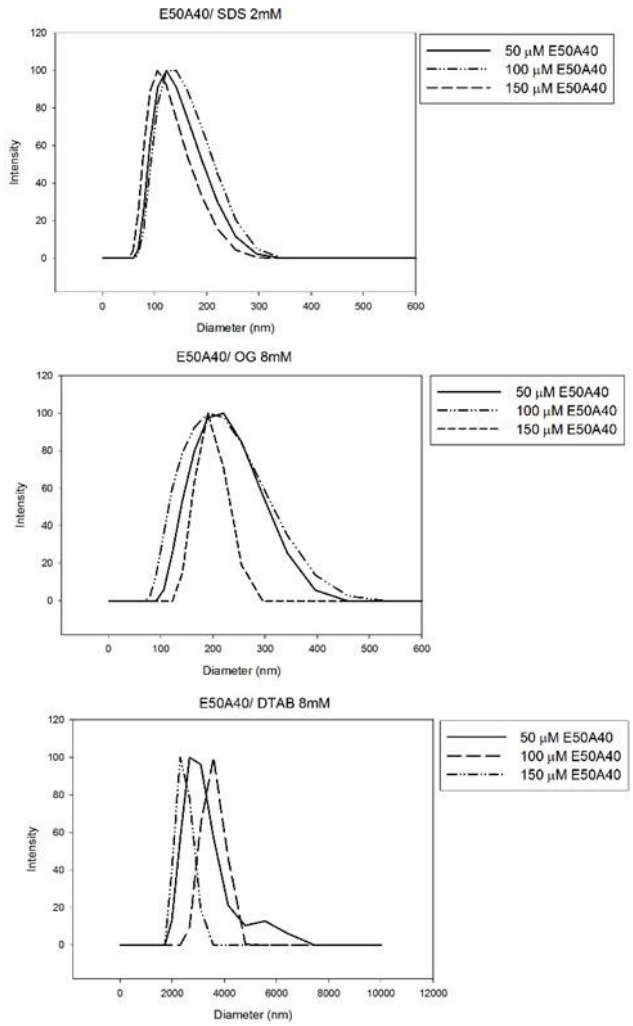

***Figure 42**: Size distribution as measured by DLS a 65°C for different concentration of ELbcR with a fixed surfactant solution.*

5.2.3. ζ-potential characterization of E50A40/surfactant complexes.

Electro-kinetic studies of the self-assembly phenomena were performed in order to gain a better insight of aggregate formation. The ζ-potential and T_t of ELbcR/surfactant complexes as a function of surfactant concentration are shown in **Figure 43** and summarized in **Table 15**.

The ζ-potential of the ELbcR/SDS complexes increased from -31.4 to -43.2 mV. Further increases in SDS concentration led to sufficiently high charge repulsion and thus suppression of the self-assembly process. As expected, no significant variation in ζ-potential was observed for the ELbcR/OG complex, with values in the range -30 to -33 mV being obtained. The addition of OG had no effect on T_t because of the invariance of the effective charge.

In contrast, the ζ-potential increased gradually from -31.4 to -2.77 mV on increasing the DTAB concentration from 0 to 6 mM, thus providing further evidence for the progressive neutralization of the anionic E-block of the ELbcR due to binding of the cationic surfactant. The ζ-potential became positive at DTAB concentrations above 6 mM as the charges of the E block had been completely neutralized due to the incorporation of excess surfactant into the complex.

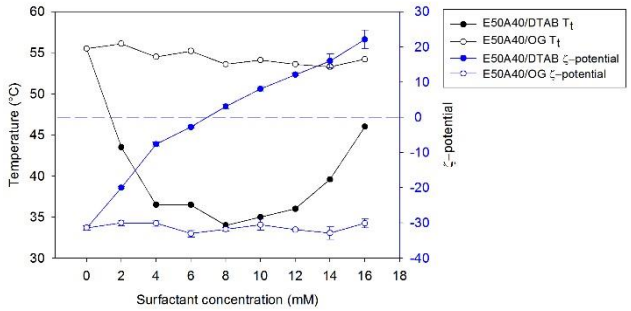

***Figure 43**: Variation in ζ-potential/T_t with DTAB/OG concentration for ELbcR complexes at 65 °C.*

This neutralizing DTAB concentration is coincident with the concentration at which T_t undergoes a large decrease, thus indicating that, once the zeta potential becomes positive, or in other words, once the number of glutamic acids blocked by DTAB is sufficiently high, the hydrophobicity of the environment increases and thus T_t decreases.

This is followed by the reverse procedure, namely an increase in T, due to the increase in the positive charge as a result of a further rise in the DTAB concentration. These results confirm the hypothesis whereby charge screening between the E-block and the polar head of the surfactant is responsible for inversion of the T_t trend with increasing DTAB concentration.

Since the electrophoretic mobilities of the assemblies are mainly governed by charges localized at or near the surface, these ζ-potential results indicate that the presence of surfactants has no impact on the distribution of the blocks in the ELbcR, with the A-block remaining at the core of the micelles and the E-block on the outside.

Table 15: *Summary of ζ-potential data.*

Concentration (mM)	E50A40/Surfactant ζ-potential(mV)		
	SDS	**DTAB**	**OG**
0	-34.40 ± 0.61	-34.40 ± 0.61	-34.40 ± 0.61
2	-43.20 ± 0.9	-20.00 ± 0.27	-30.00 ± 0.74
4	-	-7.62 ± 0.59	-30.10 ± 0.80.
6	-	-2.77 ± 0.36	-33.00 ± 1.00
8	-	3.07 ± 0.61	-31.80 ± 0.50
10	-	8.08 ± 0.65	-30.50 ± 1.50
12	-	12.10 ± 0.40	-31.90 ± 0.30
14	-	16.00 ± 1.93	-32.90 ± 1.80
16	-	22.10 ± 2.70	-30.10 ± 1.33

5.2.4. Cryo-TEM characterization of E50A40/surfactant complexes.

Particle morphology was further characterized by Cryo-TEM (**Figure 44**). The diameters of the particles determined from the Cryo-TEM data matched with the effective diameters determined by DLS, revealing the same trend in particle sizes for different surfactant concentrations as that observed from the light scattering experiments.

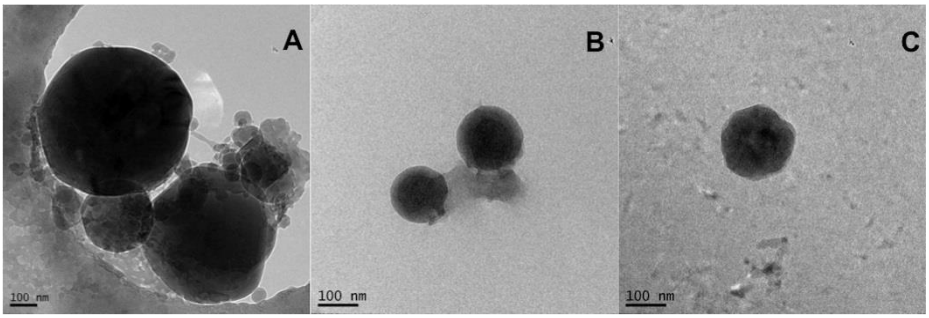

Figure 44: *Cryo-transmission electron microscope images showing the shape and size of the ELbcR structures self-assembled in aqueous solution with co-surfactants: A) 2 mM DTAB B) 2 mM OG C) 2 mM SDS. The ELbcR solutions were incubated at 65 °C in a water bath for 10 minutes before sample preparation for the microscope.*

5.2.5. Final remarks.

The effects of surfactants on the self-assembly and thermoresponsive behavior of elastin-like recombinamers have been investigated. An elastin-like diblock co-recombinamer (ELbcR) has been designed, biosynthesized, and purified. When heated to temperatures above its transition temperature (T_t), this water-soluble ELbcR (E50A40) self-assembles into micelle-like structures with a hydrodynamic diameter of 150 nm comprising a hydrophobic alanine (A) core and a water-swollen glutamic (E) corona.

These results show that the size of these micelles can be controlled by adjusting the co-surfactant concentrations, with the addition of an oppositely charged surfactant resulting in a huge increase up to the micro-scale, At sufficiently high concentration and temperature, these micelles tend to flocculate. A smaller size increase can be achieved by adding a non-ionic surfactant. A similar effect can be seen with SDS conjugation prior to complete disruption of the self-assembling process. Although these results show a considerable effect

on the sizes of the assemblies as a result of the hydrophobic interaction between the alkyl chains of the surfactants and the hydrophobic blocks of the ELbcR, the self-assembly process is mainly governed by the overall charge of the complexes. The effect of SDS and OG can vary depending on the mixing procedure, only presenting the above-mentioned effect if these surfactants are mixed with the ELbcR below its T_t.

The addition of non-ionic or similarly charged surfactants has no effect on T_t. In contrast, the addition of an oppositely charged surfactant has a marked effect on T_t in a two-step process involving an initial reduction in T_t, even at temperatures below the physiological temperature, followed by an increase in this parameter. As a result, DTAB causes a decrease in T_t associated with neutralization of the charged moieties of the recombinamer, and thus an effective increase in the effective mean hydrophobicity of the whole co-recombinamer/surfactant complex, followed by the reverse, namely the charge causing a new increase in T_t.

These results support the use of surfactants as an effective means of controlling the self-assembly of ELbcRs and increasing their applicability in uses such as controlled drug release or protein purification.

5.3. Chapter 3: Covalently bonded graphene oxide–elastin-like recombinamers as versatile composites: Electrospun nanofibers, micropatterned gels, nanoparticles and injectable hydrogels

Abstract:

Graphene possesses outstanding properties which make it the perfect material in many scientific fields. However, for biomedical applications its properties require it to be modified by coating with a highly biocompatible material, due to its low solubility in saline solvents and citotoxicity. To fulfill this need, we have synthesized elastin-like-recombinamer (ELR)–graphene oxide (GO) composites (ELR-GOs) in the form of nanofibers, hydrogels, and nanoparticles. This work proves the feasibility of covalently bonding rationally designed ELRs to GO for the construction of composite functional materials that could find uses in the biomedical field.

Graphene, which contains a monolayer of carbon atoms organized into a highly packed 2D honeycomb structure, has emerged as the rising star of modern materials science due to its unique and outstanding properties. Some of these, such as its geometry and structure, provide graphene with high thermal and electrical conductivity or a high Young's modulus/fracture strength[133], all of which make graphene an ideal material for a wide variety of applications[134].

These properties include several which make graphene an interesting material for biomedical applications, namely high surface area, which, together with the π stacking of aromatic drugs, provides a higher loading capacity than is possible with other nanomaterials[135], near-infrared energy absorption, which is useful, amongst others, for thermal cancer treatment[136], or highly sensitive electrical properties, which can be applied in nanosensors or neural scaffolds[137]. However, graphene and graphene oxide present two major drawbacks as a biomedical material, namely their poor solubility (although graphene oxide can be dispersed in water it collapses in saline conditions[144]), which is critical for such applications, and toxicity. It is commonly accepted that the in vitro cellular toxicity of this material is correlated with its surface coating, becoming more biocompatible as the biocompatibility of the material used in the coating increases[145-147]. In light of this, we have chosen elastin-like recombinamers (ELRs) as functionalizing material. As it was mentioned before, all functional ELRs present a thermoresponsive behavior in aqueous solution in which they remain "soluble" below a certain temperature (Tt) but experience a phase-separation process above Tt. This process is fully reversible upon lowering the temperature[15]. Wang et al. have exploited

these particular characteristics together with the near-IR absorption of graphene to construct a non-covalent light-controlled hydrogel actuator[187]. Other external stimuli, such as UV-vis light ion concentration, or pH[188], also have a noticeable effect on the behavior of ELRs.

ELRs are produced by recombinant DNA technologies, thus allowing an exceptionally precise control over the amino acid composition and opening up the possibility of designing ELRs with the particular characteristics needed for a specific application. This design versatility, in conjunction with their bioactivity, self-assembly behavior, and high biocompatibility, makes ELRs ideal materials for studies in the biomedical field, especially those in which toxic materials are employed and biocompatibility must be provided[189].

Two major strategies for attaching different molecules to graphene or graphene oxide, namely covalent and non-covalent modifications, have been employed. In this work we have chosen a covalent linkage due to its higher stability and stronger attachment compared with a non-covalent bond. This results in a more stable composite, which is a critical parameter for potential biomedical systems when dealing with biological environments. Furthermore, many of the non-covalent linkages used previously involve π-π stacking[190], which reduces the drug loading capacity of graphene oxide[138]. Thus, a covalent linkage represents a competitive advantage compared with non-covalent bonds as regards biomedical applications.

5.3.1. Synthesis and characterization of ELRs-GO complexes.

Due to the presence of carboxyl groups on the graphene oxide, ELRs bearing amino groups (Table 1) present in lysines were employed to perform the amidation reaction between the two groups, this reaction being mediated by carboxyl group activation using the carbodiimide methodology (**Figure 45**).

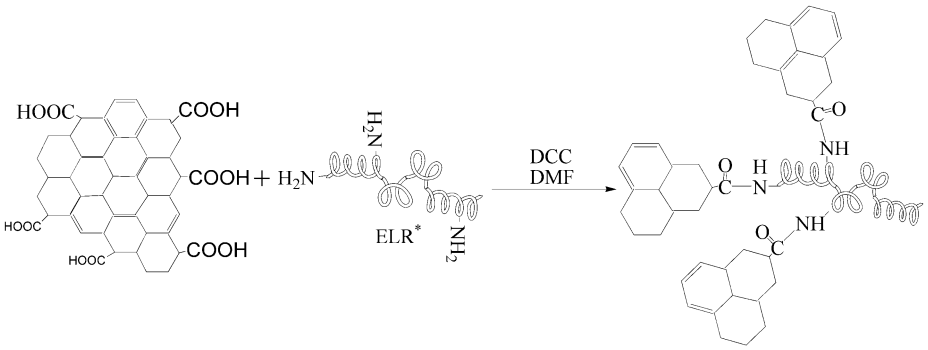

* DMAP was included in the reaction for ELR 9K-EI2RGD

***Figure 45**: Schematic representation of the synthesis of ELR-GO composites*

Once the reaction was complete, the reaction mixture was centrifuged to eliminate unreacted GO and reaction by-products and the supernatant containing ELR-GO was subjected to various purification cycles. Finally, dialysis against deionized water was required. Detailed reaction and subsequent exhaustive purification procedures can be found in the materials and methods section (**4.2.15**).

The ELRs were synthesized by bacterial expression and their monodispersity and molecular weight verified by MALDI-TOF and SDS electrophoresis (**Figure 46**, **Figure 47**.) The detailed characterization of IKx24 and HRGD6 can be found elsewhere[191, 192].

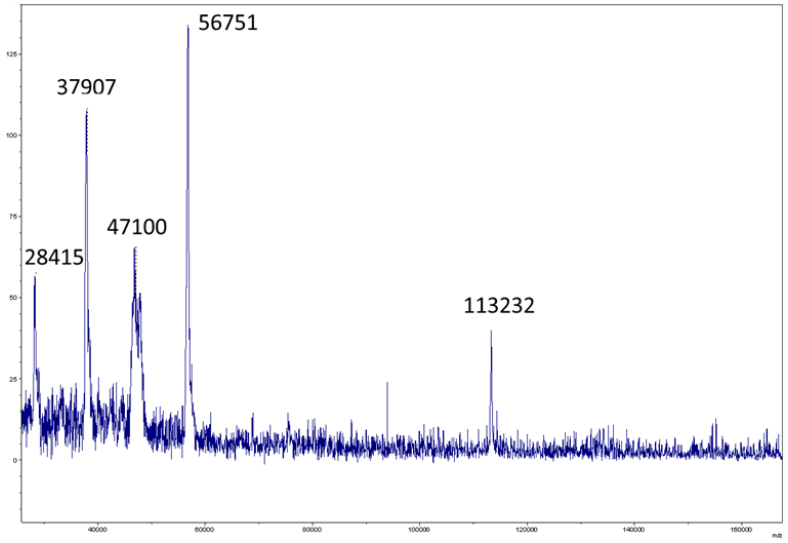

***Figure 46**: Determination of the 9K-EI2RGD molecular weight by MALDI-TOF mass spectrometry.*

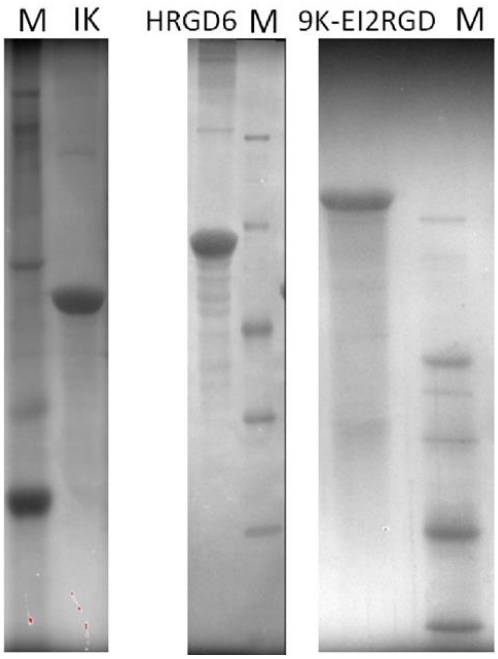

M: Protein marker. Lines: 166, 66, 45, 35, 25 kDa

***Figure 47**: Analysis of the purity of the different ELRs by SDS-PAGE after staining with copper chloride.*

Three different ELR-GO composites were designed as potential candidates for biomedical applications. The ELRs employed in this work were selected to have lysines on their sequences. In the case of physical hydrogel formation a tetra-block amphiphilic ELR with lysines on its sequence was selected .The ELRs employed are summarized in **Table 16**.

***Table 16**: ELRs evaluated in this chapter.*

ELR Nomenclature	**Amino acid sequence**
IKx24	$[(VPGIG)_2(VPGKG)(VPGIG)_2]_{24}$
HRGD6	$\{[(VPGIG)_2(VPGKG)(VPGIG)_2]_2$-(AVTGRGDSPASS)-$[(VPGIG)_2(VPGKG)(VPGIG)_2]_2\}Cccc_6$
9K-EI2RGD	3K-$[(VPGVG)_2(VPGEG)(VPGVG)_2]_{10}$-$(VGIPG)_{60}$-3K-$[(VPGVG)_2(VPGEG)(VPGVG)_2]_{10}$-$(VGIPG)_{60}$-$[(VPGIG)_{10}$-(AVTGRGDSPASS)-$(VPGIG)_{10}$-$]_2$-3K

The RGD integrin-binding domain was included in some of the constructs to enable future applications as model extracellular matrix proteins.

In order to analyze the content of graphene oxide in the ELR-GO composites TGA experiments, which measures the decomposition behavior of the sample during heating, were carried out. **Figure 48** shows the decomposition behavior of the ELR-GO and GO.

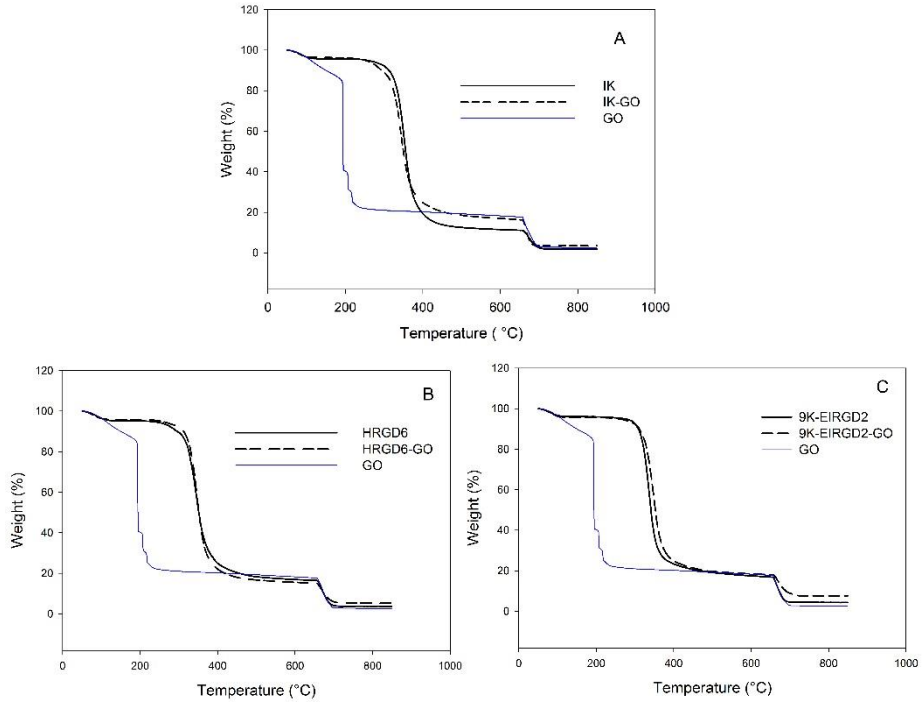

***Figure 48**: Thermogravimetric Analyses (TGA) of graphene oxide, A) IK, IK-GO; B) HRGD6, HRGD6-GO; and C) 9K-EIRGD2, 9K-EIRGD2-GO.*

It can be clearly seen that GO is not thermostable, as the loss of mass started below 100°C. This mass loss correspond to evaporation of the water stored at its π-stacked structure[193]. The majority (81%) of the GO mass was lost close to 200°C, which is attributed to the pyrolysis of those groups containing labile oxygen[194]. Changing the purge from N_2 to air at 650°C have as a result another loss of mass, as the organic carbon is transformed to CO_2 and H_2O under this atmosphere.

On the other hand, ELRs seems to be an effective coating to enhance thermal stability of graphene oxide. For all of the ELR-GO composites the maximum mass loss (approximately 80%) takes place around 350 °C. A similar behavior was found for ELRs, which

indicates the mass loss of ELR-GO composites at this stage is due to ELR decomposition. Analyzing the mass percentage of the residues at 800°C it is estimated a 2.17 wt% content of graphene oxide in the ELR-GO. Taking into account that the wt% of GO in the reaction was 3.2% it can be concluded a high reaction efficiency of 68%.

The effect of the covalently bonded GO on the ELRs properties is rapidly seen as the binding of GO to the ELRs lowers their characteristic transition temperature, as verified by differential scanning calorimetry (DSC) (**Figure 49**). This decrease in Tt can be attributed to binding of the carboxyl groups of GO to the amino groups of the ELRs, thereby reducing their number and thus the quantity of charged groups. This, in turn, reduces the overall hydrophobicity and decreases Tt[27]

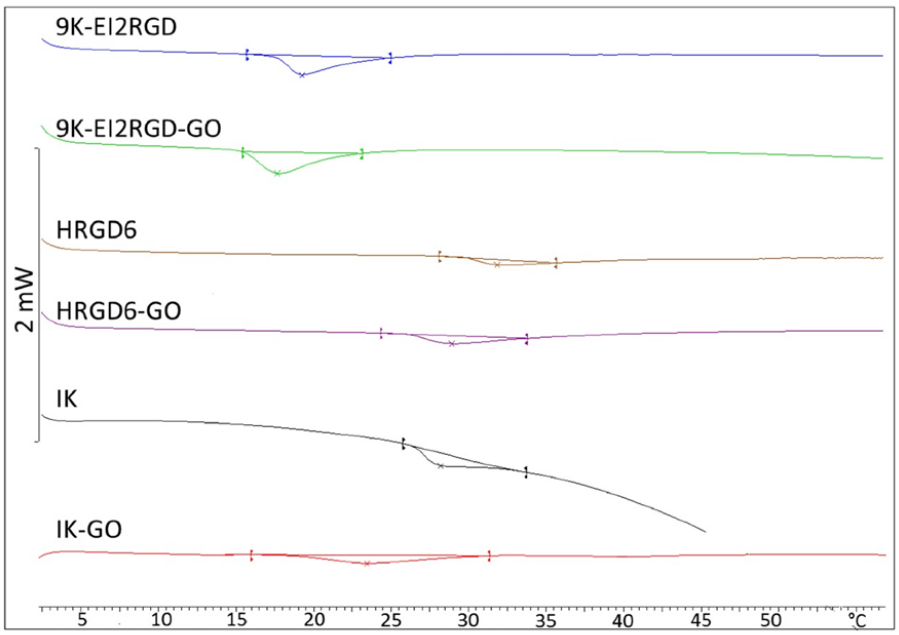

***Figure 49**: DSC thermograph for a heating cycle (5°C min^{-1}) for ELR and ELR-GO composites at 50 mg.mL^{-1} in milliQ water.*

Table 17: *Summary of transtion temperatures of ELRs and ELR-GO composites.*

ELR Nomenclature	**Tt (°C)**	**Enthalpy variation. (Jg^{-1})**
IKx24	28.17	-3.35
IKx24-GO	23.01	-4.49
HRGD6	31.85	-1.46
HRGD6-GO	28.92	-2.77
9K-EI2RGD	19.25	-5.45
9K-EI2RGD-GO	17.67	-6.30

The colloidal stability of ELR-GO composites was investigated. As it was previously mentioned, GO collapses in saline conditions[144]. In contrast, the ELR-GO composites were found to be soluble in different saline buffers (**Figure 50**), thereby suggesting that covalently bonding GO to ELRs provides with steric protection against GO aggregation, which confer stability in biological solutions.

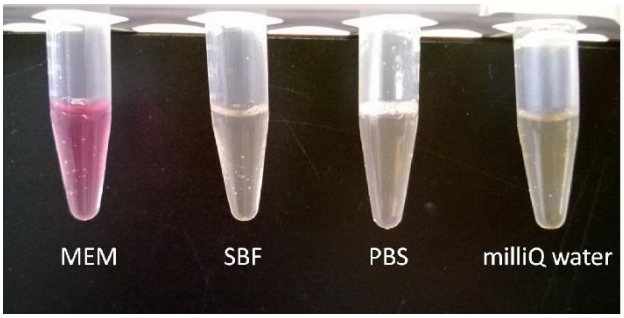

Figure 50*: Picture of 9K-EI2RGD in different solvents: culture minimum essential medium (MEM), simulated body fluid (SBF), PBS and milliQ water. Concentration 30 mg/mL.*

5.3.2. Cellular bioactivity of ELR-GO composites.

Two ELR-GO composites, one containing the RGD integrin binding motif (HRGD6-GO) and one without it, were tested for the ability to promote adhesion and spreading of human foreskin fibroblast cells in serum-free media. As it can be clearly seen in **Figure 51**, both ELR-GO composites are suitable for cell culture. Cells adhered after one hour and proliferated after 48 hours. No noticeable differences were observed comparing with ELRs alone.

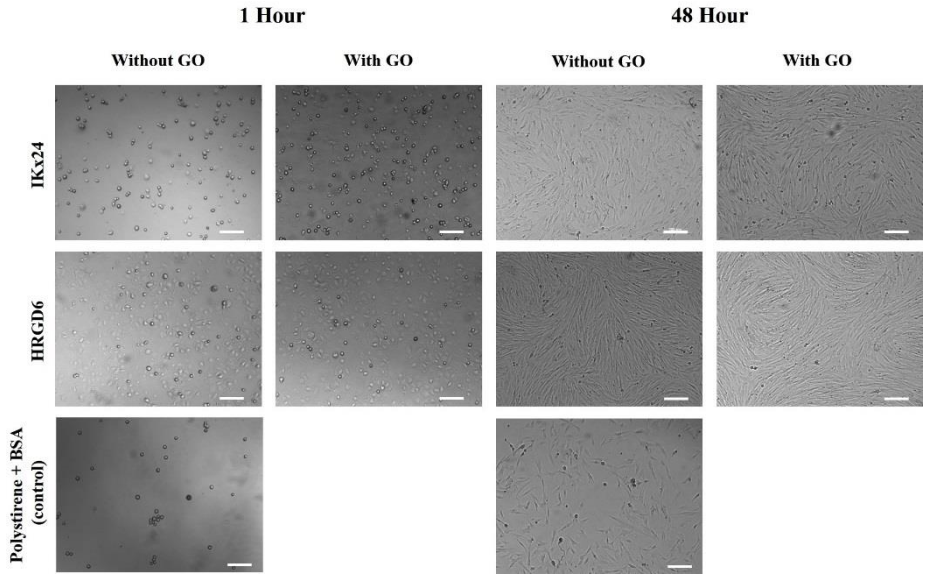

***Figure 51**: Optical micrographs of cell culture over wells covered with IK and HRGD6 both with and without the presence of GO. Images were taken 1 hour and 48 hours after seeding. Scale bar 200 µm*

Cell attachment was improved by the presence of the RGD motif in all cases. Therefore, we conclude that covalently bonding GO to ELRs greatly reduces GO toxicity. This result together with the stability in saline solutions, enables the usage of ELR-GO composites as potential candidates for biomedical applications.

5.3.3. Possible applications of ERL-GO composites in the biomedical field.

The first such application for which ELR-GO composites could be valuable candidates concerns the field of tissue engineering. One of the most widespread approaches for the assembly of cellular scaffolds is the modification of substrate topography by way of techniques such as electrospining, thus enabling the formation of fibrous systems, or tailor-made topographies by replica molding, in order to mimic the ECM conformation of natural tissues[195, 196], ELRs have shown excellent cell behavior and proliferation in such topography-modified substrates[191] and GO confers the scaffolds with specific properties, such as increased electrical conductivity, thus meaning that they could be used as scaffolds for neural stem cells[137, 197].

To this end, we have constructed different topographies using these techniques and the HRGD6-GO composite (**Figure 52**). Detailed procedures can be found in the materials and methods section (**4.2.16**)

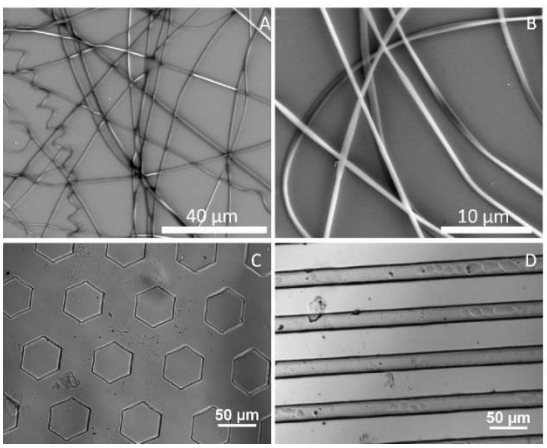

***Figure 52**: Different topologies achieved with HRGD6-GO: A, B) ESEM micrographs of electrospun nanofibers; C) optical micrographs of hexagonal micropatterned gels; D) optical micrographs of groove-micropatterned gels.*

Electrospinning of HRGD6-GO resulted in a homogeneous mass of fibers isotropically and randomly distributed over the surface with a fiber width distribution of 832 ± 126 nm, a width at which cells can sense them as individual fibers[198]. These fibers were subsequently cross-linked (by immersion in 10% HMDI/acetone solution overnight and then exhaustively washed with ultrapure deionized wate) to provide stability in aqueous media.

Chemically cross-linked HRGD6-GO hydrogels with micropatterned surfaces were also synthesized (**Figure 52 C&D**) (detailed information of the hydrogel and pattern formation can be found in **4.2.17**). The surface pattern consisted of 50 μm hexagons and grooves with a width of 20 μm separated by 50 μm, thus meaning that cells could be confined and aligned in their interior. The presence of graphene oxide in these nano-micro structures did not affect the stimuli-responsiveness nature of the ELR. When immersed in water, the HRGD6-GO hydrogel retains its thermal sensitivity, showing a clear size reduction above the Tt.

Drug delivery is another field of biomedicine in which GO could prove useful. Therefore, in light of this proposed use as a drug-delivery system, and taking advantage of the self-assembly properties of ELRs, we have developed two different ELR-GO composites in order to obtain two of the best assemblies employed in such applications, namely hydrogels and nanoparticles. To this end, an amphiphilic elastin like block-corembinamer (ELbcRs), 9K-EI2RGD, was coupled with GO to obtain a hybrid hydrogel. Unlike the ELR-GO hydrogels described previously, we have exploited in this case the self-assembly behavior of ELbcRs, which allows them to form physical

hydrogels[199]. A 15 wt% aqueous 9K-EI2RGD-GO solution was employed, and it was found that inclusion of GO did not hamper physical hydrogel formation, as verified by rheological measurements

The thermogelling properties of a 15 wt% 9K-EI2RGD-GO solution were evaluated as a function of temperature using a controlled stress rheometer at a constant strain of 0.1% and a frequency of 1 Hz (**Figure 54**). The modulus was found to be strain independent at 37°C and a frequency of 1 Hz (**Figure 53**). A strain of 0.1% was selected.

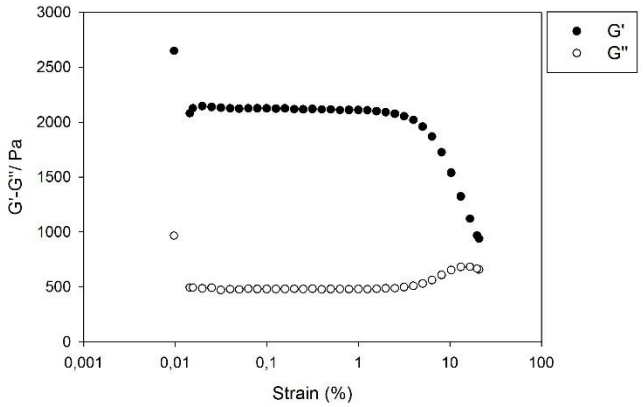

***Figure 53**: Strain dependence of the modulus of a 15 wt% 9K-EI2RGD-GO hydrogel.*

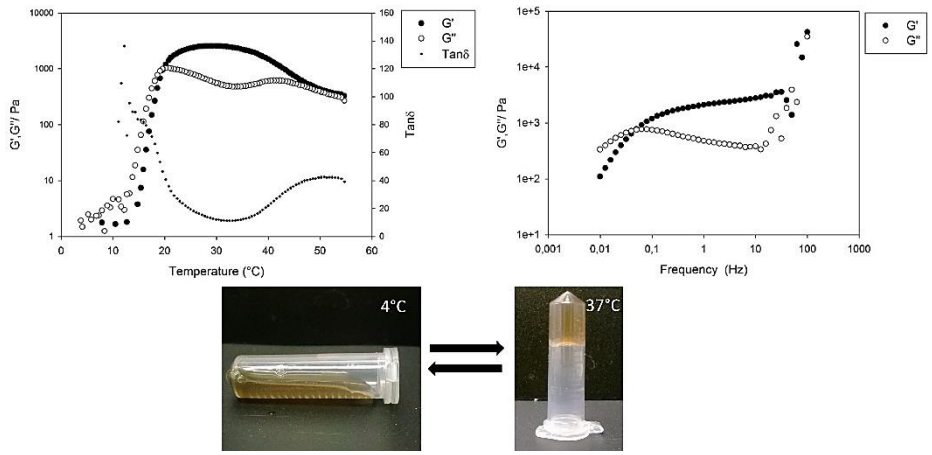

Figure 54: *Thermogelling properties of a 15 wt% 9K-EI2RGD-GO solution: a) Storage modulus (G') and loss modulus (G'') as a function of temperature. b) A plot of modulus versus frequency at 37°C.*

A plot of the thermogelling properties as a function of temperature revealed a gelation temperature (G'/G'' = 1) of 19°C and a maximum storage modulus (G') of 2580 Pa. The gel formed can therefore be considered to be a "soft gel" that may also prove to be ideal for cell culture purposes. The modulus frequency dependence observed indicates molecular relaxation with a time constant within the range of frequencies studied. A similar frequency dependence has also been observed in natural tissues such as the uterus[200].

As the trigger temperature for gel formation, which is completely reversible upon lowering the temperature, is close to body temperature, the 9K-EI2RGD-GO composite could prove useful as an injectable hydrogel for local and directed treatments. The physical hydrogel is also pH-sensitive due to the presence of glutamic acids in its sequence and absorbs in the NIR region due to the presence of GO, which may also boost the sol-gel transition. In light of their unique properties, injectable hydrogels represent an excellent system for the

sustained release of therapeutic agents[201], and this ability is enhanced upon combination with GO, thus suggesting that the ELR-GO physical hydrogel could prove to be an excellent candidate for this purpose.

Finally, we have developed an IKx24-GO composite in order to obtain one of the most widely use drug-delivery systems: nanoparticles. Nanoparticles are excellent candidates as carriers for genes, proteins or drugs, for example, due to their small size, which allows them to move freely through the circulatory system without blocking veins or arteries[122, 202]. Nanoparticles are of particular interest for drug-delivery purpose due to their ability to encapsulate hydrophobic drugs. The binding of ELRs to GO may considerably increase their loading capacity due to the high surface area of the resulting construct and its ability to π stack aromatic drugs, for example anti-cancer drugs such as doxorubicin (DOX), which are normally insoluble in aqueous media. Functionalized GO has also been used for gene transfection[138], thereby increasing the potential uses of IKx24-GO nanoparticles.

Nanoparticle formation was performed using dilute IKx24-GO solution (25 μM) by taking advantage of spontaneous ELR-based nanoparticle self-assembly above the Tt[119]. Nanoparticle formation was followed by dynamic light scattering (DLS) with monodisperse (PDI: 0.233 ± 0.017) nanoparticle distributions with a maximum at 83.51 ± 1.51 nm being obtained (**Figure 55**). The DLS autocorrelation functions were used to obtain the size distribution and polydispersity index.

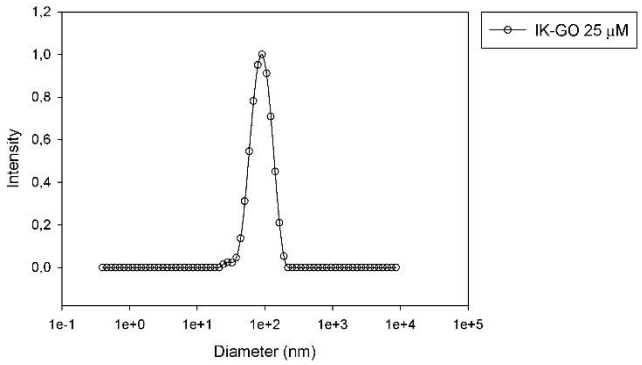

***Figure 55**: Normalized size distribution as measured by DLS for a 25 μM IK-GO solution at 37°C.*

Dilute solutions of 9K-EI2RGD-GO also led to nanoparticle formation, as the physical hydrogel formation of ELbcRs is due to the packing of individual nanoparticles[199, 203].

5.3.4. Final remarks.

In conclusion, we have shown that genetically designed amino-containing ELRs can be employed to covalently functionalize GO. Thus, GO was treated with three different ELRs to form ELR-GO composites with a high solubility in aqueous saline solution, low cytotoxicity and exhibiting a variety of structures. More specifically, electrospun fibers, micropatterned chemical hydrogels, injectable physical hydrogels, and nanoparticles have been produced using the ELR-GO composites. These composites could be highly valuable candidates for future experimentation into a wide range of biomedical applications, including tissue engineering, cell-culture, or drug/gene delivery.

5.4. Chapter 4: Self-assembly of different Elastin like recombinamers macromolecular architectures through Leucine Zipper formation: From di-blocks to brush polymers.

Abstract:

Advances in DNA recombinant technology allows the synthesis of genetically engineering elastin like recombinamers (ELRs) with complete control of chemistry and molecular weight. Despite the fact that ELRs have unique physical and biological properties, they are produced essentially with a linear structure. The main aim of this work is the obtaining of brunched recombinamers through modular design, by which, the different branches are individually recombinatly produced and later, exploiting self-assembling (bottom-up) approaches, the construction of ramified structures by simply mixing. In order to reach high levels of efficiency in this self-assembling, specifically designed helical domains (Leucine Zippers), which are able to form specific coiled-coil aggregations, are included into ELRs sequences. In this regard, five different ELR-zipper complexes have been designed, biosynthesized, and purified with a view to achieving di-blocks and brushed architectures. The formation of the different strucutures was characterized by native-PAGE electrophoresis, circular dichroism, dynamic light scattering and analytical ultracentrifugation. The results present herein shows the possibility of obtaining non-linear superstructures, such as brush assemblies, with Elastin-like recombinamers

Natural proteins normally lacks of topological variety but are usually rich of functional groups that promotes the protein folding, self-assembly and function. Those proteins presenting a non-linear architecture, such as those natural circular occurring proteins, are drawing the attention of many researchers due to their unique functions[204]. During the last decade, recombinamers[5], a new kind of recombinant protein polymers, have demonstrated outstanding capabilities in obtaining highly functional systems for the most cutting edge areas in nano(bio)technology and biomedicine. However, as compared with conventional polymers, and although recombinamers show unmatched levels of complexity of their monomer sequence and control in the synthesis, conventional synthetic polymers can draw upon others strategies to obtain advanced functionalities. One of the most successful strategies is varying the polymer architecture, and in particular, complex branched structures have proven enormous potential to reach high levels of functionality, which is clear for macromolecules having brush[205] or dendrimer[206, 207] architecture. However, recombinamers, by the way they are produced, are intrinsically linear. Thus, the controlled conjugation of peptides or proteins with synthetic polymers has been commonly used as promising candidates for biomedical applications[208]. This hybrid assembly produce responsive and molecular recognition-capable materials with improved properties such as greater biomolecule stability and increased aqueous solubility.[209, 210]

As an alternative to synthetic polymers, we are interested in the use of genetically engineered protein polymers containing folding motifs. The great advantage of utilizing biotechnological techniques is the ability to construct modular polymer-like proteins composed of

several functionally independent domains, such as structural or bioactive with a clearly superior degree of control and complexity to that achieved by conventional chemical synthesis. Within this framework, we report herein the formation of complex architectures by Elastin like recombinamers (ELRs). Nonetheless, recombinant DNA technologies allows the obtaining of protein-based polymers with linear structures which makes difficult reaching complex superstructures as those reach by chemical synthesis.

In this regard, we have selected heterodimeric coiled coil interaction through leucine zipper as linker in order to construct complex architectures. This type of interaction has been employed lately for the conjugation of biological molecules and synthetic polymers[208, 211]. The α-helical coiled coil offers an attractive simplification of complex oligomeric protein interactions and constitutes one of the most important motifs underlying many of the functionalities found in natural proteins. In this regard, leucine zippers are common three-dimensional structural motifs in proteins involved in regulating gene expression usually found as part of a DNA-binding domain in various transcription factors. The leucine zipper dimerization domain forms a coiled coil that consist of four to five heptads, in which each heptad is composed of two α-helical turns or seven amino acids, labeled **a**, **b**, **c**, **d**, **e**, **f** and **g**.[212]. Amino acids in the **a**, and **d** positions are on the same surface of the α-helix and are typically hydrophobic and interact with the complementary **a'** and **d'** amino acid positions in the opposite monomer creating a hydrophobic core essential for the dimer stability. The **g** and **e** positions typically contain charged amino acid which interact electrostatically with **e'** and **g'** regulating both homodimerization and heterodimerization determining the specificity

of coiled coil recognition. Furthermore, Van der Waals between **g** and **e'** methylene groups and the underlying **a** and **d** amino acids contribute to stability.[105, 213] This good knowledge of the folding machanism together with the flexibility of the coiled coil sequences makes this type of domains especially attractive for rational design(preferable against other less understood linkage domains used lately[214]) and the interest of inclusion of coiled-coil domains in biomaterial is increasing recently[215, 216].

In this regard, the hypothesis of this work is to exploit the amazing possibilities of the assembly found in leucine zippers to obtain superstructures such as brushed architectures from stimuli-responsive ELRs presenting unique opportunities to generate functional materials with structures and functionalities similar to those seen in nature.

5.4.1. Materials design.

The recombinant technology employed in the ELR production gives us absolute control over their composition at a gene level, thereby allowing total control of the recombinamers length and composition with a single amino acid precision. We examined two different types of ELR-Zipper complexes. In all cases the ELR employed was based on glutamic acid. This particular ELR is pH dependent, once the pH is above the pKa of the carboxyl group, the glutamic acid is deprotonated, thus negatively charged and therefore the Tt of this ELR is highly increase, remaining soluble at any temperature[217].

The basic principles to be considered for the design, comparison and description of coiled coils are their stability, association number oligomerization selectivity and the orientation of the helices. Four major parameters are responsible for coiled coil stability,

hydrophobicity of the core residues position **a** and **d**[108] , number of heptad repeats[109], electrostatic interactions between the residues in position **e** and **g**[110], and the helical predisposition of the remaining amino acids[111]. In this sense the leucine zippers domains were designed with position **b** being occupied in all the cases by an Alanine which is known have a high helical propensity and containing five heptad repeats.

All the cases present a cistein residue in position **d** in order to form a disulfide bond and provide higher stability to the protein coupling. The presence of the cistein in position **d** do not prevent the formation of leucine zippers[218]. Apart from this Cistein residue, Z3 and Z6 are composed in position **d** by 100% of leucine, resulting in a complete leucine zipper. Furthermore, all the amino acids in position **e** and **g** are of the same polarity, E for Z3 and R for Z6. On the contrary, Z5 and Z2 have a mixture of hydrophobic amino acids in position **d**, phenylalanine and luecine, and a mixture of different charge amino acids in the **e** and **g** positions (Z5 **d** positions: KKKEE and Z2 **d** positions: EEEKK) The origin of this differences is to provide specificity to the coupling, being only possible the coupling between those zippers with same **d** composition and opposite charge residues in **e** and **g** positions (Z3 pairs with Z6 and Z5 pairs with Z2) as the formation of homodimers or heterodimers is mainly determined by the electrostatic interactions between the charged amino acids placed at position **e** and **g**. Homodimers result from the presence of oppositely charged amino acids in these positions because of the attractive forces between the **e** and **g** amino acids of the two strands. Thus the heterodimer formation is expected in all cases.

The orientation of the helices is also determined by the electrostatic interaction between the amino acids residues in position **e** and **g**. Antiparallel heterodimers will result from the attractive forces between positions **e**:**e'** and **g**:**g'**, while parallel heterodimers will result from the attraction between residues in positions **e**:**g'** and **g**:**e'**.All in all, the leucine zipper domains employed in this work were designed to adopt a heterodimer parallel conformation (**Figure 56**).

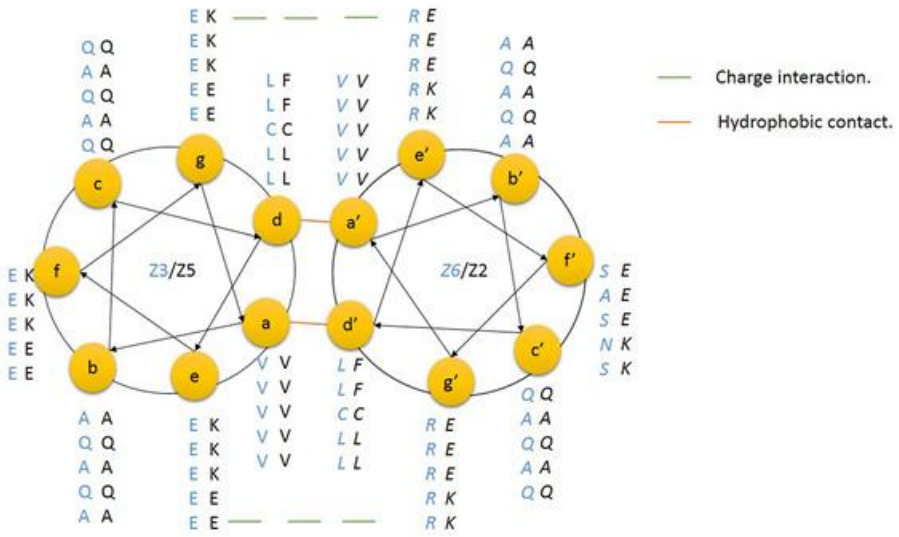

Figure 56: *Helical wheel diagram of the Z3-Z6 and Z5-Z2 heterodimer formation. Dimerization is achieved by hydrophobic contacts between position* ***a*** *and* ***d*** *amino acids and stabilized by charge interaction between position e and g amino acids.*

Taking the specificity in the zipper domains into account, five different ELR-Zippers have been produce in order to achieved diverse morphologies, such as block recombinamers or brush recombinamers. The different assemblies considered are represented in **Figure 57**.

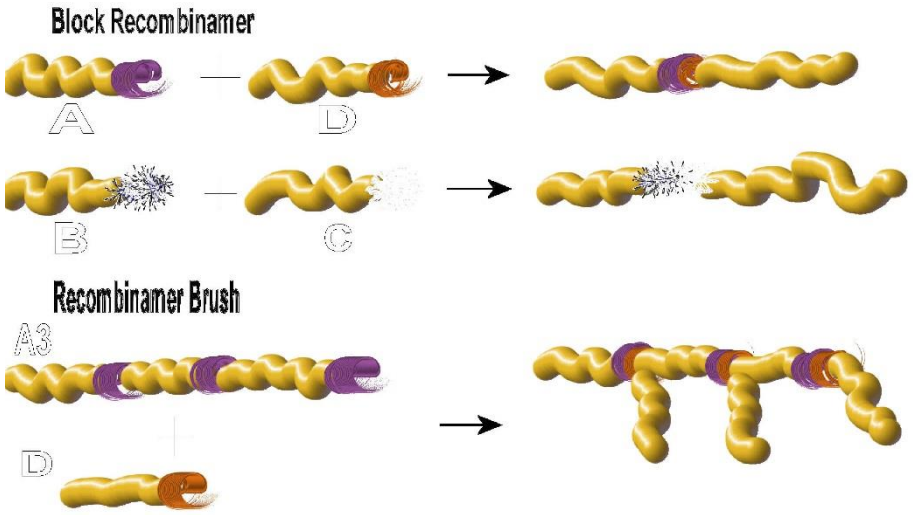

***Figure 57**: Schematic representation of the different morphologies self-assembled by the different ELR-Z couplings.*

5.4.2. ELR-Zipper gene synthesis.

In an effort to obtain different molecular structures, diverse recombinant ELRs have been design and produce. In this sense a set of genes have been design and employed in this work (**Figure 58**).

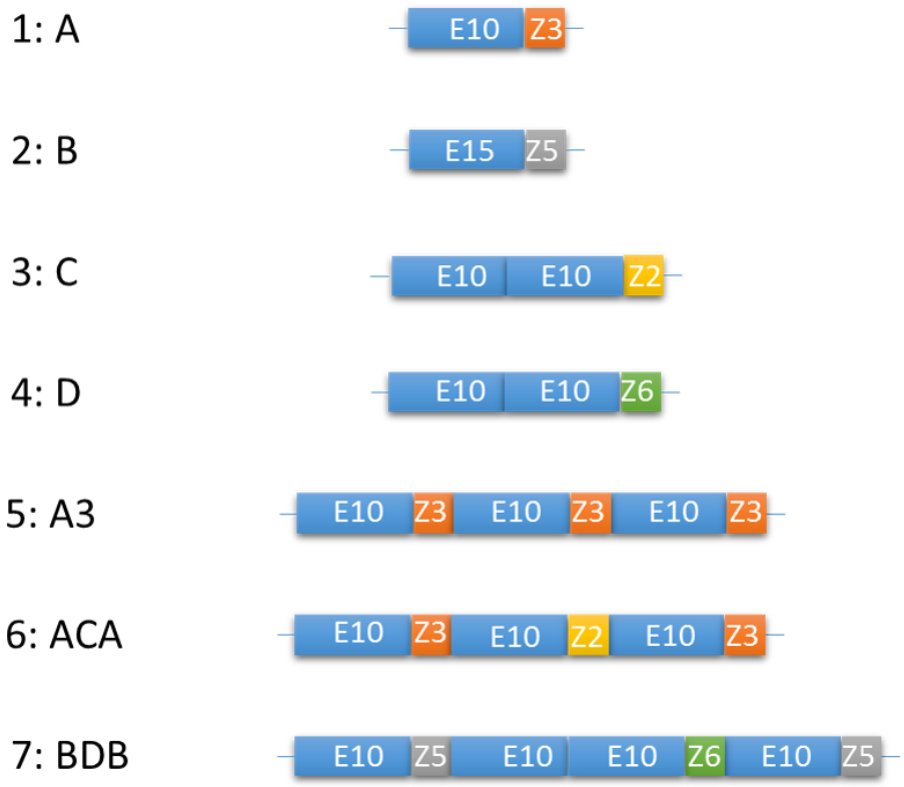

***Figure 58**: Genes constructs and abbreviations employed.*

***Table 18:** Amino acid sequence of the different building block employed in this work.*

Abbreviation	Sequence
E10	$[(VPGVG)_2(VPGEG)(VPGVG)_2]_{10}$
E15	$[(VPGVG)_2(VPGEG)(VPGVG)_2]_{15}$
Z3	VAQLEEEVQALEEEVAQCEEEVQALEEEVAQLEEE
Z5	VAQFKKKVQAFKKKVAQCKKKVQALEEEVAQLEEE
Z2	VAQFEEEVQAFEEEVAQCEEEVQALKKKVAQLKKK
Z6	VAQLRSRVQARARVAQCRSRVQALRNRVAQLRSR

The pDrive cloning vector containing the genes for the E10 and E5 were avaible from previous studies. The plasmid cloning vector (pUC57) containing the sequences encoding the leucine zipper domains was provided by GenScript. The sequences encoding the leucine zipper domains were transferred from the pUC57 to a pDrive cloning vector by Ms. Alicia Fernandez Colino.

The construction of the fuse genes described in **Figure 58** was carried out by the sequential introduction of the repetitive ELR polypeptide codifying gene segments and the gene segments codifying for zippers domains by a seamless iterative recursive strategy (**2.1.6**).

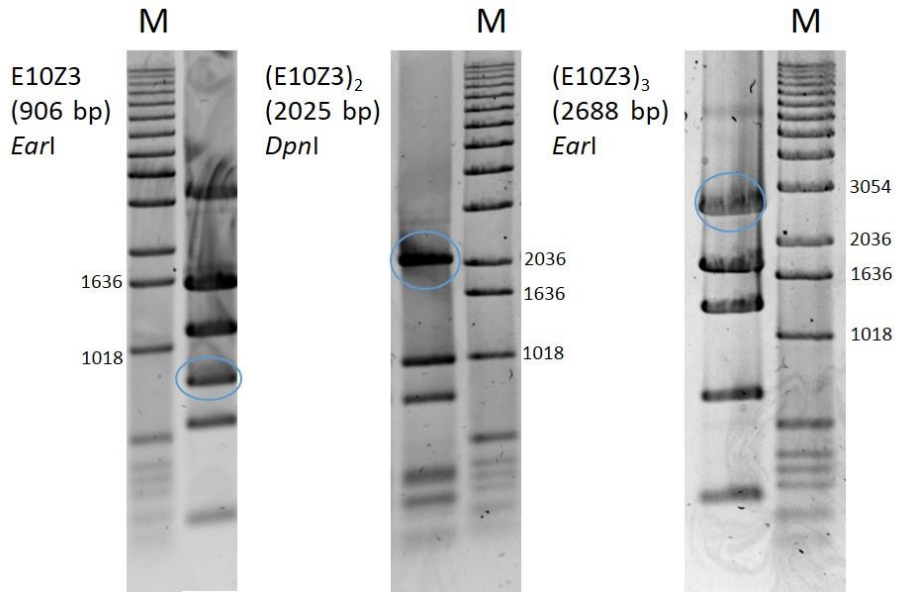

***Figure 59**: Enzymatic analysis of the different gene constructions made during the building process of the genes encoding for E10Z3x3. (E10Z3)2 was digested with DpnI which added 315 bp (2025 bp= 1710 (E10Z3)2 + 315 (DpnI cut))*

Once the desired constructions were obtained and their sequences controlled their released inserts after enzymatic digestion

with *Ear*I and *Dpn*I, which is used in order to avoid the appearance of fragments with similar size to the segment of interest, were subcloned in the modified pET 25b+ vector pET 7 expression vector. These resulting vectors were used to transform *E. coli* expression strains as described in (**4.2.8.3**).

5.4.3. ELRs expression and purification

The final gene constructions were transformed on the bacterial strain BLR (DE3) following the above mention protocol **(4.2.8.3)**. The expression of the recombinamers was made as previously described (**4.2.10.1**) The ELRs purification protocol was made based on the ITT (**4.2.10.3**) consisting on three sequentially rounds of inverse transition cycling, which rendered highly pure and monodisperse polymers, as corroborated by SDS-PAGE (**Figure 60**)

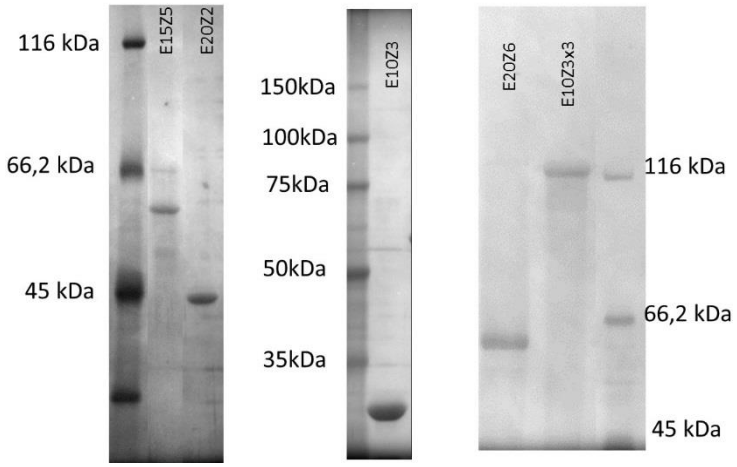

***Figure 60**: Analysis of the ELR-zipper purity after ITT purification by SDS-PAGE stained with cooper.*

The electrophoretic pattern showed an excellent level of purity for all the ELRs. No contaminant proteins form *E.coli* were found. The specimen showed retarded electrophoretic mobility as the molecular

weight found was approximately 20% bigger than expected. This behavior has been previously observed in ELRs.

In order to confirm the recombinamer's molecular weight and amino acid composition, the samples underwent MALDI-TOF (**Figure 61**) and amino acid analysis (**Table 19**).

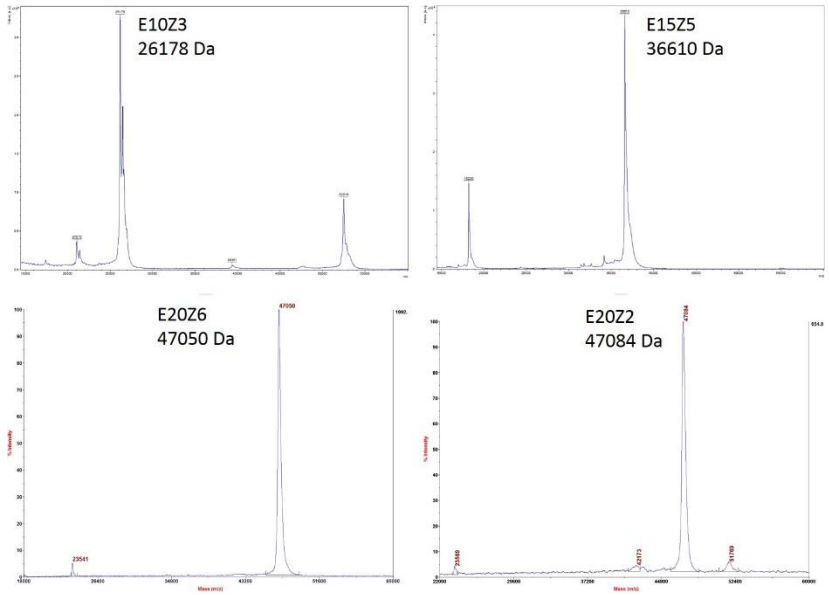

Figure 61 *Determination of the molecular weight of E10Z3, E15Z5, E20Z6, and E20Z2 by MALDI-TOF mass spectometry.*

In the case of E10Z3x3, it was obtained a molecular weight of 20990 Da when it was expected to have 77087 Da (**Figure 62**). The molecular weight obtained is in good agreement with the one expected for E10. This result indicates that the E10Z3x3 is fragmented into E10 and Z3 fragments during the MALDI-TOF process.

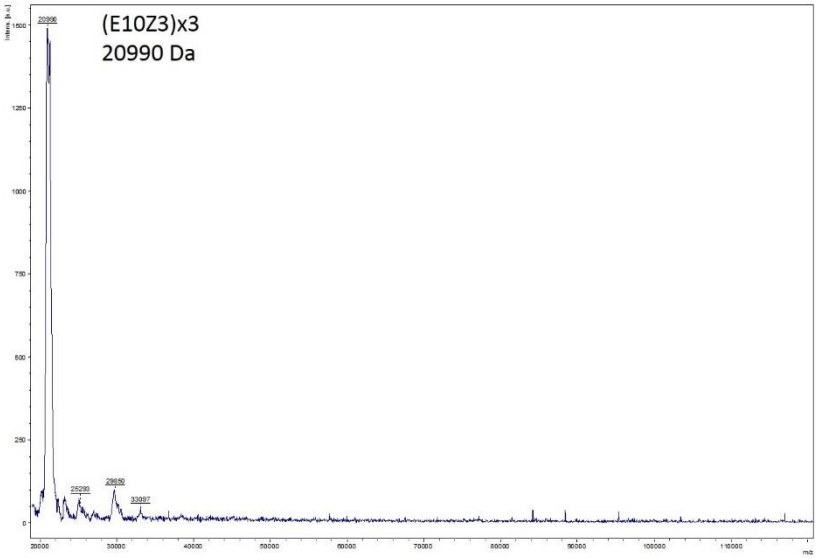

***Figure 62**: Determination of the E10Z3·x3 molecular weight by MALDI-TOF mass spectrometry.*

***Table 19:** Amino acid composition analysis (theoretical and experimental) of the ELR-zippers*

	E10Z3x3		**E20Z6**		**E10Z3**		**E15Z5**		**E20Z2**	
Aa	**Exp.**	**Pred**	**Exp.**	**Pred**	**Exp.**	**Pred**	**Exp**	**Pred**	**Exp.**	**Pred**
E	70,34	76	28,64	26	25,74	26	21,56	22	28,69	30
N			1	1						
S	1,6	1	3,65	4	1	1	1,3	1	0,98	1
Q	13,88	15			4,21	5	5,19	5		5
G	343,31	330	217,42	210	115,62	110	157,81	160	216,85	210
R			5,13	10						
A	11,64	15	3,36	6	6,06	5	5,03	5	4,74	5
C	6,39	3	0,9	1	0,8	1	1	1	1,24	1
V	287,82	289	191,01	187	99,12	97	145,36	141	189,68	187
M	1,32	1	0,89	1	1,21	1	0,95	1	1,42	1
F							3,67	2	2,65	2
L	12,74	14	4,6	6	5,2	6			3,74	4
K									6,45	6
P	151,69	151	100,35	101	51,74	51	77,12	76	99,78	101

The gene constructions 6 and 7 where designed with a view to obtaining a dendrimer structure, but although the expression was high, when they were produced and purified they suffered degradation, as checked by SDS-PAGE (**Figure 63**). The number of protease inhibitors was increased but degradation still occurred.

Size exclusion chromatography was used, under denaturing conditions urea 8M, in order to eliminate the degradation products. The separation of the degradation products was unsuccessful. Thus, this two polymers were discarded and the dendrimer formation was no longer taken into consideration

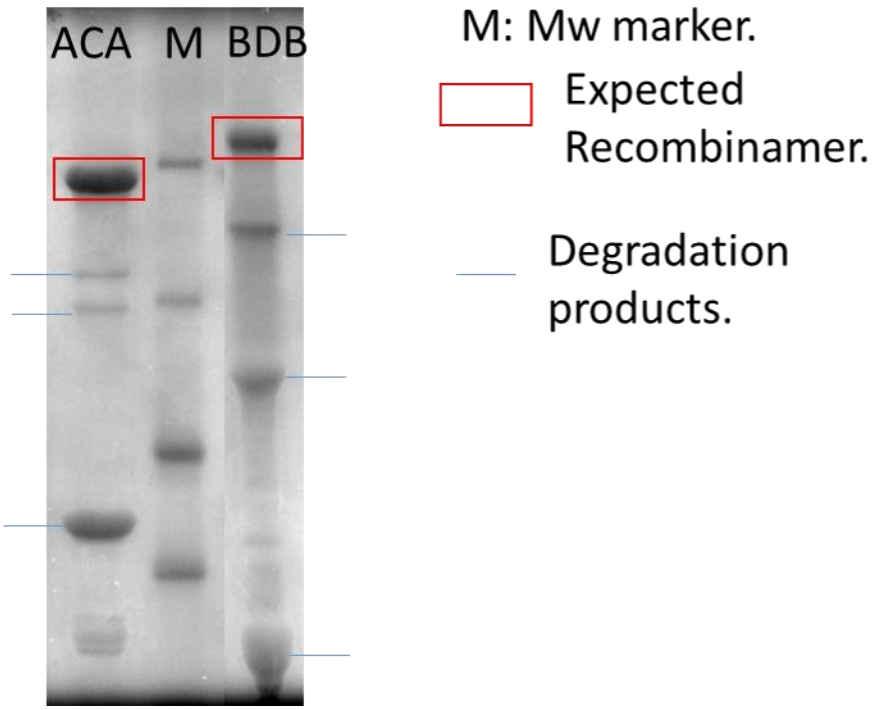

Figure 63: *SDS-PAGE of ACA and BDB samples after the purification process.Degradation products are clearly identify.*

5.4.4. Characterization of the zipper formation, protein coupling:

We hypothesized that the mixture of the single zipper domain recombinamers (A+ D and B+ C) will lead to the formation of block

recombinamers. In the same way, more complicated structures such as a brush conformation is obtained by the linkage between a three zipper domain containing ELR (A3) and his single counterpart (D). In order to test this hypothesis several experimental techniques were carried out.

5.4.4.1. Native polyacrylamide gel electrophoresis.

In a first approximation non-denaturing poly-acrylamide electrophoresis were used. Non-denaturing electrophoresis represent a simple technique to identify different protein morphologies. Under native PAGE conditions (absence of denaturing agents, such as SDS), polypeptides retain their higher-order structure, the ability of interact with other polypeptides and it is often retain enzymatic activity[157]. Thus, the migration of proteins depends not exclusively on the molecular weight, but other factors such as size, shape and native charge also play a critical role in the migration within the gel. Therefore, native PAGE is a useful technique when it comes to assaying native structures of proteins[157].

In this way, if a coupling between the different ELR-Zipper constructs take place a different band pattern should be identify in the electrophoresis. Electrophoresis were carried out both with and without the presence of β-mercapthoethanol for precluding the possible protein coupling due to disulfide bond between cisteins. The result of the electrophoresis is shown in **Figure 64**.

According to the native- PAGE analysis shown in **Figure 64**, it can be said that the conjugation of the different ELR-zippers is indeed taking place. Regarding the formation of block copolymers, lines A and D in the presence of β-mercapotethanol show a single negatively stained band, while in line A+D there is no trace of those negatively stained bands and a clear higher band appears. Taking a look to the

analysis without β-mercapotethanol, in line A appears a second negatively stained band (blue box) while in line D there is an absent of any kind of bands, but it seems to have a trace of bands on the top part of the gel(red group). The appearance of a second band in line A and the band trace at top of line D are consistent with self-aggregates formation due to disulfide bond between the cisteins. In the case of line D, the complex formed in this manner seems to be too big or too elongated to penetrate within the gel. Regarding the phenylalanine containing ELR-zippers (B & C), judging from the band pattern obtained in presence of β-mercapotethanol it seems clear that the coupling have been undertaken. Notwithstanding, some traces of the bands corresponding to the individuals specimens can be seen in line B+C (blue arrows). In the absence of β-mercapthoethanol, B shows clear a second band (black box), which indicate the formation of disulfide bonded self-aggregates. C looks less prone to self-aggregation as the intensity of the second band is clearly minority.

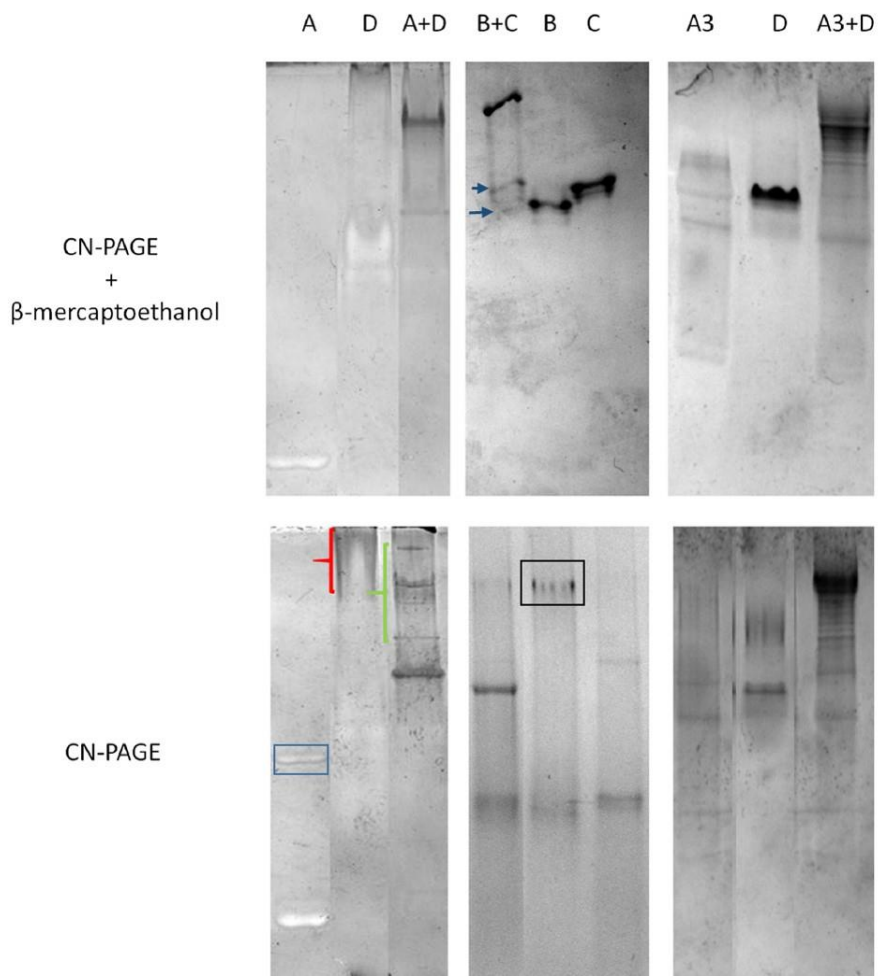

***Figure 64**: Native-PAGE analysis of the different ELR-zipper mixtures under different conditions, with and without β-mercaptoethanol.*

In light of the results of both with and without β-mercapthoethanol line A3 + D the formation of the recombinant brush polymer it also seems to be being taking place. In this case, line A3+D lacks of the bands related to the individual ELR-zippers but it does not show a clear band but a single broad band together with less intense group of bands. This multiple band appearance is consistence with the feasible different types of bonding available due to the three zippers domains present at A3. Since the migration in native PAGE is not only

related to molecular weight but also to the size or conformation of the complex, the conjugation of D to the first A domain will result in a different band compared with D being attached to the second, third or both A domains within A3.

In order to shed further light into the assembly of the ELR-zippers other experimental techniques, such as circular dichroism have been carried out. Since the presence of the cisteins does not prevent the formation of the complexes between the different ELR-zippers, the rest of the experimental techniques are carried out in absence of β-mercapthoethanol.

5.4.4.2. Circular dichroism (CD).

In order to have a clue on the secondary structure of the assemblies made by the different pairs of ELR-zipper CD spectroscopy analysis were carried out. The result of this analysis are shown in **Figure 65**.

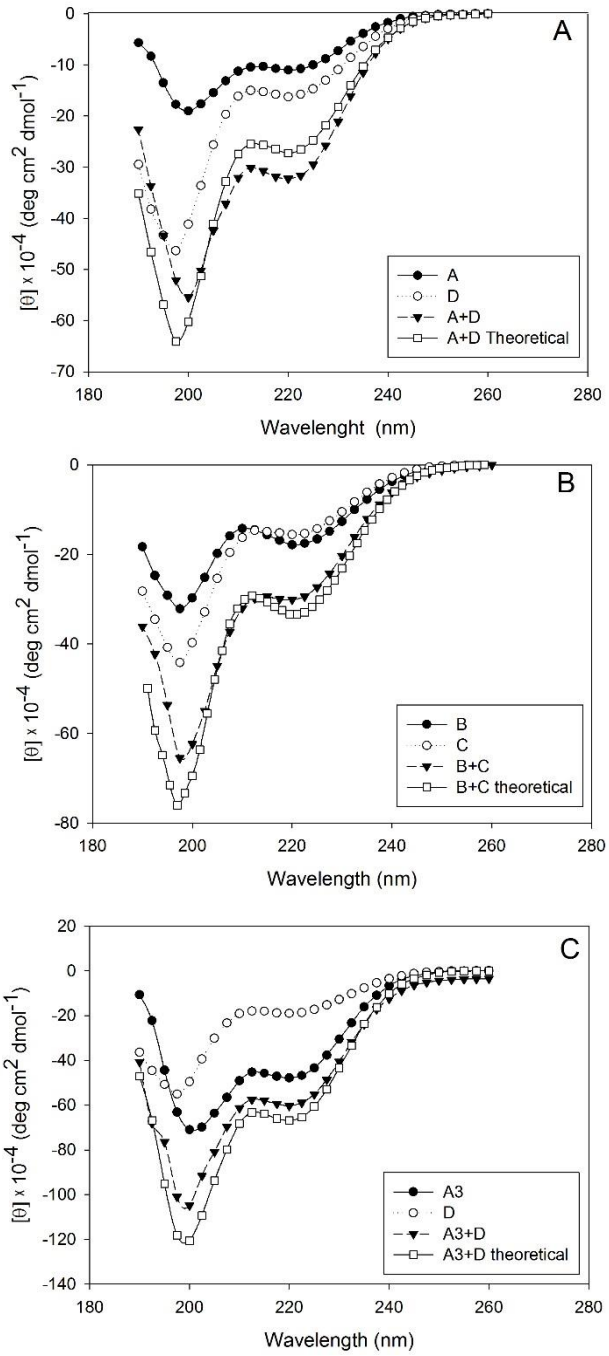

***Figure 65**: CD spectra at room temperature of A) A, D, A+D, B) B, C, B+C, C) A3, D A3+AD.*

Leucine zipper are known to adopt an α-helix, as secondary structure which present a CD spectra consisting of two characteristics negative bands at 208 and 222 nm. On the other hand, elastin like recombinamers are known to adopt a mixture of secondary structures consisting of random coils, β-turns and β-sheets assemblies[219, 220]. Regarding to the spectrum recorded (**Figure 65**), it can be said that when it comes to determining the secondary structure of the ELR – zipper assemblies the predominant part is that of the ELR, as there is a lack of the α-helix characteristic negative bands at 208 and 222nm.

Regarding the diblock formation, it can be clearly seen (**Figure 65A**) a variation of the wavelength of the first negative band in the mixture (moving to 200nm) when compared to the A and D individual spectrum. When comparing the mixture spectrum obtained with the theoretical one, which is obtained adding the spectrums recorded of the individual specimens, it can be seen that the 200 nm negative band is less intense in the experimental spectrum, which indicates a more order structure. The same behavior can be appreciated in the mixture of B and C (**Figure 65B**) and in the mixture making the brush recombinamer A3 and D (**Figure 65C**). It is worth noting that A3 shows a similar spectrum to the one obtained for the mixture, which could be identified as homo-aggregates formation. All in all, despite the fact that the main contribution of the spectrum is due to the ELRs, thus β-turn together with unordered conformation, it could be suggested a structure inducing effect played by the mixtures as a result of the α-helix formation of the zipper domains.

5.4.4.3. Dynamic light scattering (DLS):

In order to characterize the macromolecular assembly of the ELR-zippers, dynamic light scattering (DLS) measurements were

carried out. DLS have been extensively used in the characterization of the self-assembly behavior of ELRs[119, 221]. The autocorrelation functions obtained by DLS were analyzed using the CONTIN algorithm[160]. The size distributions obtained from this analysis are shown in **Figure 66**.

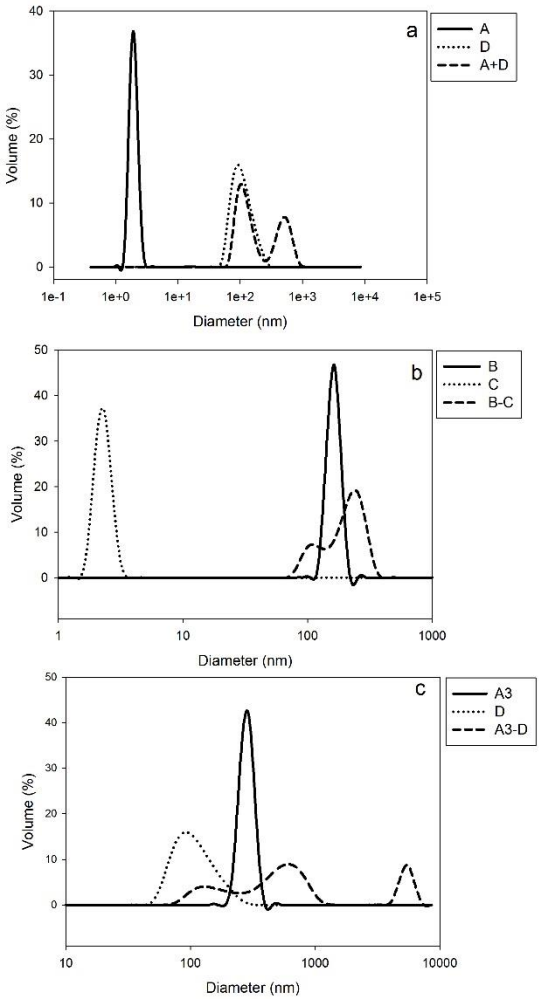

Figure 66: *Size distribution as measured by DLS at room temperature for a) A, D and A+D, b) B, C and B+C, c) A3, D and A3+D.*

ELR are dissolved relatively extended when the temperature is below their transition temperature. Under this conditions, ELR

monomers have been reported to have an hydrodynamic radius, as measured by DLS, between 1 and 10 nm[222]. As can be seen in **Figure 66a,b** E10Z3 (A) and E20Z2 (C) present an hydrodynamic radius below 10 nm, which indicate the extended, non-aggregated state of the chains of the cited ELR-zippers. The fact that this set of ELR-zippers (A & C) are in an extended state is in good agreement with the band pattern observed previously in the Native-Page analysis. Despite the fact that both samples (A & C) presented a band related with the homo-aggregates formation, it was less intense than the band corresponding to the monomer, which is compatible with the single small size distribution observes by DLS.

Regarding the A & C counterpart ELR-zippers, D & B respectively, the size distribution obtained indicate the formation of homo-aggregates as the size distribution obtained where centered at approximately 150 nm and 160 nm for D and B respectively. This sizes are incompatible with ELR single monomers. This homo-aggregation is also in good concordance with what was previously observed in the Native-Page analysis in the absence of β-mercaptoethanol. In light of the results obtained for the mixtures samples, both the di-block forming ELR-zippers pairs seems to be effectively adopting the di-block assembly. A+D shows a double size distribution (**Figure 66a)**, which are centered at approximately 150 nm and 500 nm respectively. The 500 nm distribution was not found in the individual samples, thus indicating the formation of new structures as result of the mixture. This structure formation is consistent with the di-block formation. Although the di-block formation appears to be taken place, the second size distribution observed (150 nm) is coincident with the one observed for the single D sample, which indicate that the reaction, zipper formation,

between A and D is not 100% effective, as both components were equimolarly mixed. The formation of the di-block by the phenylalanine-leucine ELR-zipper (B and C) also seems to be occurring, although the size distribution obtained in the mixture is only slightly bigger (approximately 220 nm) than that obtained for single B.

DLS data also cast some light on the brush recombinamer formation. As can be seen in **Figure 6 C**, E10Z3x3 (A3) shows a size distribution center at approximately 500 nm, which indicates the formation of a somehow self-aggregates. Regarding the A3-D mixture sample, three different size distributions (centered at approximately 150 nm, 540 nm and 5000 nm) can be observed. The first two distribution are coincident with the ones showed by the individuals ELR-zippers. The biggest distribution is not found in any of single recombinamers and therefore is attributed to the brush recombinamer formation. A summary of the DLS data is presented in **Table 20.**

***Table 20**: Summary of the light-scattering properties for ELR-Zipper.*

ELR	D_h(nm)	PDI
A	2.0 ± 0.4	0.54 ± 0.10
D	155.0 ± 63.0	0.28 ± 0.01
	120.0 ± 37.0	
A+D	512.0 ± 138.0	0.30 ± 0.05
C	162.0 ± 19.0	0.41 ± 0.03
B	2.5 ± 0.4	0.60 ± 0.15
	114.0 ± 20.0	
C+B	227.0 ± 51.0	0.38 ± 0.08
A3	516.0 ± 81.0	0.26 ± 0.06
	156.0 ± 71.0	
	544.0 ± 64.0	
A3+D	5438.0 ± 642.0	0.47 ± 0.11

The hydrodynamic diameter values obtained for the ELR-zipper solutions should be treated with caution as the polydispersity indexes are very high and the CONTIN analysis is less accurate under such conditions. Despite this, these results indicate the formation of di-blocks and brush recombinamer as a result of a coiled-coil interaction, although the sizes may not be very accurate.

5.4.4.4. Analytical centrifugation.

In order to have a precise evidence of the di-blocks and brush recombinamer formation, analytical ultracentrifugation (sedimentation velocity) experiments were carried out.

Analytical ultracentrifugation is a highly precise and accurate technique when it comes to determining properties of proteins or macromolecules in solution. The reason for this resides in that it is manly base in thermodynamics, which makes all the variables needed for the sedimentation analysis experimentally determinable[223]. The

sedimentation coefficient S, which is the velocity of the particle per unit gravitational acceleration, is defined as follows.

$$S = \frac{u}{\omega^2 r} = \frac{M(1-\bar{\nu}\rho)}{Nf}$$

Where u is the molecules velocity, ω is the angular velocity, r is the distance of the molecules to the axes of rotation, M is the molar weight of the molecules, $\bar{\nu}$ is the partial specific volume, in other words the inverse of the molecules effective density (volume occupied by each gram of solute), ρ is the density of the solvent, N is the Avogadro's number and f is the frictional coefficient, which is dependent on the size and shape of the molecules. Thus, *S* is independent of the operating conditions as it is proportional to the effective molar weight (effects of buoyancy corrected) and it is inversely proportional to the size and shape of the molecules under study.

In order to analyze the different macromolecular assemblies made by the conjugation of the ELR-zippers, sedimentation velocity experiments were carried out. In an experiment of velocity of sedimentation the molecules are under a high centrifugal field in which the centrifugal force is higher than the diffusion forces, which implies a net transport of material to the bottom of the cell. It is a hydrodynamic transport method which allows us to separate the different molecules in a solution in base of their *S*, thus their size shape and density. The result of this analysis are shown in **Figure 67** and summarized in **Table 21**..

***Table 21**: Summary of the data obtained by analytical ultracentrifugation.*

ELR	S	%
A	0.8	98.1
	3.2	1.9
D	0.5	70.6
	1.7	29.4
A+D	1.2	97.7
	3.8	2.3
B	1.3	15.3
	1.8	71.9
	2.9	10.7
	4	2.1.
C	1.1	93.2
	2.2	6.8
B+C	1.1	62.8
	1.9	33.5
	3.1	3.7
A3	1.0	82.7
	1.8	17.3
A3+D	1.2	94.3
	2.4	5.3
	3.6	0.6

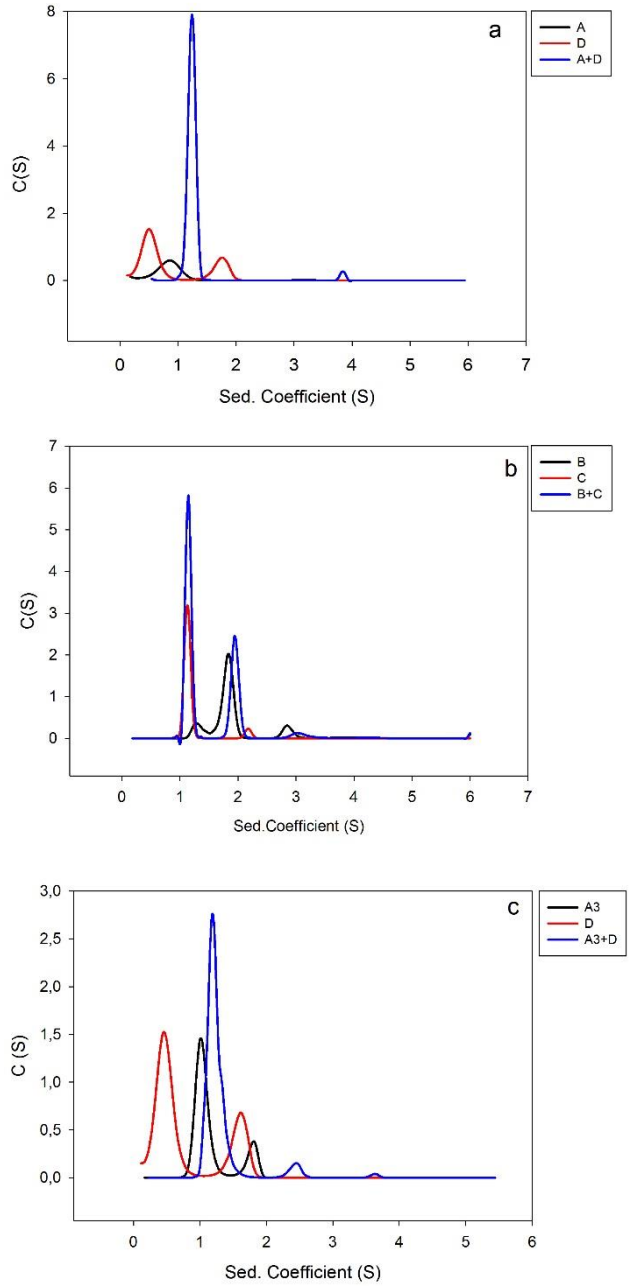

***Figure 67**: Sedimentation coefficient distribution as measured by analytical ultracentrifugation (sedimentation velocity) at room temperature for a) A, D and A+D, b) B, C and B+C, c) A3, D and A3+D.*

In light of these results, it is clear that the ELR pairs containing a pure leucine zipper (A, D and A3) assembled through coiled-coil formation with an efficiency higher than 90%. Regarding the di-block formation (A+D), it can be seen that A is manly in a monomer state with the 98.1% of the molecules presenting an S of 0.8. On the other hand, D present two main conformations, one presenting an S of 0.5, which represent the 70.6% of the total molecules in the solution and that can be attributed to the extended monomer chains, and a second one having an S of 1.7. This second type of assemblies represent almost the 30 % of the total molecules and can correspond to some kind of self-aggregation. This results are in good agreement with what was observed with the other experimental techniques employed. Once A and D are mixed, the majority of the molecules in the solution (97.7 %) showed an S of 1.2, which was not found in any of the individuals specimens. Thus, the formation of a predominant different assembly is indeed occurring. This new assembly is attributed to the di-block formation.

Regarding the brush recombinamer formation, it is also taking place with high effectiveness. A3 is found to have two different types of molecules when dissolved in water on his own. The 82.7 % of the A3 molecules possess an S of 1 while the remaining 17.3% correspond to molecules self-aggregates presenting an S of 1.8. The mixture between A3 and D give rise to the formation of three different assemblies which were not found in the individual specimens. The 94.3 % of the molecules in the mixture have an S of 1.2. Taking into account the difference in molecular weight between A3 and A, and **Equation 1**, the fact that the mixture between A and D and the mixture between A3 and D gave rise to assemblies with the same 1.2 S indicates that both

assemblies have a completely different shape, which is consistent with the formation of the di-block and the brush recombinamer.

On the contrary, the effectiveness of the assembly between the ELRs containing zipper domain with phenylalanine in some of the **d** positions (B & C) is noticeably lower. Four different assemblies were determined for B, with the 71.9 % of the molecules showing an S of 1.8. This heterogeneity together with the high S value of the predominant assembly is in good agreement with the formation of self-aggregates by this sample as previously determined by DLS and Native-PAGE. On the other hand, C is a monodisperse sample showing the 93.2% of its molecules an S of 1.1. The same 1.1 S is found for the 62.8 % of the molecules present in the B+C mixture samples. This similarity in the sedimentation coefficient together with the similarity in the hydrodynamic diameter between B and C+B (previously measured by DLS), make as think that those 1.1 S molecules of the mixture sample are indeed B molecules. The effectiveness of the di-block formation due to the assembly between C and B is restricted to the remaining 37.2 % of the molecules (1.9 S 33.5% and 3.1 S 3.7%).

5.4.5. Final remarks.

The assembly of ELR through coiled-coil into di-blocks and brush recombinamers have been investigated. A set of five ELRs containing leucine zipper domains have been designed, biosynthesized, and purified. The zipper domains were specifically designed for selectively interact with their counterpart, which has the same amino acids in positions **a** and **d** and opposite charged amino acids in position **e** and **g**, leading to the heterodimer formation. All the constructions present a cistein in the zipper domains in order to empower the union

through a covalent disulfide bong. In summary, these results show that the mixture between genetically designed ELR-zipper can be used to the fabrication of complex architectures through coiled-coil association. Di-blocks and brush recombinamers have been synthesized and characterized, being those ELR containing pure leucine zippers those reaching a higher assembly yield .In this regard, exploiting the possibilities of the assembly found in ELR-leucine zippers to obtain non-linear superstructures opens up unique opportunities to generate new functional materials with defined structures and functionalities.

CONCLUSIONS

6.0. CONCLUSIONS.

6.1. Effect of NaCl on the self-assembly of ELbcRs.

- The co-dissolution of NaCl and ELbcRs have shown an extraordinary effect on the size of the aggregates formed by the three ELbcRs studied (E50A40, E100A40, E50A40E50), with NaCl causing a substantial decrease in nanoparticle size in all cases. There is no linear dependence between particle size and NaCl concentration. At low NaCl concentrations, the self-assembled nanostructures present a wide size distribution (from 40nm to 250 nm), while once a limit NaCL is reached, the nanoparticles switch to small low polydispersed size distributions (center approx. 50nm) with further NaCl addition having no further effect on the size.
- The presence of NaCl does not change the morphology of the self-assembled nano-objects as measured by SLS and corroborated by Cryo-TEM Thus, in the compounds studied, the recombinamers were found to have the same morhoplogy (micelle/vesicle) when dissolved in both solvents (water and NaCl solutions).
- If the addition of ions is subsequent to the nano-object formation, both water (approx. 200nm) and NaCl (approx. 50nm) nanoparticle populations are found. Although both populations were found, the majority of the nanoparticles correspond to the small size distribution found when dissolved in NaCl solution which indicates that the higher ionic strength of the environment forces the already folded hydrophobic parts to adopt a different, more compacted, conformation.

- The size reduction effect is not exclusive of NaCl, as other salts (KCl, $CaCl_2$, Na_2HPO_4 and Na_2SO_4) containing different cations and anions also have a profound effect on the self-assembly behavior of these ELbcRs. A comparable salting in / salting out power of the anions and cations is required in order to obtain stable nanoparticles.
- This work support the use of NaCl as an effective way of controlling the dimensions of ELbcR-based self-assembled nanoparticles.

6.2. Effect of surfactants on the self-assembly of a model ELbcR.

- The size of the model ELbcR (E50A40) self-assembled micelles can be controlled by adjusting the co-surfactant concentration. Different effects were observed depending on the polarity of the surfactant, with the addition of an oppositely charged (cationic) surfactant resulting in a huge increase up to the micro-scale (approx. 3μm), which led to the flocculation of the micelles at sufficiently high surfactant concentration (above 2mM). A smaller size increase can be achieved by adding a non-ionic surfactant (OG). Anionic surfactant SDS causes a small size increase at low concentration, while above 2mM the self-assembling process was completely disrupted.
- The self-assembly process is mainly governed by the overall charge of the ELbcR-surfactant complexes. The hydrophobic interaction between the alkyl chains of the surfactants and the hydrophobic blocks of the ELbcR, also plays a role in the self-assembling process.

- The addition of non-ionic or similarly charged surfactants has no effect on T_t. In contrast, the addition of an oppositely charged surfactant has a marked effect on T_t in a two-step process involving an initial reduction in T_t, followed by an increase in this parameter, as the Z-potential of the complexes became positive.
- These results support the use of surfactants as a highly interesting means of controlling the self-assembly of ELbcRs in aqueous solution, as well as their use in drug delivery or purification processes

6.3. Graphene oxide- ELR composites.

- Genetically designed amino-containing ELRs can be employed to covalently functionalize GO by an amidation reaction between the carboxyl group of GO and the amino groups present at lysines of the ELRs. The effectiveness of the reaction was approximately of 70%.
- The GO-ELR composites were specifically prepared to have the ELR as the predominant compound. Thus, the GO was estimated by TGA to represent approximately the 2.5 wt% of the composite, which implied a reduction of approximately 4°C in the T_t of the composite when compared with the native ELR.
- The ELR-GO composites were found to be soluble in different saline buffers, preventing GO from aggregating. ELR-GO composites showed excellent in-vitro biocompatibility as checked by cell proliferation studies, enabling their use for potential applications in the biomedical field.
- ELR-GO have been successfully prepared into different structures which find usefulness in the biomedical field. In this

sense different microstructured ELR-GO hydrogels have been obtained showing topographies by using patterned PDMS molds. ELR-GO nanofibers have been obtained by electrospinning. ELR-GO composites have been also prepared as physical hydrogels and nanoparticles.

- This work proves the feasibility of covalently bonding rationally designed ELRs to GO for the construction of composite functional materials that could find uses in the biomedical field, such as drug delivery or tissue engineering.

6.4. Self-assembly of different Elastin like recombinamers macromolecular architectures through Leucine Zipper formation.

- A set of five ELRs containing leucine zipper domains have been designed, biosynthesized, and purified. The zipper domains were specifically designed for selectively interact with their counterpart. One pair being 100% Leucine at d position and the other pair a mixture of phenylalanine and leucine.
- All the constructions present a cistein in the zipper domains in order to empower the union through a covalent disulfide bond. The disulfide bond formation was verified by native polyacrylamide electrophoresis.
- The study of the leucine zipper formation through native polyacrylamide electrophoresis, DLS, CD and analytical centrifugation have shown the successful assembly of ELR through coiled-coil interactions into di-blocks and nonlinear recombinamers.

- The ELRs containing pure leucine zippers are those reaching a higher assembly yield with more of 95% of heterodimer formation. On the contrary, phenylalanine zippers only threw about 30% of heterodimer formation.
- This results showed the feasibility of obtaining non-linear ELR superstructures, which opens up unique opportunities to generate new functional materials with defined structures and functionalities

.

REFERENCES

7.0. REFERENCES.

1. Hu, X.; Cebe, P.; Weiss, A. S.; Omenetto, F.; Kaplan, D. L., Protein-based composite materials. *Materials Today* **2012,** 15, (5), 208-215.

2. Girotti, A.; Fernandez-Colino, A.; Lopez, I. M.; Rodriguez-Cabello, J. C.; Arias, F. J., Elastin-like recombinamers: biosynthetic strategies and biotechnological applications. *Biotechnol J* **2011,** 6, (10), 1174-86.

3. Rodríguez-Cabello, J.; Girotti, A.; Ribeiro, A.; Arias, F., Synthesis of Genetically Engineered Protein Polymers (Recombinamers) as an Example of Advanced Self-Assembled Smart Materials. In *Nanotechnology in Regenerative Medicine*, Navarro, M.; Planell, J. A., Eds. Humana Press: 2012; Vol. 811, pp 17-38.

4. MacEwan, S. R.; Chilkoti, A., Elastin-like polypeptides: Biomedical applications of tunable biopolymers. *Peptide Science* **2011,** 94, (1), 60-77.

5. Rodríguez-Cabello, J. C.; Martín, L.; Alonso, M.; Arias, F. J.; Testera, A. M., "Recombinamers" as advanced materials for the post-oil age. *Polymer* **2009,** 50, (22), 5159-5169.

6. Vrhovski, B.; Weiss, A. S., Biochemistry of tropoelastin. *Eur J Biochem* **1998,** 258, (1), 1-18.

7. Uitto, J., Biochemistry of the elastic fibers in normal connective tissues and its alterations in diseases. *J Invest Dermatol* **1979,** 72, (1), 1-10.

8. Mithieux, S. M.; Weiss, A. S., Elastin. *Advances in Protein Chemistry* **2005,** 70, 437-461.

9. Debelle, L.; Tamburro, A. M., Elastin: molecular description and function. *International Journal of Biochemistry & Cell Biology* **1999,** 31, (2), 261-272.

10. Miao, M.; Bellingham, C. M.; Stahl, R. J.; Sitarz, E. E.; Lane, C. J.; Keeley, F. W., Sequence and structure determinants for the self-aggregation of recombinant polypeptides modeled after human elastin. *Journal of Biological Chemistry* **2003,** 278, (49), 48553-48562.

11. Urry, D. W.; Hugel, T.; Seitz, M.; Gaub, H. E.; Sheiba, L.; Dea, J.; Xu, J.; Parker, T., Elastin: a representative ideal protein elastomer. *Philosophical Transactions of the Royal Society of London Series B-Biological Sciences* **2002,** 357, (1418), 169-184.

12. Cox, B. A.; Starcher, B. C.; Urry, D. W., Coacervation of Alpha-Elastin Results in Fiber Formation. *Biochimica Et Biophysica Acta* **1973,** 317, (1), 209-213.

13. Di Zio, K.; Tirrell, D. A., Mechanical properties of artificial protein matrices engineered for control of cell and tissue behavior. *Macromolecules* **2003,** 36, (5), 1553-1558.

14. Rodríguez-Cabello, J. C.; Reguera, J.; Girotti, A.; Arias, F. J.; Alonso, M., Genetic Engineering of Protein-Based Polymers: The Example of Elastinlike Polymers. *Advances in Polymer Science* **2006,** 200, 119-167.

15. Urry, D. W., *What sustains life? Consilient mechanisms for protein-based machines and materials*. Springer-Verlag: New York, 2006.

16. Rodriguez-Cabello, J. C.; Gonzalez de Torre, I.; Pinedo, G., CHAPTER 19 Elastin-like Hydrogels and Self-assembled Nanostructures for Drug Delivery. In *Smart Materials for Drug*

Delivery: Volume 2, The Royal Society of Chemistry: 2013; Vol. 2, pp 180-198.

17. Meyer, D. E.; Chilkoti, A., Quantification of the Effects of Chain Length and Concentration on the Thermal Behavior of Elastin-like Polypeptides. *Biomacromolecules* **2004,** 5, (3), 846-851.

18. Urry, D. W., Molecular Machines: How Motion and Other Functions of Living Organisms Can Result from Reversible Chemical Changes. *Angew. Chem., Int. Ed. Engl.* **1993,** 32, (6), 819-841.

19. Urry, D. W.; Trapane, T. L.; Prasad, K. U., Phase-structure transitions of the elastin polypentapeptide-water system within the framework of composition-temperature studies. *Biopolymers* **1985,** 24, (12), 2345-56.

20. Rodríguez-Cabello, J. C.; Alonso, M.; Pérez, T.; Herguedas, M. M., Differential scanning calorimetry study of the hydrophobic hydration of the elastin-based polypentapeptide, poly(VPGVG), from deficiency to excess of water. *Biopolymers* **2000,** 54, (4), 282-288.

21. Urry, D. W.; Luan, C. H.; Parker, T. M.; Gowda, D. C.; Prasad, K. U.; Reid, M. C.; Safavy, A., Temperature of polypeptide inverse temperature transition depends on mean residue hydrophobicity. *Journal of the American Chemical Society* **1991,** 113, (11), 4346-4348.

22. Urry, D. W.; Haynes, B.; Zhang, H.; Harris, R. D.; Prasad, K. U., Mechanochemical coupling in synthetic polypeptides by modulation of an inverse temperature transition. *Proc Natl Acad Sci U S A* **1988,** 85, (10), 3407-11.

23. Ribeiro, A.; Arias, F. J.; Reguera, J.; Alonso, M.; Rodríguez-Cabello, J. C., Influence of the Amino-Acid Sequence on the Inverse Temperature Transition of Elastin-Like Polymers. *Biophys. J.* **2009,** 97, (1), 312-320.

24. Kunz, W.; Henle, J.; Ninham, B. W., 'Zur Lehre von der Wirkung der Salze' (about the science of the effect of salts): Franz Hofmeister's historical papers. *Current Opinion in Colloid & Interface Science* **2004,** 9, (1-2), 19-37.

25. Franz, H., Zur Lehre von der Wirkung der Salze. *Archiv für Experimentelle Pathologie und Pharmakologie* **1888,** 24.

26. Cho, Y.; Zhang, Y.; Christensen, T.; Sagle, L. B.; Chilkoti, A.; Cremer, P. S., Effects of Hofmeister Anions on the Phase Transition Temperature of Elastin-like Polypeptides. *The Journal of Physical Chemistry B* **2008,** 112, (44), 13765-13771.

27. Reguera, J.; Urry, D. W.; Parker, T. M.; McPherson, D. T.; Rodriguez-Cabello, J. C., Effect of NaCl on the Exothermic and Endothermic Components of the Inverse Temperature Transition of a Model Elastin-like Polymer. *Biomacromolecules* **2007,** 8, (2), 354-358.

28. Thapa, A.; Han, W.; Simons, R. H.; Chilkoti, A.; Chi, E. Y.; López, G. P., Effect of detergents on the thermal behavior of elastin-like polypeptides. *Biopolymers* **2013,** 99, (1), 55-62.

29. Urry, D. W.; Hayes, L. C.; Channe Gowda, D.; Parker, T. M., Pressure effect on inverse temperature transitions: biological implications. *Chemical Physics Letters* **1991,** 182, (2), 101-106.

30. Tamura, T.; Yamaoka, T.; Kunugi, S.; Panitch, A.; Tirrell, D. A., Effects of temperature and pressure on the aggregation properties of an engineered elastin model polypeptide in aqueous solution. *Biomacromolecules* **2000,** 1, (4), 552-5.

31. Urry, D. W., Physical Chemistry of Biological Free Energy Transduction As Demonstrated by Elastic Protein-Based Polymers†. *The Journal of Physical Chemistry B* **1997,** 101, (51), 11007-11028.

32. Cappello, J.; Crissman, J.; Dorman, M.; Mikolajczak, M.; Textor, G.; Marquet, M.; Ferrari, F., Genetic-Engineering of Structural Protein Polymers. *Biotechnology Progress* **1990,** 6, (3), 198-202.

33. Lewis, R. V.; Hinman, M.; Kothakota, S.; Fournier, M. J., Expression and purification of a spider silk protein: A new strategy for producing repetitive proteins. *Protein Expression and Purification* **1996,** 7, (4), 400-406.

34. Mcpherson, D. T.; Morrow, C.; Minehan, D. S.; Wu, J. G.; Hunter, E.; Urry, D. W., Production and Purification of a Recombinant Elastomeric Polypeptide, G-(Vpgvg)19-Vpgv, from Escherichia-Coli. *Biotechnology Progress* **1992,** 8, (4), 347-352.

35. Cheng, S., Methods and reagents for the polymerase chain reaction amplification of long DNA sequences. In Google Patents: 1996.

36. McGrath, K. P.; Tirrell, D. A.; Kawai, M.; Mason, T. L.; Fournier, M. J., Chemical and biosynthetic approaches to the production of novel polypeptide materials. *Biotechnology Progress* **1990,** 6, (3), 188-192.

37. Won, J. I.; Barron, A. E., A new cloning method for the preparation of long repetitive polypeptides without a sequence requirement. *Macromolecules* **2002,** 35, (22), 8281-8287.

38. Prince, J. T.; Mcgrath, K. P.; Digirolamo, C. M.; Kaplan, D. L., Construction, Cloning, and Expression of Synthetic Genes Encoding Spider Dragline Silk. *Biochemistry* **1995,** 34, (34), 10879-10885.

39. Arévalo, C. G. Elastin-like recombinamers for advanced biomedical applications: Tissue engineering, gene delivery and nanovaccines. Universidad de Valladolid

Valladolid, 2012.

40. Roberts, R. J.; Vincze, T.; Posfai, J.; Macelis, D., REBASE - restriction enzymes and DNA methyltransferases. *Nucleic Acids Research* **2005,** 33, D230-D232.

41. Goeden-Wood, N. L.; Conticello, V. P.; Muller, S. J.; Keasling, J. D., Improved assembly of multimeric genes for the biosynthetic production of protein polymers. *Biomacromolecules* **2002,** 3, (4), 874-879.

42. Rabotyagova, O. S.; Cebe, P.; Kaplan, D. L., Protein-Based Block Copolymers. *Biomacromolecules* **2011,** 12, (2), 269-289.

43. Voet, D.; Voet, J. G., *Biochemistry*. John Wiley & Sons: 2004.

44. Duncan, R., The dawning era of polymer therapeutics. *Nat Rev Drug Discov* **2003,** 2, (5), 347-60.

45. Thomas, S.; Hannah, L.; Marzia, M.; Miriam, V. F.-M.; Lorena Ruiz, P.; Giuseppe, B., Block copolymer nanostructures. *Nano Today* **2008,** 3.

46. Nettles, D. L.; Chilkoti, A.; Setton, L. A., Applications of elastin-like polypeptides in tissue engineering. *Adv. Drug Delivery Rev.* **2010,** 62, (15), 1479-1485.

47. McDaniel, J. R.; Callahan, D. J.; Chilkoti, A., Drug delivery to solid tumors by elastin-like polypeptides. *Advanced Drug Delivery Reviews* **2010,** 62, (15), 1456-1467.

48. Huang, L.; McMillan, R. A.; Apkarian, R. P.; Pourdeyhimi, B.; Conticello, V. P.; Chaikof, E. L., Generation of Synthetic Elastin-Mimetic Small Diameter Fibers and Fiber Networks. *Macromolecules* **2000,** 33, (8), 2989-2997.

49. Lee, T. A. T.; Cooper, A.; Apkarian, R. P.; Conticello, V. P., Thermo-reversible self-assembly of nanoparticles derived from elastin-mimetic polypeptides. *Advanced Materials* **2000,** 12, (15), 1105-1110.

50. Rodriguez-Cabello, J. C.; Martin, L.; Girotti, A.; Garcia-Arevalo, C.; Arias, F. J.; Alonso, M., Emerging applications of multifunctional elastin-like recombinamers. *Nanomedicine (London, U. K.)* **2011,** 6, (1), 111-22.

51. Israelachvili, J., *Intermolecular and Surface Forces, Third Edition*. Academic Press: 2010.

52. Nagarajan, R.; Ganesh, K., Block copolymer self-assembly in selective solvents: theory of solubilization in spherical micelles. *Macromolecules* **1989,** 22, (11), 4312-4325.

53. Jones, R. A. L., *Soft Condensed Matter*. OUP Oxford: 2002.

54. Castelletto, V.; Parras, P.; Hamley, I. W.; Bäverbäck, P.; Pedersen, J. S.; Panine, P., Wormlike Micelle Formation and Flow Alignment of a Pluronic Block Copolymer in Aqueous Solution. *Langmuir* **2007,** 23, (13), 6896-6902.

55. Smart, T.; Lomas, H.; Massignani, M.; Flores-Merino, M. V.; Perez, L. R.; Battaglia, G., Block copolymer nanostructures. *Nano Today* **2008,** 3, (3–4), 38-46.

56. Discher, B. M.; Won, Y.-Y.; Ege, D. S.; Lee, J. C.-M.; Bates, F. S.; Discher, D. E.; Hammer, D. A., Polymersomes: Tough Vesicles Made from Diblock Copolymers. *Science* **1999,** 284, (5417), 1143-1146.

57. Jain, S.; Bates, F. S., On the origins of morphological complexity in block copolymer surfactants. *Science* **2003,** 300, (5618), 460-4.

58. Cui, H.; Chen, Z.; Zhong, S.; Wooley, K. L.; Pochan, D. J., Block Copolymer Assembly via Kinetic Control. *Science* **2007,** 317, (5838), 647-650.

59. Xuan, J.; Han, D.; Xia, H.; Zhao, Y., Dual-Stimuli-Responsive Micelle of an ABC Triblock Copolymer Bearing a Redox-Cleavable Unit and a Photocleavable Unit at Two Block Junctions. *Langmuir* **2013,** 30, (1), 410-417.

60. Zhu, J.; Jiang, W., Self-Assembly of ABC Triblock Copolymer into Giant Segmented Wormlike Micelles in Dilute Solution. *Macromolecules* **2005,** 38, (22), 9315-9323.

61. Dupont, J.; Liu, G., ABC triblock copolymer hamburger-like micelles, segmented cylinders, and Janus particles. *Soft Matter* **2010,** 6, (15), 3654-3661.

62. Liu; Abetz, V.; Müller, A. H. E., Janus Cylinders. *Macromolecules* **2003,** 36, (21), 7894-7898.

63. Stoenescu, R.; Graff, A.; Meier, W., Asymmetric ABC-triblock copolymer membranes induce a directed insertion of membrane proteins. *Macromol Biosci* **2004,** 4, (10), 930-5.

64. Stewart, S.; Liu, G., Block Copolymer Nanotubes. *Angew Chem Int Ed Engl* **2000,** 39, (2), 340-344.

65. Holder, S. J.; Sommerdijk, N. A. J. M., New micellar morphologies from amphiphilic block copolymers: disks, toroids and bicontinuous micelles. *Polymer Chemistry* **2011,** 2, (5), 1018-1028.

66. Jiang, X.; Wang, Y.; Zhang, W.; Zheng, P.; Shi, L., Raspberry-Like Aggregates Containing Secondary Nanospheres of Polystyrene-block-poly(4-vinylpyridine) Micelles. *Macromolecular Rapid Communications* **2006,** 27, (21), 1833-1837.

67. Li, Z.; Hillmyer, M. A.; Lodge, T. P., Laterally Nanostructured Vesicles, Polygonal Bilayer Sheets, and Segmented Wormlike Micelles. *Nano letters* **2006,** 6, (6), 1245-1249.

68. Brannan, A. K.; Bates, F. S., ABCA Tetrablock Copolymer Vesicles. *Macromolecules* **2004,** 37, (24), 8816-8819.

69. Förster, S.; Berton, B.; Hentze, H. P.; Krämer, E.; Antonietti, M.; Lindner, P., Lyotropic Phase Morphologies of Amphiphilic Block Copolymers. *Macromolecules* **2001,** 34, (13), 4610-4623.

70. Jain, S.; Gong, X.; Scriven, L. E.; Bates, F. S., Disordered Network State in Hydrated Block-Copolymer Surfactants. *Physical Review Letters* **2006,** 96, (13), 138304.

71. Giuseppe, B.; Anthony, J. R., The evolution of vesicles from bulk lamellar gels. *Nature Materials* **2005,** 4, (11), 869-876.

72. Battaglia, G.; Ryan, A. J., Effect of Amphiphile Size on the Transformation from a Lyotropic Gel to a Vesicular Dispersion. *Macromolecules* **2005,** 39, (2), 798-805.

73. Bermudez, H.; Brannan, A. K.; Hammer, D. A.; Bates, F. S.; Discher, D. E., Molecular Weight Dependence of Polymersome Membrane Structure, Elasticity, and Stability. *Macromolecules* **2002,** 35, (21), 8203-8208.

74. Findenegg, G. H., J. N. Israelachvili: Intermolecular and Surface Forces (With Applications to Colloidal and Biological Systems). Academic Press, London, Orlando, San Diego, New York, Toronto, Montreal, Sydney, Tokyo 1985. 296 Seiten, *Berichte der Bunsengesellschaft für physikalische Chemie* **1986,** 90, (12), 1241-1242.

75. Kunz, W.; Henle, J.; Ninham, B. W., 'Zur Lehre von der Wirkung der Salze' (about the science of the effect of salts): Franz Hofmeister's historical papers. *Curr. Opin. Colloid Interface Sci.* **2004,** 9, (1–2), 19-37.

76. Franz, H., Zur Lehre von der Wirkung der Salze. *Arch. Exp. Path. Pharmakol.* **1888,** 24.

77. Pandit, N.; Trygstad, T.; Croy, S.; Bohorquez, M.; Koch, C., Effect of Salts on the Micellization, Clouding, and Solubilization Behavior of Pluronic F127 Solutions. *J. Colloid Interface Sci.* **2000,** 222, (2), 213-220.

78. Jørgensen, E. B.; Hvidt, S.; Brown, W.; Schillén, K., Effects of Salts on the Micellization and Gelation of a Triblock Copolymer Studied by Rheology and Light Scattering. *Macromolecules* **1997,** 30, (8), 2355-2364.

79. Patel, K.; Bahadur, P.; Guo, C.; Ma, J. H.; Liu, H. Z.; Yamashita, Y.; Khanal, A.; Nakashima, K., Salt induced micellization of very hydrophilic PEO–PPO–PEO block copolymers in aqueous solutions. *Eur. Polym. J.* **2007,** 43, (5), 1699-1708.

80. Perreur, C.; Habas, J.-P.; Lapp, A.; Peyrelasse, J., Salt influence upon the structure of aqueous solutions of branched PEO–PPO–PEO copolymers. *Polymer* **2006,** 47, (3), 841-848.

81. Zhang, L.; Somasundaran, P.; Maltesh, C., Electrolyte Effects on the Surface Tension and Micellization of n-Dodecyl β-d-Maltoside Solutions. *Langmuir* **1996,** 12, (10), 2371-2373.

82. Baldwin, R. L., How Hofmeister ion interactions affect protein stability. *Biophys. J.* **1996,** 71, (4), 2056-2063.

83. Sedlák, E.; Stagg, L.; Wittung-Stafshede, P., Effect of Hofmeister ions on protein thermal stability: Roles of ion hydration and peptide groups? *Arch. Biochem. Biophys.* **2008,** 479, (1), 69-73.

84. Khan, M. O.; Mel'nikov, S. M.; Jönsson, B., Anomalous Salt Effects on DNA Conformation: Experiment and Theory. *Macromolecules* **1999,** 32, (26), 8836-8840.

85. Vámosi, G.; Clegg, R. M., The Helix−Coil Transition of DNA Duplexes and Hairpins Observed by Multiple Fluorescence Parameters†. *Biochemistry* **1998,** 37, (40), 14300-14316.

86. Zou, D.; Tie, Z.; Lu, C.; Qin, M.; Lu, X.; Wang, M.; Wang, W.; Chen, P., Effects of hydrophobicity and anions on self-assembly of the peptide EMK16-II. *Biopolymers* **2010,** 93, (4), 318-329.

87. López de la Paz, M.; Goldie, K.; Zurdo, J.; Lacroix, E.; Dobson, C. M.; Hoenger, A.; Serrano, L., De novo designed peptide-based amyloid fibrils. *Proc. Natl. Acad. Sci. U. S. A.* **2002,** 99, (25), 16052-16057.

88. Rosen, M. J., *Surfactants and Interfacial Phenomena*. Wiley: 2004.

89. Courtois, J.; Berret, J. F., Probing oppositely charged surfactant and copolymer interactions by isothermal titration microcalorimetry. *Langmuir* **2010,** 26, (14), 11750-8.

90. Langevin, D., Complexation of oppositely charged polyelectrolytes and surfactants in aqueous solutions. A review. *Adv. Colloid Interface Sci.* **2009,** 147–148, (0), 170-177.

91. Zhao, J.; Zhang, G.; Pispas, S., Thermo-induced aggregation behavior of poly(ethylene oxide)-b-poly(N-isopropylacrylamide) block copolymers in the presence of cationic surfactants. *J. Phys. Chem B.* **2009,** 113, (31), 10600-6.

92. Petzold, G.; Mende, M.; Kochurova, N., Polymer–surfactant complexes as flocculants. *Colloids Surf., A* **2007,** 298, (1–2), 139-144.

93. Phani Kumar, B. V. N.; Umayal Priyadharsini, S.; Prameela, G. K. S.; Mandal, A. B., NMR investigations of self-aggregation characteristics of SDS in a model assembled tri-block copolymer solution. *J. Colloid Interface Sci.* **2011,** 360, (1), 154-162.

94. Stepanek, M.; Matejicek, P.; Prochazka, K.; Filippov, S. K.; Angelov, B.; Slouf, M.; Mountrichas, G.; Pispas, S., Polyelectrolyte-surfactant complexes formed by poly[3,5-bis(trimethylammoniummethyl)4-hydroxystyrene iodide]-block-poly(ethylene oxide) and sodium dodecyl sulfate in aqueous solutions. *Langmuir* **2011,** 27, (9), 5275-81.

95. Hajduová, J.; Procházka, K.; Šlouf, M.; Angelov, B.; Mountrichas, G.; Pispas, S.; Štěpánek, M., Polyelectrolyte–Surfactant Complexes of Poly[3,5-bis(dimethylaminomethyl)-4-hydroxystyrene]-block-poly(ethylene oxide) and Sodium Dodecyl Sulfate: Anomalous Self-Assembly Behavior. *Langmuir* **2013,** 29, (18), 5443-5449.

96. Wesley, R. D.; Dreiss, C. A.; Cosgrove, T.; Armes, S. P.; Thompson, L.; Baines, F. L.; Billingham, N. C., Structure of a hydrophilic-hydrophobic block copolymer and its interactions with salt and an anionic surfactant. *Langmuir* **2005,** 21, (11), 4856-61.

97. Kumbhakar, M., Aggregation of ionic surfactants to block copolymer assemblies: a simple fluorescence spectral study. *J. Phys. Chem B.* **2007,** 111, (51), 14250-5.

98. Kelarakis, A.; Chaibundit, C.; Krysmann, M. J.; Havredaki, V.; Viras, K.; Hamley, I. W., Interactions of an anionic surfactant with poly(oxyalkylene) copolymers in aqueous solution. *J. Colloid Interface Sci.* **2009,** 330, (1), 67-72.

99. Eeckman, F.; Moes, A. J.; Amighi, K., Surfactant induced drug delivery based on the use of thermosensitive polymers. *J. Control Release* **2003,** 88, (1), 105-16.

100. Ge, X.; Conley, A. J.; Brandle, J. E.; Truant, R.; Filipe, C. D. M., In Vivo Formation of Protein Based Aqueous Microcompartments. *J. Am. Chem. Soc.* **2009,** 131, (25), 9094-9099.

101. Bryksin, A. V.; Brown, A. C.; Baksh, M. M.; Finn, M. G.; Barker, T. H., Learning from nature – Novel synthetic biology approaches for biomaterial design. *Acta Biomaterialia*, **2014,** 10, (4), 1761-1769.

102. König, H. M.; Kilbinger, A. F. M., Learning from Nature: β-Sheet-Mimicking Copolymers Get Organized. *Angewandte Chemie International Edition* **2007,** 46, (44), 8334-8340.

103. Tang, A.; Wang, C.; Stewart, R. J.; Kopeček, J., The coiled coils in the design of protein-based constructs: hybrid hydrogels and epitope displays. *Journal of Controlled Release* **2001,** 72, (1–3), 57-70.

104. Pechar, M.; Pola, R., The coiled coil motif in polymer drug delivery systems. *Biotechnology Advances* **2013,** 31, (1), 90-96.

105. Vinson, C.; Myakishev, M.; Acharya, A.; Mir, A. A.; Moll, J. R.; Bonovich, M., Classification of human B-ZIP proteins based on dimerization properties. *Molecular and Cellular Biology* **2002,** 22, (18), 6321-6335.

106. Yu, Y. B., Coiled-coils: stability, specificity, and drug delivery potential. *Advanced Drug Delivery Reviews* **2002,** 54, (8), 1113-1129.

107. Ryadnov, M. G.; Papapostolou, D.; Woolfson, D. N., The leucine zipper as a building block for self-assembled protein fibers. *Methods Mol Biol* **2008,** 474, 35-51.

108. Tripet, B.; Wagschal, K.; Lavigne, P.; Mant, C. T.; Hodges, R. S., Effects of side-chain characteristics on stability and oligomerization state of a de Novo-designed model coiled-coil: 20 amino acid substitutions in position “d”. *Journal of Molecular Biology* **2000,** 300, (2), 377-402.

109. De Crescenzo, G.; Litowski, J. R.; Hodges, R. S.; O'Connor-McCourt, M. D., Real-Time Monitoring of the Interactions of Two-

Stranded de Novo Designed Coiled-Coils: Effect of Chain Length on the Kinetic and Thermodynamic Constants of Binding†. *Biochemistry* **2003,** 42, (6), 1754-1763.

110. Zhou, N. E.; Kay, C. M.; Hodges, R. S., The net energetic contribution of interhelical electrostatic attractions to coiled-coil stability. *Protein Eng* **1994,** 7, (11), 1365-72.

111. Litowski, J. R.; Hodges, R. S., Designing heterodimeric two-stranded alpha-helical coiled-coils: the effect of chain length on protein folding, stability and specificity. *J Pept Res* **2001,** 58, (6), 477-92.

112. Harbury, P. B.; Zhang, T.; Kim, P. S.; Alber, T., A switch between two-, three-, and four-stranded coiled coils in GCN4 leucine zipper mutants. *Science* **1993,** 262, (5138), 1401-7.

113. Yang, J.; Xu, C.; Kopeckova, P.; Kopecek, J., Hybrid hydrogels self-assembled from HPMA copolymers containing peptide grafts. *Macromol Biosci* **2006,** 6, (3), 201-9.

114. Herrero-Vanrell, R.; Rincon, A. C.; Alonso, M.; Reboto, V.; Molina-Martinez, I. T.; Rodriguez-Cabello, J. C., Self-assembled particles of an elastin-like polymer as vehicles for controlled drug release. *J. Controlled Release* **2005,** 102, (1), 113-122.

115. Chilkoti, A.; Dreher, M. R.; Meyer, D. E.; Raucher, D., Targeted drug delivery by thermally responsive polymers. *Adv. Drug Delivery Rev.* **2002,** 54, (5), 613-630.

116. García-Arévalo, C.; Bermejo-Martín, J. F.; Rico, L.; Iglesias, V.; Martín, L.; Rodríguez-Cabello, J. C.; Arias, F. J., Immunomodulatory Nanoparticles from Elastin-Like Recombinamers: Single-Molecules for Tuberculosis Vaccine Development. *Mol. Pharmaceutics* **2013,** 10(2), 586-597.

117. McDaniel, J. R.; Callahan, D. J.; Chilkoti, A., Drug delivery to solid tumors by elastin-like polypeptides. *Adv. Drug Delivery Rev.* **2010,** 62, (15), 1456-1467.

118. Wu, Y.; MacKay, J. A.; McDaniel, J. R.; Chilkoti, A.; Clark, R. L., Fabrication of elastin-like polypeptide nanoparticles for drug delivery by electrospraying. *Biomacromolecules* **2009,** 10, (1), 19-24.

119. Martín, L.; Castro, E.; Ribeiro, A.; Alonso, M.; Rodríguez-Cabello, J. C., Temperature-Triggered Self-Assembly of Elastin-Like Block Co-Recombinamers:The Controlled Formation of Micelles and Vesicles in an Aqueous Medium. *Biomacromolecules* **2012,** 13, (2), 293-298.

120. Dreher, M. R.; Simnick, A. J.; Fischer, K.; Smith, R. J.; Patel, A.; Schmidt, M.; Chilkoti, A., Temperature triggered self-assembly of polypeptides into multivalent spherical micelles. *J. Am. Chem. Soc.* **2008,** 130, (2), 687-94.

121. Sallach, R. E.; Wei, M.; Biswas, N.; Conticello, V. P.; Lecommandoux, S.; Dluhy, R. A.; Chaikof, E. L., Micelle Density Regulated by a Reversible Switch of Protein Secondary Structure. *J. Am. Chem. Soc.* **2006,** 128, (36), 12014-12019.

122. Gref, R.; Domb, A.; Quellec, P.; Blunk, T.; Müller, R. H.; Verbavatz, J. M.; Langer, R., The controlled intravenous delivery of drugs using PEG-coated sterically stabilized nanospheres. *Adv. Drug Delivery Rev.* **1995,** 16, (2-3), 215-233.

123. Douglas, S. J.; Davis, S. S.; Illum, L., Nanoparticles in drug delivery. *Crit. Rev. Ther. Drug Carrier Syst.* **1987,** 3, (3), 233-61.

124. Kim, W.; Thévenot, J.; Ibarboure, E.; Lecommandoux, S.; Chaikof, E. L., Self-Assembly of Thermally Responsive Amphiphilic

Diblock Copolypeptides into Spherical Micellar Nanoparticles. *Angew. Chem., Int. Ed. Engl.* **2010,** 49, (25), 4257-4260.

125. Ramakrishna, S.; Mayer, J.; Wintermantel, E.; Leong, K. W., Biomedical applications of polymer-composite materials: a review. *Composites Science and Technology* **2001,** 61, (9), 1189-1224.

126. Speidel, M. O.; Uggowitzer, P. J., *Materials in Medicine*. vdf, Hochschulverlag AG an der ETH Zürich: 1998.

127. Strong, L. E.; West, J. L., Thermally responsive polymer-nanoparticle composites for biomedical applications. *Wiley interdisciplinary reviews. Nanomedicine and nanobiotechnology* **2011,** 3, (3), 307-17.

128. Amruthwar, S. S.; Janorkar, A. V., In vitro evaluation of elastin-like polypeptide-collagen composite scaffold for bone tissue engineering. *Dental materials : official publication of the Academy of Dental Materials* **2013,** 29, (2), 211-20.

129. Leckie, A. E.; Akens, M. K.; Woodhouse, K. A.; Yee, A. J.; Whyne, C. M., Evaluation of thiol-modified hyaluronan and elastin-like polypeptide composite augmentation in early-stage disc degeneration: comparing 2 minimally invasive techniques. *Spine (Phila Pa 1976)* **2012,** 37, (20), E1296-303.

130. Wheeler, T. S.; Sbravati, N. D.; Janorkar, A. V., Mechanical & cell culture properties of elastin-like polypeptide, collagen, bioglass, and carbon nanosphere composites. *Ann Biomed Eng* **2013,** 41, (10), 2042-55.

131. Novoselov, K. S.; Geim, A. K.; Morozov, S. V.; Jiang, D.; Zhang, Y.; Dubonos, S. V.; Grigorieva, I. V.; Firsov, A. A., Electric Field Effect in Atomically Thin Carbon Films. *Science* **2004,** 306, (5696), 666-669.

132. Novoselov, K. S.; Geim, A. K.; Morozov, S. V.; Jiang, D.; Katsnelson, M. I.; Grigorieva, I. V.; Dubonos, S. V.; Firsov, A. A., Two-dimensional gas of massless Dirac fermions in graphene. *Nature* **2005,** 438, (7065), 197-200.

133. Geim, A. K., Graphene: Status and Prospects. *Science* **2009,** 324, (5934), 1530-1534.

134. Avouris, P.; Dimitrakopoulos, C., Graphene: synthesis and applications. *Mater. Today* **2012,** 15, (3), 86-97.

135. Liu, J.; Cui, L.; Losic, D., Graphene and graphene oxide as new nanocarriers for drug delivery applications. *Acta Biomater.* **2013,** 9, (12), 9243-9257.

136. Liu, Z.; Robinson, J. T.; Tabakman, S. M.; Yang, K.; Dai, H., Carbon materials for drug delivery & cancer therapy. *Materials Today* **2011,** 14, (7–8), 316-323.

137. Zhou, K.; Thouas, G. A.; Bernard, C. C.; Nisbet, D. R.; Finkelstein, D. I.; Li, D.; Forsythe, J. S., Method to Impart Electro- and Biofunctionality to Neural Scaffolds Using Graphene–Polyelectrolyte Multilayers. *ACS Appl. Mater. Interfaces* **2012,** 4, (9), 4524-4531.

138. Zhang, L.; Lu, Z.; Zhao, Q.; Huang, J.; Shen, H.; Zhang, Z., Enhanced Chemotherapy Efficacy by Sequential Delivery of siRNA and Anticancer Drugs Using PEI-Grafted Graphene Oxide. *Small* **2011,** 7, (4), 460-464.

139. Ma, X.; Tao, H.; Yang, K.; Feng, L.; Cheng, L.; Shi, X.; Li, Y.; Guo, L.; Liu, Z., A functionalized graphene oxide-iron oxide nanocomposite for magnetically targeted drug delivery, photothermal therapy, and magnetic resonance imaging. *Nano Res.* **2012,** 5, (3), 199-212.

140. Goenka, S.; Sant, V.; Sant, S., Graphene-based nanomaterials for drug delivery and tissue engineering. *Journal of Controlled Release* **2014,** 173, (0), 75-88.

141. Sprinkle, M.; Ruan, M.; Hu, Y.; Hankinson, J.; Rubio-Roy, M.; Zhang, B.; Wu, X.; Berger, C.; Heer, W. A. d., Scalable templated growth of graphene nanoribbons on SiC. *Nature Nanotechnology* **2010,** 5, (10), 727-731.

142. Kim, J.; Cote, L. J.; Kim, F.; Yuan, W.; Shull, K. R.; Huang, J., Graphene Oxide Sheets at Interfaces. *Journal of the American Chemical Society* **2010,** 132, (23), 8180-8186.

143. Kim, F.; Cote, L. J.; Huang, J., Graphene Oxide: Surface Activity and Two-Dimensional Assembly. *Advanced Materials* **2010,** 22, (17), 1954-1958.

144. Liu, Z.; Robinson, J. T.; Sun, X.; Dai, H., PEGylated Nanographene Oxide for Delivery of Water-Insoluble Cancer Drugs. *J. Am. Chem. Soc.* **2008,** 130, (33), 10876-10877.

145. Chang, Y.; Yang, S.-T.; Liu, J.-H.; Dong, E.; Wang, Y.; Cao, A.; Liu, Y.; Wang, H., In vitro toxicity evaluation of graphene oxide on A549 cells. *Toxicol. Lett.* **2011,** 200, (3), 201-210.

146. Hu, W.; Peng, C.; Lv, M.; Li, X.; Zhang, Y.; Chen, N.; Fan, C.; Huang, Q., Protein Corona-Mediated Mitigation of Cytotoxicity of Graphene Oxide. *ACS Nano* **2011,** 5, (5), 3693-3700.

147. Bianco, A., Graphene: Safe or Toxic? The Two Faces of the Medal. *Angew. Chem., Int. Ed.* **2013,** 52, (19), 4986-4997.

148. Chen, D.; Zhu, H.; Liu, T., In Situ Thermal Preparation of Polyimide Nanocomposite Films Containing Functionalized Graphene Sheets. *ACS Applied Materials & Interfaces* **2010,** 2, (12), 3702-3708.

149. Lee, S. H.; Dreyer, D. R.; An, J.; Velamakanni, A.; Piner, R. D.; Park, S.; Zhu, Y.; Kim, S. O.; Bielawski, C. W.; Ruoff, R. S., Polymer Brushes via Controlled, Surface-Initiated Atom Transfer Radical Polymerization (ATRP) from Graphene Oxide. *Macromol Rapid Commun* **2010,** 31, (3), 281-8.

150. Fim, F. d. C.; Guterres, J. M.; Basso, N. R. S.; Galland, G. B., Polyethylene/graphite nanocomposites obtained by in situ polymerization. *Journal of Polymer Science Part A: Polymer Chemistry* **2010,** 48, (3), 692-698.

151. Kuila, T.; Bose, S.; Khanra, P.; Kim, N. H.; Rhee, K. Y.; Lee, J. H., Characterization and properties of in situ emulsion polymerized poly(methyl methacrylate)/graphene nanocomposites. *Composites Part A: Applied Science and Manufacturing* **2011,** 42, (11), 1856-1861.

152. Liu, J.; Yang, W.; Tao, L.; Li, D.; Boyer, C.; Davis, T. P., Thermosensitive graphene nanocomposites formed using pyrene-terminal polymers made by RAFT polymerization. *Journal of Polymer Science Part A: Polymer Chemistry* **2010,** 48, (2), 425-433.

153. Pan, Y.; Bao, H.; Sahoo, N. G.; Wu, T.; Li, L., Water-Soluble Poly(N-isopropylacrylamide)–Graphene Sheets Synthesized via Click Chemistry for Drug Delivery. *Advanced Functional Materials* **2011,** 21, (14), 2754-2763.

154. Shen, J.; Yan, B.; Shi, M.; Ma, H.; Li, N.; Ye, M., Synthesis of graphene oxide-based biocomposites through diimide-activated amidation. *J Colloid Interface Sci* **2011,** 356, (2), 543-9.

155. Ribeiro, A.; Arias, F. J.; Reguera, J.; Alonso, M.; Rodriguez-Cabello, J. C., Influence of the amino-acid sequence on the inverse temperature transition of elastin-like polymers. *Biophys J* **2009,** 97, (1), 312-20.

156. Laemmli, U. K., Cleavage of Structural Proteins during the Assembly of the Head of Bacteriophage T4. *Nature* **1970,** 227, (5259), 680-685.

157. Walker, J., Nondenaturing Polyacrylamide Gel Electrophoresis of Proteins. In *The Protein Protocols Handbook*, Walker, J., Ed. Humana Press: 2002; pp 57-60.

158. Koppel, D. E., Analysis of Macromolecular Polydispersity in Intensity Correlation Spectroscopy: The Method of Cumulants. *The Journal of Chemical Physics* **1972,** 57, (11), 4814-4820.

159. Provencher, S. W., CONTIN: A general purpose constrained regularization program for inverting noisy linear algebraic and integral equations. *Computer Physics Communications* **1982,** 27, (3), 229-242.

160. Brown, W., *Light scattering : principles and development*. Clarendon Press: Oxford, 1996; p xiii, 528 p.

161. Burchard, W., *Static and dynamic light scattering from branched polymers and biopolymers*

Springer Berlin / Heidelberg: 1983; Vol. 48, p 1-124.

162. Zhang, S. G., Fabrication of novel biomaterials through molecular self-assembly. *Nat. Biotechnol.* **2003,** 21, (10), 1171-1178.

163. Discher, B. M.; Won, Y. Y.; Ege, D. S.; Lee, J. C. M.; Bates, F. S.; Discher, D. E.; Hammer, D. A., Polymersomes: Tough vesicles made from diblock copolymers. *Science* **1999,** 284, (5417), 1143-1146.

164. Upadhyay, K. K.; Le Meins, J. F.; Misra, A.; Voisin, P.; Bouchaud, V.; Ibarboure, E.; Schatz, C.; Lecommandoux, S., Biomimetic doxorubicin loaded polymersomes from hyaluronan-block-poly(gamma-benzyl glutamate) copolymers. *Biomacromolecules* **2009,** 10, (10), 2802-8.

165. Chen, T. H.; Bae, Y.; Furgeson, D. Y., Intelligent biosynthetic nanobiomaterials (IBNs) for hyperthermic gene delivery. *Pharm. Res.* **2008,** 25, (3), 683-91.

166. Dash, B. C.; Mahor, S.; Carroll, O.; Mathew, A.; Wang, W.; Woodhouse, K. A.; Pandit, A., Tunable elastin-like polypeptide hollow sphere as a high payload and controlled delivery gene depot. *J. Controlled Release* **2011,** 152, (3), 382-392.

167. Chen, T.; Guo, X.; Liu, X.; Shi, S.; Wang, J.; Shi, C.; Qian, Z.; Zhou, S., A strategy in the design of micellar shape for cancer therapy. *Adv. Healthcare Mater.* **2012,** 1, (2), 214-24.

168. Reguera, J.; Lagaron, J. M.; Alonso, M.; Reboto, V.; Calvo, B.; Rodríguez-Cabello, J. C., Thermal behavior and kinetic analysis of the chain unfolding and refolding and of the concomitant nonpolar solvation and desolvation of two elastin-like polymers. *Macromolecules* **2003,** 36, (22), 8470-8476.

169. D'Souza, A. J. M.; Hart, D. S.; Middaugh, C. R.; Gehrke, S. H., Characterization of the changes in secondary structure and architecture of elastin-mimetic triblock polypeptides during thermal gelation. *Macromolecules* **2006,** 39, (20), 7084-7091.

170. Sanson, C.; Schatz, C.; Le Meins, J. F.; Brulet, A.; Soum, A.; Lecommandoux, S., Biocompatible and biodegradable poly(trimethylene carbonate)-b-poly(L-glutamic acid) polymersomes: size control and stability. *Langmuir* 26, (4), 2751-60.

171. Rekatas, C. J.; Mai, S.-M.; Crothers, M.; Quinn, M.; Collett, J. H.; Attwood, D.; Heatley, F.; Martini, L.; Booth, C., The effect of hydrophobe chemical structure and chain length on the solubilization of griseofulvin in aqueous micellar solutions of block

copoly(oxyalkylene)s. *Phys. Chem. Chem. Phys.* **2001,** 3, (21), 4769-4773.

172. Liu, S.; Weaver, J. V. M.; Tang, Y.; Billingham, N. C.; Armes, S. P.; Tribe, K., Synthesis of Shell Cross-Linked Micelles with pH-Responsive Cores Using ABC Triblock Copolymers. *Macromolecules* **2002,** 35, (16), 6121-6131.

173. Schärtl, W., *Light scattering from polymer solutions and nanoparticle dispersions*. Springer: Berlin ; New York, 2007; p xiv, 191 p.

174. Lutter, J.; Wu, T.-Y.; Zhang, Y., Hydration of Cations: A Key to Understanding of Specific Cation Effects on Aggregation Behaviors of PEO-PPO-PEO Triblock Copolymers. *J. Phys. Chem. B* **2013,** 117, (35), 10132-10141.

175. Cho, Y.; Zhang, Y.; Christensen, T.; Sagle, L. B.; Chilkoti, A.; Cremer, P. S., Effects of Hofmeister anions on the phase transition temperature of elastin-like polypeptides. *J Phys Chem B* **2008,** 112, (44), 13765-71.

176. Tomé, L.; Pinho, S.; Jorge, M.; Gomes, J.; Coutinho, J., Salting-in with a salting-out agent: explaining the cation specific effects on the aqueous solubility of amino acids. *J. Phys. Chem. B* **2013,** 117, (20), 6116-6128.

177. Reiersen, H.; Clarke, A. R.; Rees, A. R., Short elastin-like peptides exhibit the same temperature-induced structural transitions as elastin polymers: implications for protein engineering. *J Mol Biol* **1998,** 283, (1), 255-64.

178. Yamaoka, T.; Tamura, T.; Seto, Y.; Tada, T.; Kunugi, S.; Tirrell, D. A., Mechanism for the phase transition of a genetically

engineered elastin model peptide (VPGIG)40 in aqueous solution. *Biomacromolecules* **2003,** 4, (6), 1680-5.

179. Zhang, Y.; Trabbic-Carlson, K.; Albertorio, F.; Chilkoti, A.; Cremer, P. S., Aqueous two-phase system formation kinetics for elastin-like polypeptides of varying chain length. *Biomacromolecules* **2006,** 7, (7), 2192-9.

180. Ghoorchian, A.; Cole, J. T.; Holland, N. B., Thermoreversible Micelle Formation Using a Three-Armed Star Elastin-like Polypeptide. *Macromolecules* **2010,** 43, (9), 4340-4345.

181. Chilkoti, A.; Christensen, T.; MacKay, J. A., Stimulus responsive elastin biopolymers: Applications in medicine and biotechnology. *Curr Opin Chem Biol* **2006,** 10, (6), 652-7.

182. Ortona, O.; D'Errico, G.; Paduano, L.; Vitagliano, V., Interaction between cationic, anionic, and non-ionic surfactants with ABA block copolymer Pluronic PE6200 and with BAB reverse block copolymer Pluronic 25R4. *J. Colloid Interface Sci.* **2006,** 301, (1), 63-77.

183. Luan, C.-H.; Urry, D. W., Elastic, Plastic, and Hydrogel Protein-based Polymers. In *Polymer Data Handbook*, Mark, J. E., Ed. Oxford University Press: New York, 1999; pp 78-89.

184. Nagapudi, K.; Brinkman, W. T.; Leisen, J.; Thomas, B. S.; Wright, E. R.; Haller, C.; Wu, X. Y.; Apkarian, R. P.; Conticello, V. P.; Chaikof, E. L., Protein-based thermoplastic elastomers. *Macromolecules* **2005,** 38, (2), 345-354.

185. Vitorazi, L.; Berret, J.-F.; Loh, W., Self-Assembly of Complex Salts of Cationic Surfactants and Anionic–Neutral Block Copolymers. Dispersions with Liquid-Crystalline Internal Structure. *Langmuir* **2013,** 29, (46), 14024-14033.

186. Qi, L.; Fresnais, J. r.; Berret, J.-F. o.; Castaing, J.-C.; Destremaut, F.; Salmon, J.-B.; Cousin, F.; Chapel, J.-P., Influence of the Formulation Process in Electrostatic Assembly of Nanoparticles and Macromolecules in Aqueous Solution: The Interaction Pathway. *J. Phys. Chem. C* **2010,** 114, (39), 16373-16381.

187. Wang, E.; Desai, M. S.; Lee, S.-W., Light-Controlled Graphene-Elastin Composite Hydrogel Actuators. *Nano Lett.* **2013,** 13, (6), 2826-2830.

188. Arias, F. J.; Santos, M.; Fernandez-Colino, A.; Pinedo, G.; Girotti, A., Recent Contributions Of Elastin-Like Recombinamers To Biomedicine And Nanotechnology. *Curr Top Med Chem* **2014,** 18, 18.

189. Fahmi, A.; Pietsch, T.; Bryszewska, M.; Rodríguez-Cabello, J. C.; Koceva-Chyla, A.; Arias, F. J.; Rodrigo, M. A.; Gindy, N., Fabrication of CdSe-Nanofibers with Potential for Biomedical Applications. *Adv. Funct. Mater.* **2010,** 20, (6), 1011-1018.

190. Wang, E.; Desai, M. S.; Heo, K.; Lee, S.-W., Graphene-Based Materials Functionalized with Elastin-like Polypeptides. *Langmuir* **2014**.

191. Garcia-Arevalo, C.; Pierna, M.; Girotti, A.; Arias, F. J.; Rodriguez-Cabello, J. C., A comparative study of cell behavior on different energetic and bioactive polymeric surfaces made from elastin-like recombinamers. *Soft Matter* **2012,** 8, (11), 3239-3249.

192. Pierna, M.; Santos, M.; Arias, F. J.; Alonso, M.; Rodríguez-Cabello, J. C., Efficient Cell and Cell-Sheet Harvesting Based on Smart Surfaces Coated with a Multifunctional and Self-Organizing Elastin-Like Recombinamer. *Biomacromolecules* **2013,** 14, (6), 1893-1903.

193. Jung, I.; Dikin, D.; Park, S.; Cai, W.; Mielke, S. L.; Ruoff, R. S., Effect of Water Vapor on Electrical Properties of Individual

Reduced Graphene Oxide Sheets. *The Journal of Physical Chemistry C* **2008,** 112, (51), 20264-20268.

194. Stankovich, S.; Dikin, D. A.; Piner, R. D.; Kohlhaas, K. A.; Kleinhammes, A.; Jia, Y.; Wu, Y.; Nguyen, S. T.; Ruoff, R. S., Synthesis of graphene-based nanosheets via chemical reduction of exfoliated graphite oxide. *Carbon* **2007,** 45, (7), 1558-1565.

195. Beachley, V.; Wen, X., Polymer nanofibrous structures: Fabrication, biofunctionalization, and cell interactions. *Progress in Polymer Science* **2010,** 35, (7), 868-892.

196. Alison, P. M.; Derek, A. B.; Ana, G.; Manish, B.; George, M. W., Cell Encapsulation in Sub-mm Sized Gel Modules Using Replica Molding. *PLoS ONE* **2008,** 3, (5).

197. Ning, L.; Qi, Z.; Song, G.; Qin, S.; Rong, H.; Long, W.; Liwei, L.; Jianwu, D.; Mingliang, T.; Guosheng, C., Three-dimensional graphene foam as a biocompatible and conductive scaffold for neural stem cells. *Sci. Rep.* **2013,** 3.

198. McPherson, D. T.; Morrow, C.; Minehan, D. S.; Wu, J.; Hunter, E.; Urry, D. W., Production and Purification of a Recombinant Elastomeric Polypeptide, G-(VPGVG)19-VPGV, from Escherichia coli. *Biotechnol. Prog.* **1992,** 8, (4), 347-352.

199. Martin, L.; Javier Arias, F.; Alonso, M.; Garcia-Arevalo, C.; Rodriguez-Cabello, J. C., Rapid micropatterning by temperature-triggered reversible gelation of a recombinant smart elastin-like tetrablock-copolymer. *Soft Matter* **2010,** 6, (6), 1121-1124.

200. Kiss, M. Z.; Hobson, M. A.; Varghese, T.; Harter, J.; Kliewer, M. A.; Hartenbach, E. M.; Zagzebski, J. A., Frequency-dependent complex modulus of the uterus: preliminary results. *Phys. Med. Biol.* **2006,** 51, (15), 3683-95.

201. Bae, K. H.; Wang, L.-S.; Kurisawa, M., Injectable biodegradable hydrogels: progress and challenges. *Journal of Materials Chemistry B* **2013,** 1, (40), 5371-5388.

202. Kim, W.; Thévenot, J.; Ibarboure, E.; Lecommandoux, S.; Chaikof, E., Self-Assembly of Thermally Responsive Amphiphilic Diblock Copolypeptides into Spherical Micellar Nanoparticles. *Angew. Chem., Int. Ed.* **2010,** 49, (25), 4257-4260.

203. Wright, E. R.; Conticello, V. P., Self-assembly of block copolymers derived from elastin-mimetic polypeptide sequences. *Advanced Drug Delivery Reviews* **2002,** 54, (8), 1057-1073.

204. Conlan, B. F.; Gillon, A. D.; Craik, D. J.; Anderson, M. A., Circular proteins and mechanisms of cyclization. *Peptide Science* **2010,** 94, (5), 573-583.

205. Rühe, J.; Knoll, W., Functional polymer brushes*. *Journal of Macromolecular Science, Part C* **2002,** 42, (1), 91-138.

206. Inoue, K., Functional dendrimers, hyperbranched and star polymers. *Progress in Polymer Science* **2000,** 25, (4), 453-571.

207. Vögtle, F.; Gestermann, S.; Hesse, R.; Schwierz, H.; Windisch, B., Functional dendrimers. *Progress in Polymer Science* **2000,** 25, (7), 987-1041.

208. Pechar, M.; Pola, R.; Laga, R.; Ulbrich, K.; Bednárová, L.; Maloň, P.; Sieglová, I.; Král, V.; Fábry, M.; Vaněk, O., Coiled Coil Peptides as Universal Linkers for the Attachment of Recombinant Proteins to Polymer Therapeutics. *Biomacromolecules* **2011,** 12, (10), 3645-3655.

209. Sahin, E.; Kiick, K. L., Macromolecule-Induced Assembly of Coiled-Coils in Alternating Multiblock Polymers. *Biomacromolecules* **2009,** 10, (10), 2740-2749.

210. Vandermeulen, G. W. M.; Tziatzios, C.; Duncan, R.; Klok, H.-A., PEG-Based Hybrid Block Copolymers Containing -Helical Coiled Coil Peptide Sequences: Control of Self-Assembly and Preliminary Biological Evaluation. *Macromolecules* **2005,** 38, (3), 761-769.

211. Apostolovic, B.; Deacon, S. P. E.; Duncan, R.; Klok, H.-A., Cell Uptake and Trafficking Behavior of Non-covalent, Coiled-coil Based Polymer–Drug Conjugates. *Macromolecular Rapid Communications* **2011,** 32, (1), 11-18.

212. Oshea, E. K.; Klemm, J. D.; Kim, P. S.; Alber, T., X-RAY structure of the gcn4 leucine zipper, a 2-stranded, parallel coiled coil. *Science* **1991,** 254, (5031), 539-544.

213. Mason, J. M.; Arndt, K. M., Coiled coil domains: stability, specificity, and biological implications. *Chembiochem* **2004,** 5, (2), 170-6.

214. Zhang, W.-B.; Sun, F.; Tirrell, D. A.; Arnold, F. H., Controlling Macromolecular Topology with Genetically Encoded SpyTag–SpyCatcher Chemistry. *Journal of the American Chemical Society* **2013,** 135, (37), 13988-13997.

215. Walker, A. A.; Weisman, S.; Kameda, T.; Sutherland, T. D., Natural Templates for Coiled-Coil Biomaterials from Praying Mantis Egg Cases. *Biomacromolecules* **2012,** 13, (12), 4264-4272.

216. Walker, A. A.; Warden, A. C.; Trueman, H. E.; Weisman, S.; Sutherland, T. D., Micellar refolding of coiled-coil honeybee silk proteins. *Journal of Materials Chemistry B* **2013,** 1, (30), 3644-3651.

217. Ribeiro, A.; Arias, F. J.; Reguera, J.; Alonso, M.; Rodríguez-Cabello, J. C., Influence of the Amino-Acid Sequence on the Inverse Temperature Transition of Elastin-Like Polymers. *Biophysical Journal* **2009,** 97, (1), 312-320.

218. Zhou, N. E.; Kay, C. M.; Hodges, R. S., Disulfide bond contribution to protein stability: Positional effects of substitution in the hydrophobic core of the two-stranded .alpha.-helical coiled-coil. *Biochemistry* **1993,** 32, (12), 3178-3187.

219. Nicolini, C.; Ravindra, R.; Ludolph, B.; Winter, R., Characterization of the Temperature- and Pressure-Induced Inverse and Reentrant Transition of the Minimum Elastin-Like Polypeptide GVG(VPGVG) by DSC, PPC, CD, and FT-IR Spectroscopy. *Biophysical Journal* **2004,** 86, (3), 1385-1392.

220. Amiram, M.; Quiroz, F. G.; Callahan, D. J.; Chilkoti, A., A highly parallel method for synthesizing DNA repeats enables the discovery of 'smart' protein polymers. *Nat Mater* **2011,** 10, (2), 141-8.

221. Pinedo-Martín, G.; Castro, E.; Martín, L.; Alonso, M.; Rodríguez-Cabello, J. C., Effect of Surfactants on the Self-Assembly of a Model Elastin-like Block Corecombinamer: From Micelles to an Aqueous Two-Phase System. *Langmuir* **2014,** 30, (12), 3432-3440.

222. Dreher, M. R.; Simnick, A. J.; Fischer, K.; Smith, R. J.; Patel, A.; Schmidt, M.; Chilkoti, A., Temperature Triggered Self-Assembly of Polypeptides into Multivalent Spherical Micelles. *Journal of the American Chemical Society* **2007,** 130, (2), 687-694.

223. Lebowitz, J.; Lewis, M. S.; Schuck, P., Modern analytical ultracentrifugation in protein science: a tutorial review. *Protein Sci* **2002,** 11, (9), 2067-79.

APPENDIX